Smart Operation of Four-Quadrant Electric Vehicle Chargers in Distribution Grids

by

Mauricio Restrepo Restrepo

A thesis
presented to the University of Waterloo
in fulfillment of the
thesis requirement for the degree of
Doctor of Philosophy
in
Electrical and Computer Engineering

Waterloo, Ontario, Canada, 2017

EXAMINING COMMITTEE MEMBERSHIP

The following served on the Examining Committee for this thesis. The decision of the Examining Committee is by majority vote.

External Examiner	Dr. Ali Emadi Professor, McMaster University
Supervisor	Dr. Claudio Cañizares Professor, University of Waterloo
Supervisor	Dr. Mehrdad Kazerani Professor, University of Waterloo
Internal Member	Dr. Kankar Bhattacharya Professor, University of Waterloo
Internal Member	Dr. Catherine Rosenberg Professor, University of Waterloo
Internal-external Member	Dr. Srinivasan Keshav Professor, University of Waterloo

I hereby declare that I am the sole author of this thesis. This is a true copy of the thesis, including any required final revisions, as accepted by my examiners.

I understand that my thesis may be made electronically available to the public.

Abstract

Many policies and programs adopted in the context of climate change mitigation and substitution of fossil fuels are contributing to the continuous development and growth of Electric Vehicles (EVs) in urban mobility systems, reaching 1.26 million units on the roads through the end of 2015. Even though the increasing number of EVs will create problems in distribution systems, which can be mitigated using smart charging strategies, there will also be economic opportunities for EV owners to provide services to the grid while their vehicle are parked and plugged in, a concept known as Vehicle-to-Grid (V2G). Most of the studies on V2G have concentrated on the provision of services such as frequency regulation or spinning reserves, which may reduce the battery life because of the required extra charging/discharging cycles, and little attention has been paid to the possibility of providing reactive power control services to the grid by using the ac/dc converter and the dc link capacitor available in most advanced chargers, a practice that does not compromise the vehicle battery life. These kinds of chargers, which are known as four-quadrant EV chargers due to the capability of being operated in all quadrants of the P-Q plane, can be used in distribution networks to improve the power factor and help regulate voltage, thus facilitating larger EV penetrations, as discussed in this thesis.

In the first part of this thesis, a new average model of a single-phase, four-quadrant EV charger is developed. The steady-state and step responses of the proposed model for different P-Q requests, corresponding to the operation in the four quadrants of the P-Q plane, are used to validate its performance against a four-quadrant EV charger prototype. The model is shown to be useful for efficient time-domain simulations and studies that include a number of EV chargers, such as EV integration studies in Low-Voltage (LV) distribution networks. A practical case study is presented to demonstrate and test the performances of the four-quadrant charger and its model, investigating the voltage interactions of several chargers in an LV residential network during the provision of three vehicle-to-grid (V2G) strategies for active and reactive power.

In the second part, a novel three-stage algorithm to coordinate the operation of four-quadrant EV chargers with other volt/var control devices in Medium-Voltage (MV) and LV distribution feeders is proposed. The first stage of the algorithm is operated on a day-ahead basis and defines the Load Tap Changer (LTC) and capacitor schedules while minimizing the peak load associated with EVs in the distribution system. The second and third stages update their operation every five minutes, to fairly allocate the aggregated and individual EV loads in the MV and LV feeders, respectively, while minimizing active power losses and voltage deviations. The proposed technique is applied to CIGRE's North-American MV

and LV benchmark systems to demonstrate its ability to properly allocate EV loads, and improve distribution system performance in terms of losses and voltage profiles.

Acknowledgements

First and foremost, I would like to express my sincere gratitude to my supervisors, Prof. Claudio Cañizares and Prof. Mehrdad Kazerani, for their invaluable guidance and support during my graduate studies at the University of Waterloo. It has been a great honor and privilege to have completed my studies under their supervision, learning from the example of two excellent professionals and human beings.

I would like to thank Prof. Catherine Rosenberg, Prof. Kankar Battacharya, and Prof. Srinivasan Keshav from the University of Waterloo, for serving on my Advisory Committee, and for their insightful comments and feedback. I am also very thankful to Prof. Ali Emadi from McMaster University, for serving as the external thesis examiner and for his wise comments and observations.

I am very thankful with all my friends and colleagues of EMSOL and Power Electronics Labs, which I have met during the course of my studies: Adarsh, Alfredo, Ahmad, Akash, Amir, Andrés, Bharat, Behnam, Chioma, Daniel Olivares, Daniel Remón, Darío, David, Edson, Ehsan, Elham, Fabián, Fabricio, Felipe Ramos, Felipe Valencia, Francisco, Indrajit, Isha, Iván, Jordan, José Daniel, Juan Carlos, Mahmoud, Mariano, Marten, Mehrdad, Mostafa, Nafeesa, Nitin, Rajib, Shubha, Sofía, Talal, Víctor, and Zuher. My deepest thanks for enriching these years of studies, for their friendship, and for sharing with me their knowledge.

I wish to express my deepest gratitude to my parents, Iván and María Eugenia, and my sisters, Claudia and Adriana, who have always supported and encouraged me in pursuing this personal goal.

Finally, I sincerely acknowledge the financial support provided by Natural Sciences and Engineering Research Council of Canada (NSERC), Ontario Research Fund (ORF), Hydro One Networks Inc., IBM Corporation, and the University of Waterloo, which made possible this research.

Table of Contents

List of Tables

List of Figures

List of Acronyms

ADC Analog-to-Digital Converter

BAU Business-as-Usual

BMS Battery Management System

CAD Canadian Dollar

CC Constant Current

CCU Central Control Unit

CI Confidence Interval

CP Constant Power

CT Current Transformer

CV Constant Voltage

DG Distributed Generation

DOPF Distribution Optimal Power Flow

DP Dynamic Programming

DSM Demand-side Management

DSO Distribution System Operator

EV Electric Vehicle

EVSE Electric Vehicle Supply Equipment

GA Genetic Algorithm

ICE Internal Combustion Engine

LDC Local Distribution Company

LC Line-Drop Compensator

Li-Ion Lithium-Ion

LTC Load Tap Changer

LP Linear Programming

LV Low-Voltage

MCS Monte Carlo Simulation

MILP Mixed-Integer Linear Programming

MINLP Mixed-Integer Nonlinear Programming

MPC Model Predictive Control

MSS Maximum Sensitivity Selection

MV Medium-Voltage

NiMH Nickel-Metal Hydride

NLP Non-linear Programming

OPF Optimal Power Flow

PCC Point of Common Coupling

PDF Probability Distribution Function

PLL Phase-Locked Loop

PR Proportional-resonant

PSO Particle Swarm Optimization

PV Photo-voltaic

PWM Pulse width modulation

QP Quadratic Programming

SoC State-of-charge

SQP Sequential Quadratic Programming

SVR Step Voltage Regulator

TOU Time-of-use

V2B Vehicle-to-Building

V2G Vehicle-to-Grid

V2H Vehicle-to-Home

V2V Vehicle-to-Vehicle

NHTS National Household Travel Survey

Nomenclature

Parameters

α, β	Second Stage objective function weight factors
γ	Heuristic method scaling factor
ω	Angular frequency [rad/s]
$\overline{cap}$	Maximum switching capacitor position
$\overline{E}$	Maximum energy capacity [kWh]
$\overline{I}$	Maximum line current [p.u.]
$\overline{P}$	Maximum active power capacity [kW]
$\overline{S}$	Maximum apparent power [kVA]
$\overline{tap}, \underline{tap}$	Maximum and minimum tap positions
$\overline{V}, \underline{V}$	Maximum and minimum voltage limits [p.u.]
τ_1, τ_2	Time steps for stages 1 and 2
$\mathbf{Y}$	Line admittance phasor [S]
$\mathbf{Z}$	Line impedance phasor [Ω]
θ	Line admittance angle [rad]
A, B, C, D	Distribution line parameter matrices
Bc	EV battery capacity [kWh]
C	Capacitance [mF]
C_{MP}	Medium-peak time electricity tariff [$/kWh]
C_{OP}	Off-peak time electricity tariff [$/kWh]
C_P	Peak time electricity tariff [$/kWh]

Cr	EV charger rating [kVA]
CT_p	Number of turns in primary winding of current transformer
CT_s	Number of turns in secondary winding of current transformer
k_i	Integral gain constant
k_p	Proportional gain constant
L	Inductance [mH]
LN	Number of load nodes in the MV system
Mop	Maximum number of operations per hour
N	Number of nodes in the MV system
N_v	Number of EVs connected in each phase
N_{pt}	Number of turns in primary winding of potential transformer
n_p, n_q	Voltage exponents of exponential load models
P_{max}	Maximum allowable peak demand
R	Resistance [Ω]
SW	Switch
T	Period [s]
T_{max}	Maximum time
U	Identity matrix
V_{L_O}	Load nominal voltage [V]
W	Initial sample
w_p	Initial sample point
Y	Line admittance magnitude [S]
Y_{abc}	Line admittance matrix
Z	Impedance magnitude [Ω]
Z_1, Z_2	Secondary winding impedances [Ω]
Z_H	Primary winding impedance [Ω]
Z_{abc}	Line impedance matrix

Variables

δ	Voltage angle [rad]
Ψ^B	Set of bootstrap samples
$\mathbf{I}$	Current phasor [A]
$\mathbf{V}$	Voltage phasor [V]
θ	Angle [rad]
Θ^B	Set of bootstrap sample statistics
θ^b	Statistic of bootstrap sample W_b
θ^*	Bootstrap statistic
cap	Switched capacitor position
D	Duty cycle
E	Energy [kWh]
i, I	Instantaneous and RMS current [A], [p.u.]
I_{abc}	Vector of line currents
K	Aggregated EV droop constant
M	Modulation index
m	Modulation signal
P	Active power [kW]
Q	Reactive power [kVAR]
S	Apparent power of load [kVA]
SF	Switching Function
SoC	State of Charge
tap	Tap position
v, V	Instantaneous and RMS voltage [V], [p.u.]
V_L	Load voltage [V]
V_{LTC}	Load tap changer voltage
V_{rel}	Relay voltage
VD	MV voltage deviation index [p.u.]
W^b	Bootstrap sample

w_p^b	Bootstrap sample point
λ	Binary variable indicating if EV is activated
μ_D	Average distribution system load
d	SQP subproblem direction
$V_{lg_{abc}}$	Vector of line-to-ground voltages
x	Vector of decision variables

Sub- and Super-scripts

α	α-axis component in $\alpha\beta$ transform
β	β-axis component in $\alpha\beta$ transform
$agev$	Aggregated EV index
b	Battery
bl	Base load
c	Coupling
d	Direct-axis
dc	Direct current
ev	EV index
f	Filter
fin	Final
i	Equality constraint index
i_t	Tap index
ini	Initial
j	Inequality constraint index
j_c	Switched capacitor index
k	Iteration index
k_m	MV bus number
l	Line
L_E	Exponential load
L_I	Constant current load

L_m, L_l	MV and LV load indexes
l_m, l_l	MV and LV line indexes
L_P	Constant power load
L_Z	Constant impedance load
$meas$	Measured
mod	Modulation
n	Node
n_m, n_l	MV and LV node indexes
$nev_{n_m,t}$	Number of EVs at node n_m at time t
oc	Open circuit
p	Phase index
q	Quadrature-axis
r	Line's receiving end
ref	Reference
req	Request
s	Line's sending end
sys	System
t	Time index
ss	Substation

Chapter 1

Introduction

1.1 Motivation and relevance

The United Nations conference on climate change (COP21), held in Paris in 2015, introduced a new global agreement for alleviating the causes of climate change and stopping the increase in average earth temperature [1]. This agreement encourages the signatory countries to develop and adopt clean technologies, in which Electric Vehicles (EVs) within urban mobility systems play a major role. In this context, the federal and provincial governments of Canada have started to implement policies to promote the use of EVs. Particularly, the province of Ontario, in its 2016-2020 Climate Change Action Plan, contemplates investments of 250 million CAD to fund incentives and programs to expand the use of EVs in the province [2]. Thus, thanks to these policies and programs, it is expected that EVs will rapidly become a common mobility alternative.

Although the global EV fleet is still small, with 1.26 million EVs circulating on the roads through the end of 2015 (404,090 in the United States and 18,450 in Canada), the growth of EVs has been continuous since 2010, reaching an almost 70% increase between 2014 and 2015 [3]. This expansion will continue in the coming years, and may reach up to 100 million EV units by 2030 [4]. This growth of the global EV fleet will come with a proportional growth in charging stations. Through the end of 2015, 1.45 million charging stations were operating worldwide, out of which 13% were public and 87% were private stations, primarily located in residential units and office buildings [3].

The increase of EVs is creating new challenges for the power industry. Traditionally, distribution networks have been sized to support the maximum coincident load for short

periods of time, considering different load characteristics [5]. In contrast, in the new context of clean transportation, EVs will be connected to secondary distribution networks for several hours per day, increasing the maximum coincident demand and reducing diversity factors. This fact may cause short and long-term problems in distribution systems, such as overloads in transformers and cables, out-of-range voltages, voltage imbalance, losses, harmonics, and accelerating transformer aging [6]. Similarly, transmission and generation systems will face additional stress because of the extra energy needed to feed EVs; thus, in transmission systems, EV loads may create congestion and increase the system operation costs [7], whereas in generation systems, fuel consumption may increase and additional fast-response generation resources may be needed to satisfy new EV loads [8].

Most of the aforementioned problems imply that existing power systems, especially distribution systems, will not support high levels of EV penetration. Thus, to overcome this issue, utilities have the options of grid reinforcements, which imply high capital investments, and smart charging, which relies on communication and control technologies to optimize the use of existing infrastructure. The latter consists of controlling the time and power demand of EV chargers [9], that can be performed centrally by an agent such as a utility or a fleet aggregator, or locally by the EV charger, and is useful in reducing charging costs and alleviating EV charging impacts on the grid by decreasing the peak power and shifting the load [10]. Furthermore, when EV chargers have the ability of bidirectional power flow, they can supply energy to the grid while parked, operating as Vehicle-to-Grid (V2G) systems [11]. This control approach gives EVs the opportunity of providing grid services such as peak shaving, frequency regulation, spinning reserve, reactive regulation, renewable transients, and motor starting, which present an economic opportunity to EV owners [12]. Both smart charging and V2G concepts have been tested in several demonstration projects [13–15], and some companies and utilities are actively implementing smart charging solutions [16].

Despite the feasibility and economic opportunities of bidirectional chargers in V2G schemes, none of the chargers used in existing EVs have bidirectional power flow capabilities [10], since V2G services add to the wear of the battery [12]. Although there is an economic benefit for providing services to the grid [10, 11], under most conditions these revenues do not cover the replacement costs of the battery, which are high. Nevertheless, most studies on bidirectional EV chargers have concentrated on injecting active power to provide grid services like frequency regulation or spinning reserve, and little attention has been paid to the possibility of reactive power control services for the grid by using the ac/dc converter and the dc link capacitor of two-stage chargers, which do not compromise the vehicle battery life [17–19]. These kinds of chargers, which hereafter will be called four-quadrant EV chargers, can be used in residential networks to improve the power factor and help

regulating voltage, and thus facilitate the integration of EVs onto the grid.

Even though EVs in general, and smart charging applications in particular, have been studied broadly during the last decade, there is still research to be done on the subject of four-quadrant EV chargers, and especially, on their use in LV residential distribution grids for providing energy services to households and the grid. This part of the distribution grid is relevant for smart charging because more than 80% of chargers are private and installed in residential units and office buildings, as previously mentioned [3], and thus their negative impacts such as excessive transformer loading, cable loading, and voltage drops should also be considered at this level of the grid.

Based on the aforementioned discussion, this thesis will focus on the modeling and testing of four-quadrant EV chargers, and the design and simulation of distribution system control strategies that incorporate these type of chargers to provide reactive power support services.

1.2 Literature Review

The evolution of EVs and the increasing availability of this technology has motivated research efforts during the last decade concerning the impact of EVs on the electricity grid, as well as development of smart charging strategies to maximize EV penetration. These control strategies consider a communication infrastructure that allows exchange of information between the EV owner and the entity that is responsible for the control, which can be an EV aggregator or a Local Distribution Company (LDC). Thus, in this section, a comprehensive literature review on smart charging for EVs is presented, highlighting some gaps in the existing work as well as the elements that are relevant to this research. Particularly, the focus of this review is on the literature that explores different objective functions and control architectures for smart charging of EVs in distribution feeders and secondary distribution systems. Moreover, this review examines the past work on modeling and prototyping of four-quadrant EV chargers and volt/var control of distribution feeders considering EVs, since this is relevant to the work reported herein.

1.2.1 Smart Charging for Electric Vehicles

EV charging can be classified into three categories: uncoordinated charging, smart charging and V2G. Uncoordinated or uncontrolled charging takes place when EV batteries are plugged in until the batteries are fully charged, with no control of the charging demand

and starting time from an external agent [20]. In jurisdictions that have implemented Time-of-use (TOU) tariffs, EV owners have incentives to plug their EVs during hours of low demand and thus, save in charging costs; this is considered a passive charging strategy [21]. In smart charging, EV charging set points are determined by an external agent or the EV according to a set of economical and operational goals. In V2G, EV batteries can be discharged to provide services to the grid and receive economic incentives [11].

An extensive body of literature has covered many aspects of smart charging, exploring several objectives and control architectures. Some of the objectives used in smart charging controllers are designed to satisfy the EV owner's perspective, while others consider the utility's perspective [22]. Minimization of charging costs and prioritization of battery charging over other loads are objective functions reflecting the EV users' goals. From the utility's point of view, the objectives cover economic aspects such as minimization of generation costs and maximization of profits; technical aspects like minimization of losses, load leveling, or load variance; ancillary services, including frequency and voltage regulation; and reduction of CO_2 emissions.

Two control architectures are identified in EV charging management: centralized and decentralized. In centralized architectures, EV information is received and treated at a central point, optimization algorithms are implemented easily, and a better network management is achieved; however, a considerable amount of data is required, which can be difficult to gather in real applications. In decentralized architectures, the information is processed in a distributed way, and the final decision is taken by the EVs, which requires them to have an on-board control unit. Although in the latter there is uncertainty about the final result of the control actions, the controllers process less information, and changes can be easily done to the control programs [21].

Smart Charging from the Utility's Perspective

A group of publications on smart charging focus on planning applications, with the goal of assessing the impact of uncoordinated charging on distribution networks and the potentials of passive strategies (e.g. TOU tariffs) and smart charging control to alleviate these effects. Although these studies show the use of smart charging to enhance the application of EVs, their conclusions are case dependent, since they are based on particular mobility data and distribution systems. In [20], the authors analyze the impact of EVs on a 15 kV semi-urban Portuguese distribution grid under three strategies: "dumb" charging, a dual tariff policy that considers reduced electricity price during off-peak hours, and a centralized smart charging control. The congestion of lines and voltage levels at nodes are examined for different EV penetration scenarios. The smart charging algorithm works in steps of

one hour maintaining the maximum quantity of EVs that the grid can support without violating operational limits. The study concludes that smart charging allows up to 52% EV penetration, compared to 10% for dumb charging and 14% for a TOU tariff approach.

In [23], the impact of EV charging on the Australian National Electricity market load profiles is studied. The model proposed in this work incorporates Australian travel data and investigates the impact of uncoordinated charging, TOU tariff charging, and coordinated charging. Major findings of this study are that, in average, the evening peak load increases up to 820 W per vehicle in the uncoordinated case. In the TOU tariff scheme, the peaks are shifted to the late night and early morning, when prices are low. Finally, in the coordinated charging case, the charging peaks appear at the hour of minimum demand. After analyzing several penetration scenarios, the study concludes that TOU tariffs are a good option for low EV penetration stages, since the load factor is improved, but is not recommended for high EV penetration as this effect is not observed. The study in [24] made a similar analysis for the United States, using the National Household Travel Survey (NHTS) data [25], to estimate the impact of EV charging on electricity demand. A conclusion of this study is that, in average, the system peak load increases by 560-910 W per vehicle. Also, when people can only charge their vehicles at home, the home peak demand increases up to 29.4% compared to the case where people are able to charge at several locations, which indicates that the availability of charging stations is a key factor to decrease the pressure on residential charging systems.

The study in [26] estimates the impacts of EV charging on real LV distribution systems for Germany, Denmark, and The Netherlands. The authors of this paper apply a tool suite called NEMO, which integrates transportation and power system models to analyze and design EV charging infrastructure. This study shows that, for the three analyzed cases, voltage violations take place before overcurrents in cables, that smart charging is able to mitigate most of the problems seen with uncoordinated charging, and that all problems can be solved with grid reinforcement by increasing cable and transformer sizes.

Minimization of energy losses in distribution systems is a typical objective function included in smart charging controllers from the perspective of utilities. This is the case in [27], which analyzes the impact of uncoordinated and coordinated EV charging strategies in residential distribution grids, using a loss minimization approach. This work explores Quadratic Programming (QP) and Dynamic Programming (DP) solution approaches for the loss minimization problem, and a stochastic programming formulation to study the effect of residential load forecasting errors on the optimal charging schedules. The proposed algorithm is tested in a downscaled version of the IEEE 34-node test feeder, showing fewer voltage deviations and losses for the coordinated case, as well as better algorithm performance when a QP technique is employed. The authors in [28] suggest an alternative

approach to minimization of losses when coordinating the charging of EVs; they demonstrate that the minimization of losses is equivalent to the maximization of the load factor or the minimization of the load variance under certain conditions. These approaches lead to Linear Programming (LP) and convex QP problems, whith solution techniques that are more efficient than in the loss minimization strategy.

Reference [29] presents a centralized, real-time algorithm for defining the charging rates of EVs while minimizing electricity costs and losses. The allocation of charging capacity among the EVs is made using a Maximum Sensitivity Selection (MSS) optimization approach, which is based on sensitivity factors of the total losses with respect to the change in power consumption at EV nodes, calculated directly from the Jacobian matrix of the system. Every five minutes, the algorithm verifies the changes in the demand and new vehicle arrivals, and runs power flows to update the sensitivity factors and allocate charging capacity. In [30], the same authors improved the MSS algorithm by implementing a fuzzy-logic technique which combines system losses, voltage deviations, and maximum demand sensitivities to EV loads to determine charging set points.

Valley filling and load shifting are two techniques employed in controllers from the perspective of utilities, which aim to reduce the coincidence of EV loads with the base load peaks. An example for these strategies is found in [31], where authors report decentralized EV charging controller for valley filling, in which EV chargers decide their charging rates based on optimal electricity prices that account for base and EV demand. This charging algorithm is tested using a Beijing's power system model, showing good valley-filling results, even with inaccuracies in load predictions and a reduced number of EVs responding to the price signals. However, this controller is incomplete since it does not model the distribution system and EV locations, which may affect the calculation of price signals. This limitation is also observed in the decentralized EV charging controller reported in [32], which performs valley-filling and load-tracking functions by broadcasting charging control signals directly to EVs, which modify the signals according to their own preferences and constraints, and send the final set points back to the main controller to guarantee coordination with other chargers.

Most studies about smart charging from the perspective of utilities have focused on different objective functions based on control of active power, with little consideration of control of reactive power. Moreover, many of these studies only consider aggregated EV loads connected to the MV distribution system, without paying too much attention to the actual EV setpoints at the LV residential feeders. This thesis addresses these shortcomings by proposing a novel, distributed, smart charging scheme that considers the MV and LV distribution system operation variables, employing four-quadrant EV chargers to control reactive power throughout distribution feeders, while considering objective functions such

as loss minimization and voltage regulation.

Smart Charging from the Perspective of Users

A typical objective function in smart charging control from the perspective of users is the minimization of charging costs. Thus, the work in [33] presents a combination of a central control architecture and minimization of charging costs. The reported algorithm generates an EV charging schedule based on the minimization of charging costs while meeting trip energy needs of EVs and grid congestion constraints, which are incorporated in a network model that considers line currents, but not node voltages; the optimization is performed from the viewpoint of an aggregator or fleet operator. In [34], the same authors extend the previous work by incorporating a power flow method to calculate voltages and currents throughout the distribution system, describing the relations between an EV aggregator, a Distribution System Operator (DSO), and a retailer, who exchange EV and system information to minimize charging costs. The method is tested in a Danish distribution system, showing a significant reduction in voltage and current limit violations compared to the case of uncoordinated charging; however, the method relies heavily on adequate trip forecasts.

Centralized schemes based on distribution system Optimal Power Flows (OPFs), which explore several objective functions, including the minimization of charging costs, are found in [35] and [36]. In [35], the centralized distribution optimal power flow model reported in [37] is used, which calculates, one day ahead, the optimal tap and switched capacitor positions in a distribution feeder. Thus, based on this model, the authors investigate the impact of EV charging in residential distribution feeders under different objective functions, such as minimization of charging costs, minimization of losses, minimization of energy drawn from the substation, and minimization of energy costs from the external grid. The work in [36] discusses the impact of TOU tariff scheme in Ontario, Canada, wind and solar Distributed Generation (DG), and EV charging in distribution feeder operation under two objective functions: minimization of charging costs and minimization of losses. The main disadvantage of both works is the consideration of EVs as aggregated loads at the MV distribution system, without calculating the actual set points of EVs in the LV network. This problem is addressed in [38], which implements a centralized controller to define EV charging set points in an LV distribution network by minimizing charging costs. This approach uses a meta-heuristic solution method to get optimal EV charging set points; however, distribution system constraints and the MV grid are not fully considered in this model.

The work in [39] presents an EV charging control algorithm, which guarantees fulfillment of energy requirements of EVs while minimizing charging costs. The method implements a rolling optimization which calculates the optimal charging rates for 12 hours, including residential and EV loads forecasts, but only implementing the EV charging rates for the next 30 minutes. The algorithm formulation is based on voltage and current sensitivity factors extracted from the system's Jacobian matrix.

The maximization of charging rates is another objective function explored from the perspective of EV users. Thus, the authors in [40] propose and implement a smart charging controller in a real parking lot, considering a combination of EV users' preferences, including expected disconnection time and acceptable electricity prices, and hourly electricity prices calculated from historical data, to define charging priorities and allocate the available feeder capacity. However, this work does not consider the effects of EV charging on the upstream distribution system.

In [41], a smart charging algorithm with the objective of maximizing the energy delivered to EVs, calculated as the maximization of power of each charger and for each time interval, is reported. The problem formulation includes node voltages and transformer loading constraints, which are expressed in terms of sensitivity factors to the EV load variations, calculated from an unbalanced power flow at each time step. Another objective function, which accounts for the effect of proximity of EV loads to transformers, is also explored in this work. The algorithm is tested on a Dublin's LV feeder model, and shows good results for voltage and loadability, even though battery packs of a few vehicles do not reach full charge at the end of the period. The need of computing the sensitivity factors, which are shown in this thesis not to be very accurate in general smart charging control, can be a major barrier when large distribution systems and big EV fleets are considered.

The work described in [42] compares the centralized scheme in [41] with a local control approach in which each EV charger maximizes its charging rate without communicating with other chargers, keeping the terminal voltage and the service cable current within operational limits. Sensitivity factors are calculated at the beginning of the simulation and are used throughout the process, which differs from the centralized approach in [41]. This local approach is also tested on a Dublin's distribution feeder model, showing more violations of voltage limits, since chargers do not see how others are acting. This is a drawback of this model, since it requires additional measures to guarantee that the operational variables of the grid are kept within acceptable limits.

In [43], a two-stage smart charging algorithm is proposed. In the first stage, the algorithm maximizes the energy delivered to EVs, while in the second stage it minimizes losses and peak demand charges. The control scheme relies on a prediction unit to model the EV

load and guarantee feasibility of charging set points. Furthermore, it explores a scheme of Vehicle-to-Vehicle (V2V), in which some EVs discharge their batteries to supply others. The algorithm shows adequate results when tested on a 38-bus MV distribution system; however, no results are presented for LV networks.

The work in [44] describes a decentralized EV charging controller which maximizes the charging rate of EVs, while avoiding overloading in distribution lines and transformers. The algorithm applies the concept of fair rate control to allocate EV charging capacity, inspired by rate control in data networks. In this approach, each EV charger maximizes its charging rate, considering the congestion state of upstream lines and transformers, which are calculated and broadcasted from a central controller as congestion prices. The main drawback of this algorithm lies in not considering reactive power control and node voltage constraints.

A hierarchical demand control system of EVs in LV distribution networks is analyzed in [45]. The authors introduce the concept of EV managers, which are connected at the LV level and depend on supervisory EV managers at higher levels, leading to a hierarchical structure. These EV managers maximize the summation of the utility functions of downstream EV agents, making sure that service cable limits are respected, and the desired State-of-charges (SoCs) for all EVs are reached. The supervisory EV agents guarantee that loading of substation transformers and MV lines, and voltage levels, are kept within limits. The algorithm is tested and its performance is compared to that of an uncoordinated case for a distribution system model of Zurich, Switzerland, showing that voltage and congestion constraints are not infringed; however, the desired SoC is not reached in some of the vehicles, which is interpreted by the authors as a necessity for reinforcement. A drawback of this method is the definition of adequate utility functions for each EV agent, which implies a proper knowledge of priorities and behavior of their owners.

Research on smart charging strategies from the perspective of users has mostly focused on minimization of charging costs. However, this approach requires TOU pricing schemes for electricity retailing, which is not the case in many jurisdictions, making it difficult to implement in practice. Other methods, such as maximization of charging rate or maximization of energy delivered to EVs, merely depend on control strategies that can be readily implemented. Thus, to include the perspective of users, this thesis adopts the maximization of charging rate approach in the proposed smart charging scheme, since it does not need particular tariff structures and maximizes the EV battery SoC for mobility purposes, which is the primary objective of EV users.

Uncertainty in Smart Charging

A challenge in smart charging control design is the inclusion of the uncertainties associated with EV operation, which are seen in variables such as arrival time, departure time, and energy consumption. Many works on smart charging controllers have considered these uncertainties as part of the models, using techniques such as Monte Carlo Simulation (MCS), Stochastic Programming, and Model Predictive Control (MPC). These techniques are applied to guarantee that operations of distribution system and EV fleet are robust, and controller outputs are correct, irrespective of the operation times and energy needs of individual EVs.

In [46], a day-ahead distribution feeder controller, which determines optimal transformer tap and switched capacitor positions, as well as aggregated EV charging set points, is reported. This controller implements a non-parametric bootstrapping technique as an alternative to MCS, to deal with uncertainties of EV population, such as arrival and departure times, and energy consumption. The controller minimizes the feeder's peak demand including typical constraints of an unbalanced Distribution Optimal Power Flow (DOPF) model. A limited number of EV fleet realizations are used in the optimization problem and solved with a Genetic Algorithm (GA) tool. Then, the Bootstrap resampling technique is used to obtain the expected values and confidence intervals of the control variables. This approach is extended for real-time operation in [47], which introduces a second stage that takes the calculated transformer tap and switched capacitor positions as parameters, and maximizes the charging rate of EVs in real-time, following a proportional fairness method.

The authors in [48] present an MPC approach for EV charging in distribution networks. The model in this paper aims to minimize charging costs, while complying with user's charging preferences, and power set points provided by the LDC. The chargers in this model have bidirectional power flow capability, and the battery wear and tear costs are incorporated into the objective function. The model is responsive to events such as the connection of a new vehicle, the change of user preferences (e.g. anticipated time of disconnection), and changes in power references as a consequence of Demand-side Management (DSM) actions. The authors linearize the original control algorithm, mainly the cost function, resulting in a Mixed-Integer Linear Programming (MILP) problem. Several events, such as the arrival of vehicles, the early departure of a user, and the change of power reference caused by a DSM signal are simulated, showing a good performance in terms of costs. However, the main drawback of this algorithm is that it does consider network constraints; therefore, the aggregator in this case is not aware of how its actions are affecting the network operation.

An obstacle to implement any smart charging approach that considers uncertainty is

the generation of reliable forecasts and scenarios, which given the current penetration of EVs, are still inaccurate. Most of the previous studies have been carried out based on mobility studies of Internal Combustion Engine (ICE) vehicles, which may not apply to EVs. In the current stage of EV adoption, forecasting the daily behavior of EVs is a difficult task, although the increasing penetration of EVs is giving more information about their uses and limitations. Thus, this thesis provides new insights regarding uncertainty in smart charging by using real EV data, which is considered to study the effect of reactive power control with four-quadrant EV chargers in distribution feeders and its coordination with other volt/var control devices.

1.2.2 Four-Quadrant EV Chargers

The previous subsection reviewed relevant works about impacts, objective functions, control architectures, and uncertainty management in smart charging. In this subsection, a review of prototyping and modeling of four-quadrant EV chargers is presented.

As mentioned before, V2G approach requires EVs to be equipped with bidirectional chargers, whose technical feasibility has been demonstrated in several works, exploring various converter topologies and control strategies. These chargers include three-level Pulse width modulation (PWM) ac/dc converters based on neutral point clamped control [49], single-phase half-bridge rectifier for power quality compensation [50], and split-phase three-phase converter with protective earth on one of the legs and a Proportional-resonant (PR) controller [51]. Also, several works have looked at four-quadrant EV chargers and the possibility of exchanging reactive power with the grid. Thus, in [52], the potential of reactive power support operation of various single-phase EV charger topologies is explored, concluding that bidirectional chargers can operate in all four quadrants of the PQ plane independently of battery charging within the volt-ampere capability of the charger; however, the dc link capacitor size needs to be enlarged in this case since the dc link voltage ripple increases when the charger provides reactive power support. Other papers in this subject have explored various topologies and control strategies for four-quadrant EV chargers, such as PR controllers to regulate the utility line current with full bridge ac/dc converters [18]; single-phase, three-wire charger with unbalanced current compensation [53]; single-phase charger with power angle control [54]; three-phase off-board charger with boost rectifier [55]; and single-phase two-stage bidirectional EV charger for V2G reactive power operation [56].

The aforementioned works demonstrate the practical feasibility of bidirectional and four-quadrant EV chargers; however, there is a need to study their voltage interactions

with other chargers and loads in distribution systems, which can last from tens of milliseconds to a few seconds, depending on the dynamic characteristics of the electrical devices connected to the distribution network. Usually, the impacts of these interactions are analyzed on the primary distribution system, considering EVs as aggregated loads (e.g., [34, 35]). Furthermore, very few studies have been performed on the effects of EVs on the LV distribution system, even though an EV charger demand can be as high as a typical household peak demand, thus impacting directly voltage levels in distribution systems, and the loadability of distribution transformers. To understand the effects of EV chargers in LV networks, and implement control strategies to mitigate those effects, it is required to model, in detail, the equipment connected to the secondary distribution network. Such a model should consider switching dynamics, thus requiring small simulation time steps in order to account for the high switching frequency (that can be in the order of 20kHz), demanding time-consuming and costly computations [57]. This is impractical for distribution network type of studies which involve multiple chargers and various other equipment models.

To overcome the previously mentioned problem, average modeling is commonly used in power electronic systems. This modeling approach concentrates on converter cycle-to-cycle behavior, and neglects the switching dynamics within a switching period, improving the simulation efficiency without sacrificing the capability of predicting the converter steady-state and dynamic responses [58], thus allowing to simulate EV chargers in distribution system studies. Nevertheless, not much has been reported on EV charger average modeling. For example, in [57], an average model is proposed for a unidirectional EV charger composed of a diode bridge rectifier, a power factor corrector stage (boost converter), and a dc/dc converter, which is then used to study voltage regulation effects of EV chargers on a distribution network. On the other hand, for bidirectional chargers with single-stage topologies, average models have been reported, mainly for full-bridge ac/dc converters [59, 60]; however, these papers have focused on small-signal modeling for controller design and not for grid impact analysis. For two-stage and integrated bidirectional charger topologies, some works have proposed average models for the study of individual stages of these chargers (e.g., [61], [62]), but not for the complete topologies. Thus, this thesis will contribute to closing this gap by modeling and validating with actual measurements the proposed model of a two-stage, four-quadrant smart charger hardware, composed of a single-phase ac/dc converter and a bidirectional dc/dc converter, and will demonstrate the application, benefits and limitations of the model for four-quadrant EV charger integration into LV system studies.

1.2.3 Volt/Var Control with EV Chargers

Volt/var regulation functions are typically performed in distribution systems with LTCs, Step Voltage Regulators (SVRs) and capacitor banks. Recently, due to the penetration of DGs with the possibility of regulating reactive power, new challenges have emerged in the conventional volt/var function, which have been addressed in several works (e.g., [63–66]). In the near future, the inclusion of EV chargers with reactive power control will modify the conventional volt/var control function, coordinating the aforementioned control devices, DGs, and EVs.

In [67], a cooperative method to compensate for undervoltages based on local voltage measurements, EV chargers with reactive power injection capacity, and communication links is presented; however, the algorithm does not consider the coordination with other volt/var regulation devices, and does not prioritize the charging function over the reactive power provision. These drawbacks are also seen in [68] and [69]. Thus, in [68], a two-stage optimization algorithm is proposed for controlling four-quadrant EV chargers to flatten the demand curve, reduce the system currents, and minimize losses, and [69] formulates a multi-objective optimization algorithm that minimizes parking and charging costs from the user perspective, and minimizes reactive power service costs provided by EVs from the utility point of view.

The authors in [70] propose a receding horizon control framework for scheduling four-quadrant EV chargers considering technical constraints such as maximum DC current ripples in EV chargers and battery degradation costs; however, in this framework, neither the power system topology nor other volt/var control devices are considered. The authors in [71] investigate a centralized volt/var optimization engine which considers LTCs, SVRs, capacitor banks, and four-quadrant EVs to minimize power losses and capacitor operation costs, accounting for distribution system topology and the operation constraints of the volt/var regulation devices; however, EVs are considered only to inject reactive power and are aggregated in different MV nodes, without calculating the individual EV charger set points.

A real-time, three-stage scheme for voltage regulation in distribution feeders, which considers simultaneous operation of LTCs, solar Photo-voltaic (PV) systems, and EVs is reported in [72]. This scheme gives priority to EV charging and PV active power injection, and uses the remaining reactive power operation capacity of PV inverters and EVs to reduce the number of operations of LTCs; however, it does not calculate the individual set-points for EVs, and does not allocate the charging and generated power among PVs and EVs in a fair manner.

From the above literature review, it is clear that the subject of controlling four-quadrant

EV chargers, and particularly their ability to provide reactive power services combined with smart charging approaches, has not received appropriate coverage. Thus, this thesis aims to contribute in this field by proposing a control scheme for optimal operation of these chargers in distribution feeders for the provision of ancillary services using their reactive power capacity, while charging EV batteries to an acceptable level. Even though four-quadrant chargers are not part of EV models currently available for sale, the fact that some automotive companies are actively collaborating in V2G demonstration projects, and the interest of utilities to use distributed generators to provide reactive power support, point to the need to study the integration of this kind of chargers into future EV models.

1.3 Objectives and Expected Contributions

Based on the review of the state-of-the-art in smart charging and four-quadrant EV chargers, and the identified shortcomings in previous works, the objectives and expected contributions of this thesis are as follows:

- Develop an accurate and adequate average model for a single-phase, four-quadrant EV charger, validated with an actual prototype, which can be easily integrated into time-domain simulations to analyze the impacts of these types of chargers in distribution networks.
- Apply the developed four-quadrant EV charger average model in realistic LV distribution system dynamic studies.
- Develop and validate a three-stage approach to minimization of system losses and peak load, providing adequate volt/var support, and fairly allocating EV charging load, based on a four-quadrant EV smart charger connected at the LV distribution system level.
- Incorporate the uncertainty of EV driving behavior based on actual measured EV charging profiles and statistics, to properly model the active and reactive power demands of four-quadrant EV smart chargers, and determine optimal appropriate day-ahead transformer tap and capacitor schedules.
- Consider both MV and LV networks, in which EV chargers represent a significant load compared to other household loads, to generate practical smart charging strategies and control signals for individual EVs connected at the LV level.

- Test the proposed approach on realistic MV and LV North-American distribution networks, and compare it with an existing volt/var regulation strategy, demonstrating its benefits and practical feasibility.

1.4 Thesis Outline

The remaining of this thesis is organized as follows:

- Chapter 2 reviews the background subjects on which this thesis is based, including an overview of distribution feeders, EV charging, mathematical programming, and non-parametric bootstrapping.
- Chapter 3 presents the modeling, testing and validation of a single-phase, four-quadrant EV charger developed in the lab, and describes dynamic studies performed on a low-voltage distribution system model using the proposed charger model.
- Chapter 4 proposes and discusses a three-stage distribution feeder control architecture, which incorporates four-quadrant EV chargers into the volt-var control function.
- Chapter 5 summarizes the thesis content, and presents the main conclusions, contributions and future work resulting from the presented research.

Chapter 2

Background Review

2.1 Introduction

This chapter presents a background review of EV charging in distribution systems. The focus of this chapter is on describing the general characteristics, modeling approaches and control functions of the systems involved in the EV charging process, from the distribution substation to the EV chargers connected to the secondary distribution network. Thus, section 2.2 presents an overview of distribution feeders, including MV primary feeders, LV secondary systems, loads, and general control approaches applied in these networks. Section 2.4 presents a general overview of EV charging, including a description of the Electric Vehicle Supply Equipment (EVSE), the standardized charging levels, the types of EV chargers, the characteristics and modeling of EV batteries, and typical EV charging coordination strategies. Section 2.5 presents a review of mathematical programming and the two solution tools that are used in this work, i.e., GA and Sequential Quadratic Programming (SQP). Finally, Section 2.6 introduces the Nonparametric Bootstrapping method, an alternative to MCS, which is adopted in this work to deal with EV uncertainties.

2.2 Distribution Feeders

Distribution feeders are the part of the distribution system that transport the electricity from the distribution substation to end users. A simple distribution feeder and its most important components are presented in Figure 2.1. A distribution feeder is composed of the three-phase primary feeder, laterals (single-phase or three-phase), step voltage regulators,

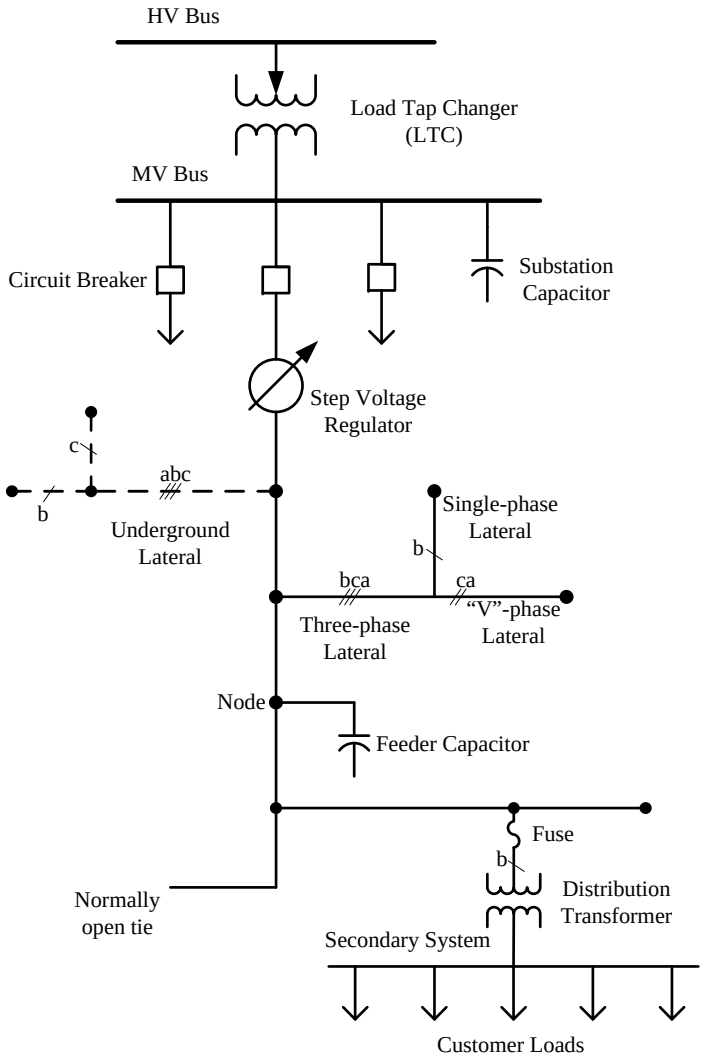

Figure 2.1: Distribution feeder components.

capacitor banks, distribution transformer, secondary network and loads, which are three-phase or single-phase [73]. Distribution feeders are by nature unbalanced because of the non-symmetrical conductor arrangements in distribution lines and the large number of single-phase loads.

2.2.1 Primary Feeders

Primary feeders are the circuits that transport the energy from the distribution substation to distribution transformers. Primary feeders are typically radial, with the main primary circuit branching into laterals that feed the MV/LV distribution transformers. Since the current magnitude is the largest when leaving the substation, the ampacity of a radial feeder is larger near the substation, and decreases at branches far from the substation. Radial systems are widely used, as they are less expensive compared to other proposed distribution configurations, but have low reliability due to the fact that a fault at the primary feeder causes loss of power in downstream loads [5].

Loop and network configurations are also used in distribution systems. The loop system is formed by connecting the ends of two feeders through a tie switch or a tie breaker, such that the loads are fed from the two feeders in normal operation. This configuration implies that the sizes of both feeders should be the same and they should withstand their own load and the load of the other feeder in the case of a contingency. The network system is characterized by the interconnection of primary feeders to different substations, having a circuit breaker at each end. Although the network configuration is the best in terms of reliability, voltage regulation and losses, its cost is high, and it is therefore only used in heavy-load centers [5]. Nevertheless, in practice, these configurations are normally operated as radial feeders.

Common voltage levels for primary feeders in North America are 4.16, 4.8, 12.47, 13.2, 13.8, 24.94, and 34.5 kV [74]. In Ontario, and specifically in Hydro One grid, the voltage levels for primary distribution are 44, 27.6, 25 and 13.8 kV [75].

Three-phase distribution lines and transformers are the devices generally modeled to analyze power flows and voltage levels in primary feeders. A three-phase overhead line or cable model consists of a π arrangement of series impedances and shunt admittances, as shown in Figure 2.2. The series impedance is composed of a real part, which depends on the resistance of the conductor, and an imaginary part, that depends on the magnetic coupling between the phases and the neutral. The typical assumptions of transposed and equally loaded lines in transmission systems cannot be made in distribution systems; thus, the self and mutual inductances should be calculated separately and not presented as a single-phase inductance, as it is common in transmission systems. The shunt admittance depends on the capacitive coupling between the phases and the ground. This π model can then be expressed as a matrix of parameters that relate the phasors of voltages $\boldsymbol{V}$ and currents $\boldsymbol{I}$ at the sending (s) and receiving (r) ends, as follows [73]:

$$\begin{bmatrix} V_{lg_{abcs}} \\ I_{abcs} \end{bmatrix} = \begin{bmatrix} A & B \\ C & D \end{bmatrix} \begin{bmatrix} V_{lg_{abcr}} \\ I_{abcr} \end{bmatrix} \tag{2.1}$$

where, as per Figure 2.2:

$$A = U + \frac{1}{2} Z_{abc} Y_{abc} \tag{2.2}$$

$$B = Z_{abc} \tag{2.3}$$

$$C = Y_{abc} + \frac{1}{4} Y_{abc} Z_{abc} Y_{abc} \tag{2.4}$$

$$D = U + \frac{1}{2} Z_{abc} Y_{abc} \tag{2.5}$$

$$Z_{abc} = \begin{bmatrix} \boldsymbol{Z}_{aa} & \boldsymbol{Z}_{ab} & \boldsymbol{Z}_{ac} \\ \boldsymbol{Z}_{ba} & \boldsymbol{Z}_{bb} & \boldsymbol{Z}_{bc} \\ \boldsymbol{Z}_{ca} & \boldsymbol{Z}_{cb} & \boldsymbol{Z}_{cc} \end{bmatrix} \tag{2.6}$$

$$Y_{abc} = \begin{bmatrix} \boldsymbol{Y}_{aa} & \boldsymbol{Y}_{ab} & \boldsymbol{Y}_{ac} \\ \boldsymbol{Y}_{ba} & \boldsymbol{Y}_{bb} & \boldsymbol{Y}_{bc} \\ \boldsymbol{Y}_{ca} & \boldsymbol{Y}_{cb} & \boldsymbol{Y}_{cc} \end{bmatrix} \tag{2.7}$$

$$U = \begin{bmatrix} 1 & 0 & 0 \\ 0 & 1 & 0 \\ 0 & 0 & 1 \end{bmatrix} \tag{2.8}$$

$$V_{lg_{abc}} = \begin{bmatrix} \boldsymbol{V}_{ag} & \boldsymbol{V}_{bg} & \boldsymbol{V}_{cg} \end{bmatrix}^T \tag{2.9}$$

$$I_{abc} = \begin{bmatrix} \boldsymbol{I}_a & \boldsymbol{I}_b & \boldsymbol{I}_c \end{bmatrix}^T \tag{2.10}$$

Where all parameters, variables, and indices are defined in the Nomenclautre section at the start of the thesis. When distribution lines are single-phase, this model can be used by assigning certain elements of the impedance and admittance matrices zero values. For

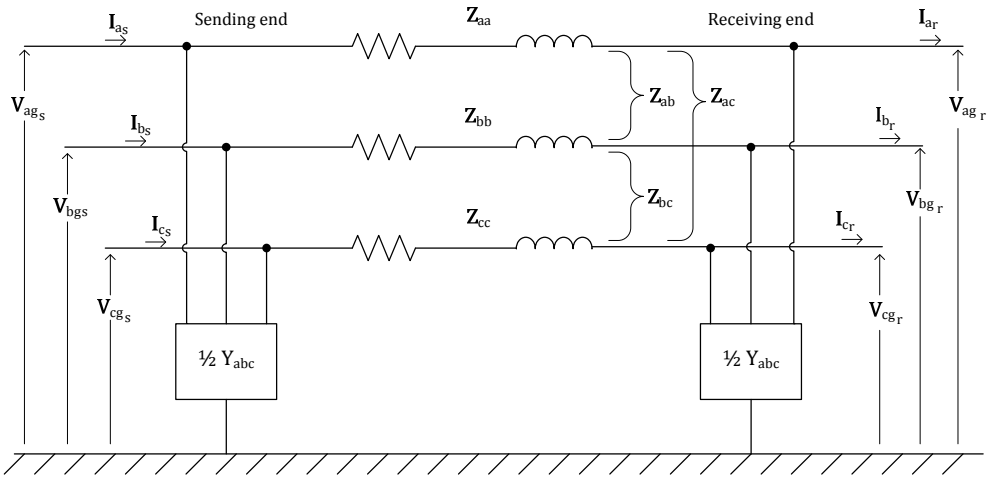

Figure 2.2: Distribution line model.

example, if the single-phase line is connected to phase a, only $\boldsymbol{Z}_{aa}$ and $\boldsymbol{Y}_{aa}$ are considered, and the rest of the elements in the corresponding matrices are set to zero. Equation (2.1) can also be used for modeling three-phase transformers. In this case, the ABCD parameters will depend on transformer connection (wye or delta), the primary-to-secondary turns ratio, considering LTCs, and the impedance of windings.

2.2.2 Secondary Grid

The secondary or LV grid, or simply the secondary, is the circuit in charge of transporting the electricity from the MV/LV distribution transformer to the loads. LV grids can be single-phase or three-phase, depending on the loads to be supplied. The voltage level in an LV grid is lower than in the primary feeder. The common practice in Ontario is to have voltage levels of 120/240 V in single-phase, three-wire systems, and 120/208 V or 347/600 V in three-phase, four-wire systems [75]. The typical configuration of LV grids is radial, in which a common secondary main, supplied by one transformer, feeds a group of customers, normally in residential, rural, and light-load commercial areas. The advantages of radial LV grids are their simplicity and low cost; their main disadvantage is low reliability, since a fault in a transformer, fuse or cable leads to a power outage for all customers served by the circuit. Other unusual configurations used in LV grids are the secondary banking, in which two or more distribution transformers are connected in parallel to feed the load,

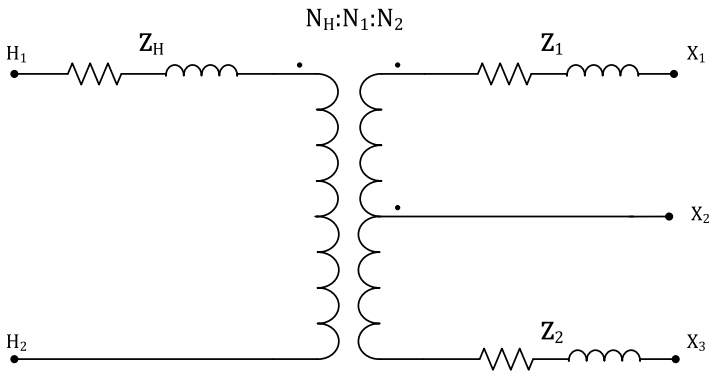

Figure 2.3: Single-phase, 3-wire transformer model.

and the secondary network, in which an area that demands high reliability is fed through a secondary mesh that at the same time is fed through several distribution transformers connected to different primary feeders [5].

MV/LV distribution transformers reduce the voltage level to serve the loads in the secondary network. In North-America, distribution transformers are normally single-phase, and have two series windings in the secondary to feed loads at 120V and 240V. This type of transformer is modeled as shown in Figure 2.3, having a series impedance in the high voltage winding, and two series impedance in the secondary windings, which may be equal, depending on the internal arrangement of the transformer. Typical capacities of single-phase transformers are 25, 50, 75, 100, and 150 kVA, with most common transformer capacities for residential customers being 25 and 50 kVA. Utilities typically calculate a peak load between 10 and 20 kVA per household served by the same transformer [74].

For modeling an LV line, the common approach is to use a series impedance representing the corresponding resistance and inductance values. When the LV line is an underground cable, a π model can be used to account for the capacitive effect of the insulation.

2.2.3 Loads

Modeling of loads is necessary to study distribution systems. Load models for power system analysis are classified in two categories: static and dynamic. Static models, which are typically used in power and distribution system studies, are not time-dependent with P and Q values that are merely a function of the voltage magnitudes and/or frequency values. Dynamic models, which are mostly used in transmission system dynamic studies, depend

not only on the present values, but also on the past values of voltage and/or frequency variables, and are represented by differential equations [76].

The following static load models are applicable to distribution system studies:

- Constant Power: This model represents a load that consumes a constant value of P and Q, independently of the voltage magnitude.
- Constant Impedance: This model represents a load with P and Q values that are dependent on the square of the voltage magnitude, which is the behavior of a constant impedance.
- Constant Current: In this model, the load P and Q values that are dependent on the voltage magnitude corresponding to a constant current load.
- ZIP model: The load is expressed as a combination of constant-power, constant-current and constant-impedance loads.
- Exponential model: The load P and Q values are calculated as exponential functions of the load voltage. It is considered a generalized form of the ZIP model [77].

Table 2.1 presents the mathematical expressions for each type of static load.

Table 2.1: P and Q expressions for static loads with voltage V_L.

	P_L	Q_L
Constant Power	P_{L_P}	Q_{L_P}
Constant Current	$P_{L_I}\left(\frac{V_L}{V_{L_O}}\right)$	$Q_{L_I}\left(\frac{V_L}{V_{L_O}}\right)$
Constant Impedance	$P_{L_Z}\left(\frac{V_L}{V_{L_O}}\right)^2$	$Q_{L_Z}\left(\frac{V_L}{V_{L_O}}\right)^2$
ZIP Load	$P_{L_P} + P_{L_I}\left(\frac{V_L}{V_{L_O}}\right) + P_{L_Z}\left(\frac{V_L}{V_{L_O}}\right)^2$	$Q_{L_P} + Q_{L_I}\left(\frac{V_L}{V_{L_O}}\right) + Q_{L_Z}\left(\frac{V_L}{V_{L_O}}\right)^2$
Exponential	$P_{L_E}\left(\frac{V_L}{V_{L_O}}\right)^{n_p}$	$Q_{L_E}\left(\frac{V_L}{V_{L_O}}\right)^{n_q}$

Residential loads can be modeled as a combination of approximately 33% constant impedance and 67% constant power loads during summer, and 60% constant impedance and 40% constant power loads during winter [74]. More recently, with the widespread use of air conditioning systems (motor loads) in residential buildings, constant-current load models have become more relevant [78]. Some studies, as the one in [79], propose experimental ZIP model coefficients for modern residential loads, classifying them by strata according to the annual consumption in kWh .

2.2.4 Control of Distribution Feeders

The control problem in distribution feeders has been traditionally treated as a volt/var problem [37]. For this, four devices are commonly used: LTCs at the main substation, capacitors at the substation level, capacitors at the feeder level, and SVRs. The objectives of these devices in a volt/var function are to minimize voltage deviations, maintain a power factor near unity through the feeder, minimize the power losses in the system, keep the loading of lines and transformers within the limits, and minimize the total number of tap changing and capacitor switching operations [37, 80].

LTCs operate automatically with the load, and are used to maintain the primary distribution voltage approximately constant when the sub-transmission voltage or the load vary. The SVR is an auto-transformer with a tap changer mechanism in the series winding, normally standardized to perform changes in a range of $\pm 10\%$ of the nominal value in 32 steps. In general, tap positions in LTCs and SVRs, and switching operations in capacitors, are determined by voltage relays which monitor the voltage at the bus they are connected to. Moreover, to regulate the voltage in a remote location, local voltage relays can be complemented with a Line-Drop Compensator (LC), which emulates the voltage drop produced along a distribution line, as seen in Fig. 2.4. In this scheme, the line current measured by the Current Transformer (CT) is injected into a measuring impedance $R' + jX'$, which is equivalent to the feeder impedance between the measuring point and the regulation point, producing a comparable voltage drop.

DGs, such as PV panels, may also participate in the volt/var function to provide reactive power support. The original standard IEEE 1547-2003 [81], which defines the procedures to interconnect distributed energy resources to power systems, established that DGs could not regulate the voltage at the Point of Common Coupling (PCC) and had to operate at unity power factor; however, a recent 2014 amendment to the standard modified this requirement by allowing DGs, in coordination with the DSO, to regulate voltage at the PCC by controlling the active and reactive power injection [82]. Nevertheless, a big challenge for controlling reactive power with PV panels is the variability of power output due to shading. Since the reactive power limits of PV panels could change continuously, the dispatch of reactive power is difficult to perform. However, authors in [83] have proposed local controllers that use PVs to mitigate short-term voltage quality issues, such as sags and swells, and strategies to minimize losses during the night hours, where PV panels can be fully used for reactive power operation.

In future smart grids, EVs will become a highly available resource that can be coordinated with other DGs, such as PV panels, to provide reactive power services to the grid. However, the uncertainty related to the connection times and SoC in the case of EVs, and

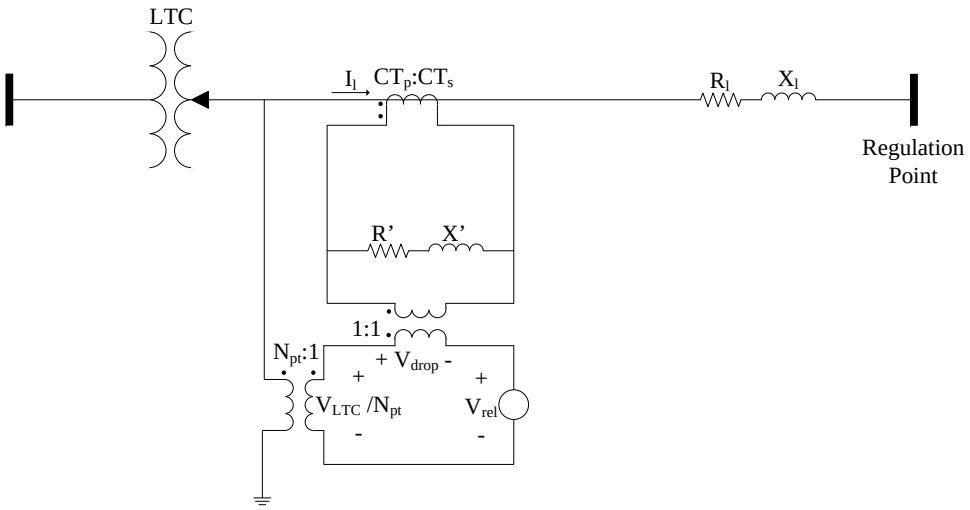

Figure 2.4: Line drop compensator.

shading in the case of solar PV panels, would require forecasting of the available reactive power capacity, thus imposing an operation challenge that should be tackled by the distribution grid management system.

Optimal feeder reconfiguration is another control function that is often used in distribution feeders. This type of control is used in loop systems, typically operated radially, to determine the normal position of switches according to the season and the optimal sequences for system reconfiguration after contingencies [84]. The optimal feeder reconfiguration is not operated in practice in real-time, and is in principle different from volt/var control, because it considers big areas or even the entire distribution system, while volt/var control concentrates on a reduced number of feeders; therefore, this type of control is not considered in this thesis. Bus voltages and protection system parameters (e.g., fault currents) are taken as constraints for the feeder reconfiguration problem [84].

2.3 Modeling of Power Electronics Converters

In the context of power electronics, simulation is a very important part of designing and analyzing any converter, since it allows to predict its electrical behavior in terms of voltages and currents, estimate the electrical stress in all components, and design appropriately the controllers that guarantee an output that follows the desired setpoints [85]. Since modeling

is a fundamental task in simulation, as it describes the electrical relationships of different components of a power electronics converter through algebraic and differential equations, model development is important. This can be done in several levels of detail, depending on the desired application, which results in the following model categories:

- Switched Models: : These types of models are the result of an elementary circuit analysis of a converter, in which all components are modeled in detail, resulting in continuous, time-varying, nonlinear state-space models that account for the effects of high switching frequencies, such as the fast transients during the operation of a switch [86, 87]. It is the most complete type of model, but it requires very short simulation time steps to accurately reproduce the converters behavior; therefore, these are mainly used for short simulation times in studies that require analyzing switching losses, studying the stress on converters components, or evaluating the transient performance of converters controllers.

- Average models: These types of models focus on the converter cycle-to-cycle behavior, neglecting the effects of high switching frequency. They can be obtained by averaging the switched state-space equations of the converter over a switching period, assuming that voltages and currents do not vary significantly on the averaging interval. These models can also be extracted from the average of waveforms associated with each component of the converter, a method known as circuit averaging [58, 87]. The outcome of this process is a set of average non-linear algebraic and differential equations that properly predict the steady-state and dynamic responses of the converter in frequencies well below the switching frequency, from which equivalent circuits can be derived. Since these types of models do not include switching effects, they can be implemented in simulation packages with larger integration time steps, thus significantly reducing simulation times. Average models are well suited for designing controllers for converters, testing the effect of converter parameters on dynamic and steady-state responses, and studying the interaction of several converters in a large electrical system.

- Sampled-data models: These types of models use discretizing techniques to approximate the continuous switched state-space equations with discrete equations that can predict the converter cycle-to cycle behavior, without focusing on switching dynamics [58, 87]. They are well suited for designing and analyzing digital controllers, and for obtaining small-signal models to study converters' stability issues around a steady-state operation point.

2.4 EV Charging

2.4.1 Charging Equipment

Electric Vehicle Supply Equipment

The EVSE is the interface between the electric grid and the EV, and it is composed of a supply device, a power cord, and a connector [88]. The supply device supplies the energy to the EV, and contains protection and control equipment. The supply device does not normally contain the battery charger, which is located on-board the vehicle; however, in fast-charging stations, the EVSE contains the charger. A power cord carries the current from the supply device to the connector, which plugs the equipment to the charging sockets located on the EV.

EV Charging Connectors

The automotive industry in North America uses SAE J1772 standard for EV connectors. This standard describes single connectors for ac slow charging (Level 1 and 2), and combo connectors for both ac slow and dc fast charging. In the European Union, automotive companies have adopted the standard VDE-AR-E-2623-2-2 [89], commonly known as Mennekes connector, for slow charging. Another standard known as CHAdeMO [90], developed by Tokyo's distribution company and other Japanese automakers, is used in several EV models for fast charging. Furthermore, automakers such as Tesla have implemented their own connectors (e.g., Supercharger connector), although interfaces with the common standards are provided.

Charging Levels

Charging levels describe the admissible voltage and current values for EV charging process, and are defined by standards. Thus, SAE J1772, which in addition to connectors defines charging levels, establishes two levels for ac charging and two levels for dc charging. AC Level 1 is used mainly in residential and workplace charging, and does not require any additional infrastructure; the charging in this case is performed on-board. AC Level 2 is the primary method for dedicated and public facilities, and is also on-board and single-phase. The ac Level 3 for fast charging with off-board converters in three-phase configuration has been proposed, but still has not been standardized. DC Level 1 and 2 are used in fast

charging facilities, and require off-board chargers that are not really feasible for residential areas [9]. Table 2.2 presents the main features of charging levels according to SAE J1772 standard [91].

Table 2.2: Charging levels according to SAE J1772 standard

AC Level 1	**AC Level 2**	**DC Level 1**	**DC Level 2**
120 V ac Single phase	240 V ac Single phase	200 to 450 V dc	200 to 450 V dc
12 A - 1.44 kW 16 A - 3.3 kW	16 A - 1.92 kW 30 A - 6.6 kW up to 80 A - 19.2 kW	19.2 kW (residential) 36 kW (public) up to 80 A	up to 200 A - 90 kW
EV includes on-board charger	EV includes on-board charger	EVSE includes off-board charger	EVSE includes off-board charger

Types of EV Chargers

EV chargers are classified according to the power flow direction as unidirectional and bidirectional. Unidirectional EV chargers are only capable of injecting energy to the battery, and are simple to control. All of the EV chargers that are presently in the market are unidirectional, and are composed of an ac-dc converter, a full bridge diode rectifier in most cases, and a dc-dc converter, which can be buck or boost type depending on the relative levels of the dc link and the battery voltages. These chargers are designed to operate at nearly unity power factor.

Bidirectional EV chargers allow active power flow in two directions, i.e., from the grid to the battery (charging operation) or from the battery to the grid (discharging operation). A bidirectional charger necessarily uses controllable switches, such as MOSFETs or IGBTs; thus, their cost is higher compared to a unidirectional charger, and their control is more complex [9]. In this thesis, the term four-quadrant EV charger is used to refer to bidirectional chargers that can inject or absorb active and reactive power independently of the charging process. This type of chargers require the dc link capacitors to be oversized according to reactive power operational needs [52].

2.4.2 Characteristics and Modeling of EV Batteries

Nickel-Metal Hydride (NiMH) is a mature battery technology that has been used for EVs and HEVs. In NiMH batteries, the positive electrode (anode) has an active material of

$Ni(OH)_2$, and the negative electrode (cathode) is made of a metal hydride, basically an alloy of rare earth materials, separated by an aquous solution of KOH. The specific energy of a NiMH battery is 60-80 Wh/kg, and the specific power is 220 W/kg [92].

Lithium-Ion (Li-Ion) battery family is the current preferred technology in PHEVs and EVs. Moreover, it is this battery type that is being improved the most in terms of energy performance and cost. A Li-Ion battery is composed of a negative electrode of metal oxide that contains lithium ($LiCoO_2$, $LiMn_2O_4$, $LiFePO_4$), and a positive electrode that is made in most cases of graphite; the electrolyte is a mixture of organic carbonates [93]. A Li-Ion battery has a specific energy of 100-200 Wh/kg and a specific power of 360 W/kg [92] .

Although the specific energy of Li-Ion battery is higher than that of NiMH, when battery cells are connected in series, a forced liquid cooling system is needed for the lithium battery. This makes NiMH batteries a better option in this case, since they only need natural air cooling. In general, these two battery technologies show similar performance in EV applications in terms of energy and power density; however, since a large-enough number of these batteries have not been in service for a long-enough periods, degradation and life cycle of these batteries based on real data is not available yet [93]. Most EVs and PHEVs in the market are equipped with a Li-Ion battery pack. Table 2.3 presents the most common battery (BEV) and plug-in hybrid (PHEV) EVs in Canada, including battery capacities and electric operation ranges.

Table 2.3: Li-Ion battery capacity and electric range of common EV models [94].

Model	**Type**	**Battery Capacity (kWh)**	**Range on Electric (km)**
BMW i3	BEV	22	130
Chevrolet Volt	PHEV	18	85
Ford C-Max Energi	PHEV	8	32
Ford Focus Electric	BEV	21	122
KIA Soul EV	BEV	27	149
Mitsubishi i-MiEV	BEV	16	100
Nissan Leaf	BEV	30	172
Smart Fortwo	BEV	17	145
Tesla Model S	BEV	90	435
Tesla Model X	BEV	90	413
Tesla Roadster	BEV	53	393
Toyota Prius	PHEV	4.4	23

Battery manufacturers describe the charging and discharging capabilities of the batteries in terms of the Maximum Continuous Discharge Current, and the Maximum 30 second discharge pulse control. Also, the C rate, which is the rate at which the battery is charged or discharged in terms of the current corresponding to one-hour full-charge/discharge, is used to define the recommendations for charging and discharging [95].

For charging batteries, two basic strategies are followed to reach the desired SoC. The first method is the Constant Voltage (CV) charging, in which the same voltage value is applied to the battery terminals until a low current limit is reached (normally 0.02 C rate), indicating that the battery is charged at the desired level. The disadvantage of this method is that it requires a high power level at the beginning, since the battery is depleted and the open circuit voltage is much lower that the voltage applied to its terminals [93]. The second method for charging batteries is Constant Current (CC), in which the charging voltage is controlled in order to keep the charging current constant throughout the process. The main challenge of this method is to determine at which point the charging should stop, since keeping a constant current after the battery has reached its full SoC increases the electrolyte temperature and could shorten the battery life [93].

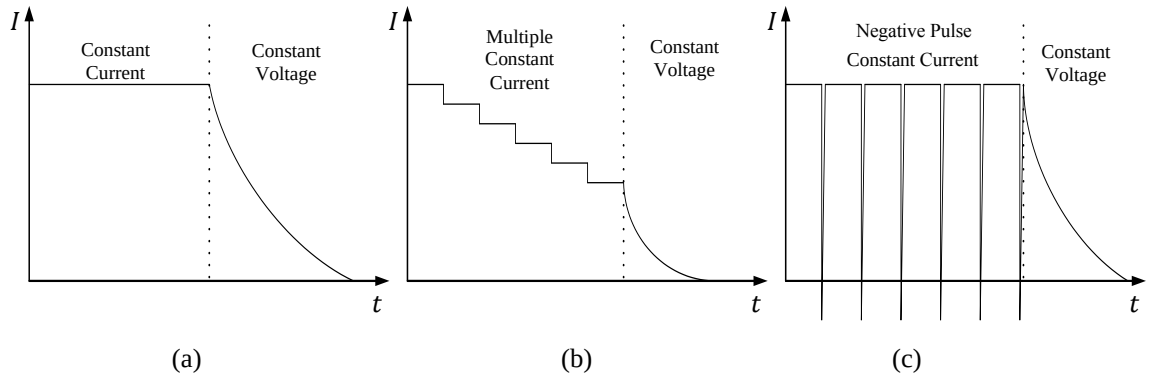

Figure 2.5: Charging methods for Li-ion batteries.

EV batteries are typically charged using a combination of CC and CV methods (Figure 2.5(a)). In the first stage, a constant current, ranging from 0.1C to 1C is applied to the battery until a cut-off voltage is reached. At this point, the method changes to CV until a low charging current is reached, indicating full SoC [96]. Since the battery is a very sensitive device that can suffer damage when not charged correctly, additional criteria are taken into consideration to interrupt the charging process; these include time, cut-off temperature, and the rate of change in temperature and rate of change in voltage [93].

Other methods for charging EV batteries have also been proposed. These include the multistage constant current, constant voltage (MCC-CV), in which several decreasing constant current stages are applied to the battery terminals, until the cut-off voltage is reached, and CV charging starts (Figure 2.5(b)); the CC-CV with negative pulse, which slightly discharges the battery in constant intervals to improve charging acceptance (Figure 2.5(c)); and the variable frequency pulse charge, that applies pulses of different frequencies during the charge period to better distribute the ions in the battery [96].

Battery models focus on different aspects of device operation. The first category concentrates on describing the electrochemical processes that occur within the battery, and the second category tries to describe the electrical performance of the battery using voltage sources, resistors and capacitors. The latter is preferred by electrical engineers, since such models can be easily incorporated into circuit simulations [93].

Many battery models have been proposed describing the electrical behavior of the device in an electrical circuit. Among these, three basic categories can be identified: Thevenin equivalent model, ac impedance model, and run-time model [97]. The Thevenin equivalent model incorporates a voltage source that is dependent on the SoC, a self-discharge resistor, a series resistor, and a parallel arrangement of capacitor and resistor that represents the transient behavior (Figure 2.6(a)). The ac model incorporates an ac arrangement that reflects the battery behavior at different frequencies, and a voltage source behind an equivalent impedance whose value is dependent on the battery state of charge (Figure 2.6(b)). Factors like the battery state of health, the ambient temperature, and the internal temperature influence the values of the model parameters. Some models, like the one proposed in [97], try to merge in a single circuit the transient behavior, the ac response, and the open circuit voltage dependence on the SoC (Figure 2.6(c)). Other models add diodes in series with resistive-capacitive arrangements to include different impedances during charging or discharging [93].

2.4.3 Electric Vehicle Charging Strategies

The charging of EVs is classified in four categories: uncoordinated charging ("dumb" charging), multiple tariff charging, smart charging, and V2G [98]. Uncoordinated charging refers to the scheme in which EV owners are free to decide the moment and the place to perform the charging of the battery. Normally, the charge process starts immediately after the arrival of the EV owner at the destination by plugging in the vehicle [9, 98, 99]. This scheme normally works with flat electricity tariffs; therefore, the owner does not have incentives to delay the connection to the grid. Majority of studies on uncoordinated

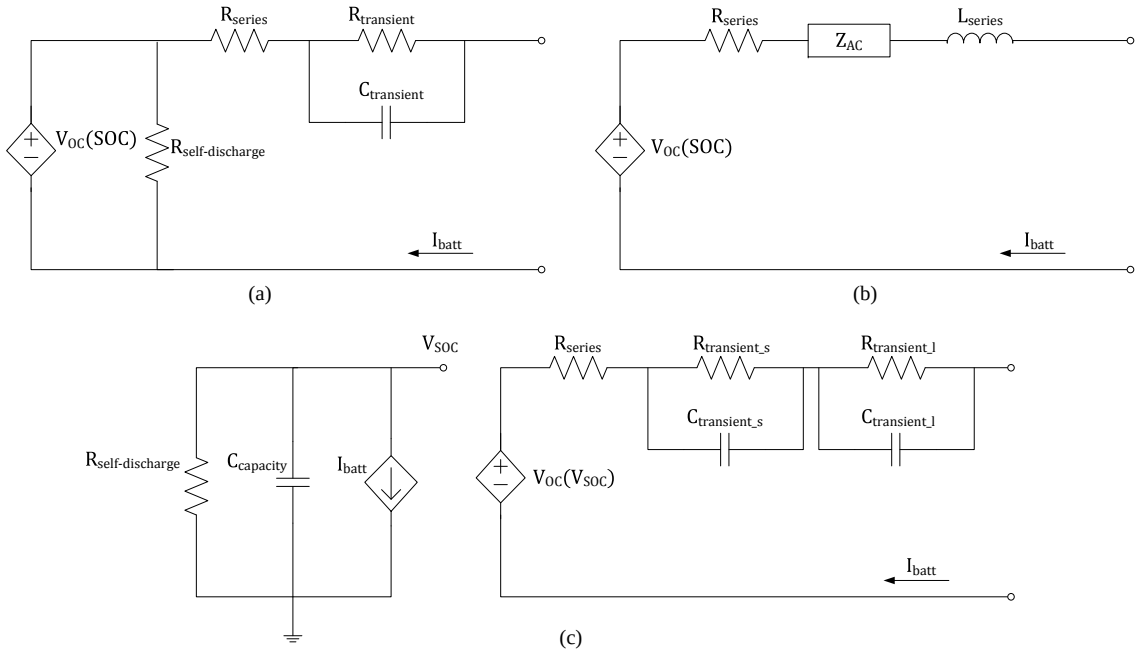

Figure 2.6: Typical battery models: (a) Thevenin model, (b) ac model, and (c) complete model.

charging in large EV fleets conclude that this strategy produces overloading in distribution lines and transformers [35, 98].

The second strategy, known as multiple-tariff charging, is different from uncoordinated charging in the existence of economic incentives for EV owners through differentiated tariffs according to the time of use. This incentive is intended to shift the energy consumption to valley hours, thus reducing the effect of EV charging during hours of high consumption [98]. A scheme of TOU tariff exists in Ontario, with different price categories that depend on the hours of the day, the type of day (week or weekend), and the season (winter or summer); the categories are: peak, mid-peak, and off-peak [100]. However, the existence of a TOU tariff does not guarantee that the EV load is effectively shifted; to take advantage of TOU tariffs, the EV owner must be aware of the economic advantages of charging at off-peak hours [98].

The third strategy is known as coordinated charging or smart charging, implying an intelligent control that actively decides the time and the rate of charging [35, 98, 99]. The objective of this method is to charge the EV when it is most beneficial, for example, when electricity price or the demand are the lowest, or when there is an excess of generation

capacity [101]. The control over the chargers can be managed by the utility or system operator [35, 101], or even by a market entity referred to as an EV aggregator, which can operate a large fleet of EVs simultaneously and take advantage of business opportunities in electricity markets [98, 99].

Various strategies have been recommended to perform the smart control of EV chargers. Some of them are listed next in the form of minimization or maximization of an objective function to control EV charging:

- Minimization of losses in distribution grids [27, 35]:

$$\min_{P_{s,l,t},P_{r,l,t}} \quad \sum_{t=1}^{T_{max}} \sum_{l=1}^{n_{lines}} (P_{s,l,t} - P_{r,l,t}) \tag{2.11}$$

- Minimization of charging costs [35, 102]:

$$\min_{P_{ev,n,t}} \quad \sum_{n=1}^{n_{nodes}} \left(\sum_{t=T_{startOP}}^{T_{endOP}} C_{OP} P_{ev,n,t} + \sum_{t=T_{startMP}}^{T_{endMP}} C_{MP} P_{ev,n,t} + \sum_{t=T_{startP}}^{T_{endP}} C_P P_{ev,n,t} \right) \tag{2.12}$$

- Maximization of load factor [28]:

$$\max_{S_{n,t}} \quad \frac{\mu_D}{max\left(\sum_{n=1}^{n_{nodes}} S_{n,t}\right)} \tag{2.13}$$

- Minimization of load variance [28]:

$$\min_{S_{n,t}} \quad \sum_{t=1}^{Tmax} \left(\frac{1}{T} \left(\sum_{n=1}^{n_{nodes}} (S_{n,t} - \mu_D) \right)^2 \right) \tag{2.14}$$

- Maximization of energy delivered to EVs [27]:

$$\max_{P_{ev,n,t}} \sum_{t=1}^{T_{max}} \sum_{n=1}^{n_{nodes}} P_{ev,n,t}\, \Delta t\, \lambda_{ev,n,t} \tag{2.15}$$

- Minimization of energy drawn by the feeder [35]:

$$\min_{P_{ss,t}} \sum_{t=1}^{T_{max}} P_{ss,t}\, \Delta t \tag{2.16}$$

- Maximization of charging rate [47]:

$$\max_{P_{ev,n,t}} \prod_{n=1}^{n_{nodes}} \frac{P_{ev,n,t}}{\overline{P_{ev,n,t}}} \tag{2.17}$$

The fourth strategy, which is an extension of the third one, is the so called V2G. In this approach, the EV has bidirectional power flow capability; therefore, EVs can inject power into the grid [98]. EV aggregators or system operators can take advantage of this capability to provide high-value grid services, and balance renewables with the EV storage capacity [99]. However, the increased use of the battery other than providing energy for EV operation reduces the battery life and increases the costs for owners; thus, strong economic incentives should be provided to cover these wear costs [98]. The concepts of Vehicle-to-Home (V2H) and Vehicle-to-Building (V2B), which concentrate on the interaction between the EV and the household or building loads, can be included in this category. These operation strategies take advantage of the bidirectional power transfer capability of the EV chargers to interact with other energy devices in order to offset the peak load and minimize the energy costs. While operating in V2H of V2B mode, the EV battery could serve as a backup supply to the building to support normal operation when outages are present in the distribution grid [17, 103].

Other charging strategies are occasionally mentioned in the literature. These include V2V [17], in which EVs with bidirectional chargers, located in the same parking lot, exchange active power to optimize the use of charging resources, and reactive V2G, or V2GQ [72], where EVs can inject or absorb reactive power to or from the grid and is the focus of this thesis.

2.5 Mathematical Programming

Optimization can be defined as the process of finding the maximum or minimum of a function, which in engineering context can represent the benefit or the effort related to a system [104]. The term mathematical programming refers to mathematical models that provide the framework for addressing and solving optimization problems [105]. These models are

expressed in terms of objective functions and constraints, which together represent a measure of the system's performance, and establish the feasible region for all the variables of the system.

An optimization problem can be represented by a set of equations and inequalities, as follows:

$$\begin{aligned} \min_{x} \ & f(x) \\ \text{s.t. } & g_i(x) = 0 \ \forall i \\ & h_j(x) \geq 0 \ \forall j \end{aligned} \tag{2.18}$$

where x is the vector of decision variables, $f(x)$ represents the objective function, $g(x)$ the equality constraint functions, and $h(x)$ the inequality constraint functions. If an optimization problem only contains an objective function $f(x)$, and $g(x)$ and $h(x)$ do not exist, the problem is unconstrained; otherwise, the problem is constrained. According to the nature of $f(x)$, $g(x)$, and $h(x)$, an optimization problem can be classified under one the following categories [104]:

- Linear Programming Problem (LP): The objective function and constraints are linear, and all decision variables are continuous.
- Quadratic Programming Problem (QP): The objective function is a convex quadratic function, the constraints are linear, and the decision variables are continuous.
- Non Linear Programming Problem (NLP): The objective function or the constraints are non linear functions, and decision variables are continuous.
- Mixed-Integer Linear Programming Problem (MILP): The objective function and the constraints are linear, and some or all decision variables are integer numbers.
- Mixed-Integer Non Linear Programming Problem (MINLP): The objective function or the constraints are non linear, and some or all decision variables are integer numbers.

No single solution method is able to solve all types of optimization problems; thus, the solution algorithm should be chosen depending on the particular characteristics of the problem under consideration. In this thesis, constrained NLP and MINLP models are used to represent a DOPF problem that includes four-quadrant EV chargers as controllable active and reactive power loads. Constrained NLPs can be solved using methods based on

search directions, and methods that do not use information from derivatives. The former include the penalty function method, augmented Lagrangian, SQP, and interior point method, whereas the latter include the Nelder-Mead simplex method, and metaheuristic methods such as GA and Particle Swarm Optimization (PSO). For NLP problems, the SQP method is employed in this work, which is discussed in more detail in Section 2.5.2.

MINLP methods are intrinsically difficult to solve. Most MINLP solvers implement decomposition techniques to obtain sub-problems that are solved using well-known methods for NLP and MILP problems. Thus, the extended cutting planes and the branch-and-bound methods, which are typically used for MILP problems, can be applied for MINLP problems, generally applying successive LP relaxations over the variables and constraints. Furthermore, modern metaheuristic methods, such as GA and PSO, can also be applied to MINLP problems since they can easily handle integer variables.

In this work, the GA method is used to solve the day-ahead dispatch of transformer taps and switched capacitors considering four-quadrant EV chargers. Although this method converges slowly, it is used here since the optimization is performed a day ahead of the actual implementation, and GA provides solutions that are more likely to be close to the global optimum. Moreover, it can be easily implemented using parallel computing paradigms to reduce solution times, and can be readily integrated with existing commercial software packages for solving parts of the optimization problem, such as the power flow equations. More details of the GA method used in this thesis are presented next.

2.5.1 Genetic Algorithms

A Genetic Algorithm is a metaheuristic optimization method based on a global search strategy that mimics the natural selection process in biological systems [104]. Compared to typical mathematical programming methods, it does not use derivatives, which has two main implications. First, the method can be slow since it does not use a search direction extracted directly from the objective function, merely depending on a high number of function evaluations to find improved solutions. Second, the method converges to a point that cannot be guaranteed to be either a local or a global optimal point. However, compared to classical optimization methods based on function derivatives, the GA is more likely to find a solution near the global optimum, since they search in a wider space in the feasible region and normally do not get stuck in a local minimum, which often happens with classic methods that start searching from a single initial point [104]. Additionally, the GA can easily account for integer variables, which make them very useful for solving complex optimization problems such as nonconvex MINLP [104].

A GA typically operates by converting the variables of an optimization problem into binary numbers, which represent the genes, and joining them to create binary chains that simulate the chromosomes of the individuals. The method starts by setting up an initial population of feasible individuals with random chromosomes. Then, the chromosomes of all members of the initial population are used to evaluate the objective function and obtain a fitness value for each individual. Some individuals are considered to integrate a mating pool, from which new individuals will be created, while the others are discarded, as occurs in the natural selection process of biological systems. The mating pool can be obtained by choosing a fixed number of individuals based on the order of their fitness values, or by defining a threshold and keeping the individuals that have a better fitness value in the mating pool [106].

Once the mating pool is built, some operators are applied over selected individuals to obtain new offsprings. These basic operators are pairing, crossover, and mutation. In pairing, two individuals from the mating pool are chosen to create new offsprings. The pairing operator can be performed either by the order in the fitness values, by a total or weighted random selection, or by a selection tournament. In the latter, a limited number of individuals is randomly taken from the mating pool, and the one with the best fitness value is picked. In crossover, the two individuals selected by pairing create two new offsprings by crossing or exchanging the genes of their chromosomes at a fixed position. In mutation, an individual is randomly taken from the current generation and one or various of its genes are changed, creating a different offspring. Finally, a new generation is created by choosing the best individuals of the mating pool, the new offsprings created by crossover, and the new offsprings produced by mutation [106].

The convergence of the GA method is tested by measuring the improvement in the fitness values of the population using statistics such as the mean, the standard deviation, or the minimum or maximum values. The method is normally said to converge when these measures improve by less than a defined tolerance in two consecutive generations. GA algorithm is also stopped based on the maximum number of iterations and the time limit [106].

The aforementioned mechanisms of GA normally deal with unconstrained optimization problems. For constrained problems, the penalty method [104] is applied to equality and inequality constraints to obtain a single objective function, which is solved using the GA method.

It is important to mention that, although GA can be slow because of the high number of function evaluations that has to be done for each generation, these evaluations are not necessarily sequential. Thus, the solution speed can be increased significantly if parallel

computing is employed [106].

2.5.2 Sequential Quadratic Programming (SQP)

SQP is an optimization method designed for solving general NLP problems with nonlinear constraints. This method is based on the consecutive solution of quadratic problems that approximate iteratively the original problem. In SQP, the constraints of the general optimization problem described by equation (2.18) are linearized to produce the following QP problem [107]:

$$\begin{aligned} \min_{d} \; & f_k + \nabla f_k^T d + \frac{1}{2} d^T \nabla_{xx}^2 \mathcal{L}_k d \\ \text{s.t.} \; & \nabla g_i(x_k)^T d + g_i(x_k) = 0 \; \forall i \\ & \nabla h_j(x_k)^T d + h_j(x_k) \geq 0 \; \forall j \end{aligned} \tag{2.19}$$

where k represents the iteration index, and d is the step direction used to calculate the next iteration point, $x_{k+1} = x_k + d_k$. These problems are solved using methods for QP such as the active-set method, and the gradient project method [107].

Line search methods require the Hessian at the current point x_k to be positive definite to obtain a minimum. If the optimization problem is highly nonconvex, this requirement is often not observed, and thus, many solution tools adopt a positive definite Hessian approximation that is updated in every iteration until it converges to the actual Hessian of the original problem [104].

The SQP method is implemented in SNOPT [108], where a quasi-Newton approximation for the Hessian and iteration step length controls using an augmented Lagrangian method are used. It is available for various optimization modeling languages, including GAMS, AMPL and AIMMS.

2.6 The Nonparametric Bootstrapping Method

The nonparametric bootstrapping is a resampling method used to estimate the distribution function of a population statistic [109]. The term nonparametric is used for this method to indicate that it does not use the population Probability Distribution Function (PDF), which is very useful when the PDF is not available or is difficult to calculate. This method is employed as an alternative to MCS as it reduces the computational burden and allows,

from few sample points, to closely estimate population statistics such as the mean, the median, or the standard deviation [110].

The method starts from a sample $W = \{w_1, w_2, ..., w_n\}$ of n points, and then, m resamples, called bootstrap samples, are created from W using sampling with replacement, which consider that each element taken from the original sample is returned after each observation and, therefore, can be selected for each bootstrap sample more than once. In this procedure, m should be sufficiently large; a rule of thumb indicates that more than 1000 samples are necessary for calculating 95% confidence intervals [111]. Bootstrap samples are represented by $W^b = \{w_1^b, w_2^b, ..., w_n^b\}$, and should contain n units, as the original sample.

The next step consists of creating $\Psi^B = \{W^1, W^2, ..., W^b, ..., W^m\}$, the set of bootstrap samples, and calculating the desired statistic θ^b for each W^b, from which the set of bootstrap statistics, $\Theta^B = \{\theta^1, \theta^2, .., \theta^b, ..., \theta^m\}$, is created. Finally, the bootstrap statistic θ^* is computed using the following expression:

$$\theta^* = E(\theta^b) \tag{2.20}$$

where $E(\cdot)$ is the expected value function. The PDF of the bootstrap statistics, known as the bootstrap distribution, can be approximated with a frequency histogram of Θ^B, assuming each θ^b has the same probability.

A common application of the bootstrapping method is calculating Confidence Intervals (CIs) of the parameter estimation, having a PDF estimate that is symmetrical with respect to θ^*. If the desired CI is (100-β)%, the percentiles ($\beta/2$)% and (100-$\beta/2$)% should be computed from Θ^B, and then the CI can be estimated as per [112]: :

$$CI_{(100-\beta)\%} = \left[2\theta^* - \theta^b_{(100-\beta/2)\%}, 2\theta^* - \theta^b_{(\beta/2)\%}\right] \tag{2.21}$$

2.7 Summary

In this chapter, a general description, and typical modeling and control approaches for distribution feeders were presented. General concepts of EV charging, including charging equipment, battery characteristics and modeling, and general strategies for EV charging, were also explained. A general explanation of mathematical programming, and the two optimization methods used in this work (GA and SQP), were described. Finally, the nonparametric bootstrap method, which is used in this work as an alternative to MCS to deal with EV uncertainties, was briefly explained.

Chapter 3

Modeling and Testing of a Four-Quadrant EV Charger

3.1 Introduction

This chapter presents the modeling and testing of a four-quadrant EV charger prototype, and describes the application of the proposed model for residential network impact studies. Thus, Section 3.2 presents the characteristics of the four-quadrant charger that is studied in this work, and Section 3.3 describes the proposed average model for the chosen charger topology. In Section 3.4, the average model is validated by comparing its responses in steady state and dynamic conditions with those of a developed charger prototype. Finally, Section 3.5 illustrates the use of the average model for the study of the impact of several four-quadrant chargers in a realistic residential LV distribution network.

3.2 Four-Quadrant EV Charger

3.2.1 Charger Topology

The four-quadrant charger analyzed in this work is a Level 1 charger rated at 1.92 kVA/120 V, implementing a two-stage topology composed of a full-bridge ac/dc converter (Stage 1), and a bidirectional buck-boost dc/dc converter (Stage 2), as shown in Figure 3.1. This configuration was chosen because of its popularity and simplicity [113–116]. Compared to a single-stage topology composed only of a full-bridge ac/dc converter, this two-stage

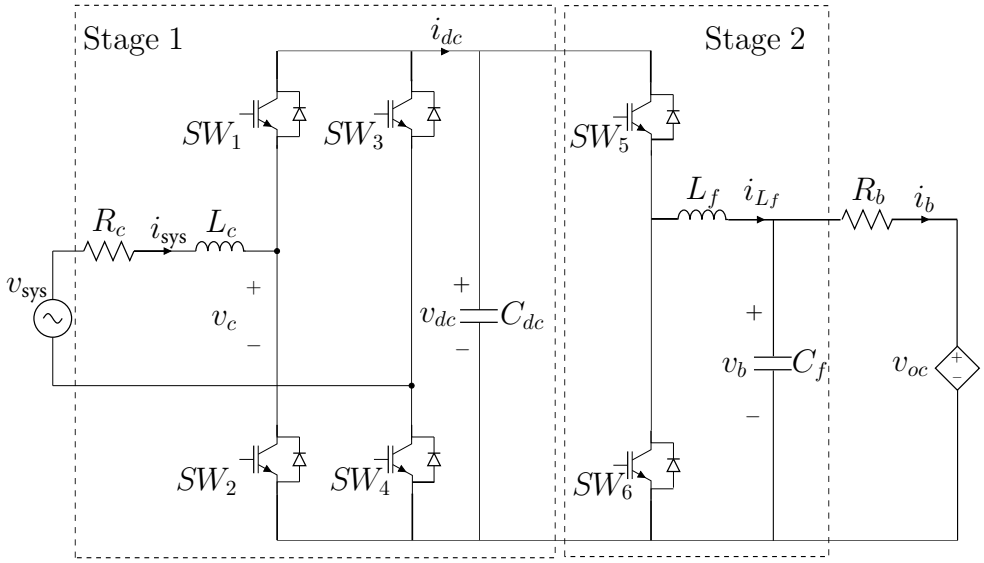

Figure 3.1: Single-phase bidirectional battery charger topology.

topology provides a better current quality for the battery, since the bidirectional dc-dc converter acts as an low-pass filter at the output, reducing the second harmonic ripple coming from the dc link. Also, a full-bridge ac/dc converter, albeit having two more switches with respect to a half-bridge converter, is more suitable for high power applications, since for the same power level, the switch current is one half of the switch current in a half-bridge converter [113]. The limitation of this topology is lack of galvanic isolation, although it does not compromise its functionality.

Stage 1 is in charge of keeping the dc-link voltage (V_{dc}) and the power factor at the ac side within a predefined range, according to reactive power setpoints, whereas Stage 2 follows the active power setpoints to control the battery current. Thus, since active and reactive power can be decoupled in this topology, their control can be done independently, as presented in the next sections, where the control strategies that ensure decoupled control of active and reactive power are explained.

3.2.2 AC/DC Converter Controller

Stage 1 controller, depicted in Figure 3.2, implements a current-control (CC) PWM in a dq frame, used in the majority of PWM voltage-source converters (VSC). The CC PWM tech-

nique is preferred in this case because of the good current and dc-link voltage regulation, and the inherent compensation of switch voltage drops and dead times [117]. Moreover, this control is implemented in a synchronous dq frame because of their ability to achieve zero steady-state error; however, there are other control options with similar attributes in VSC applications, such as PR controllers [118].

Synchronous frame controllers apply linear control strategies over time-invariant quantities obtained by transformation from ac voltages and currents. The dq0 transform is typically applied in three-phase systems for this purpose, but it cannot be applied directly in single-phase systems since it requires at least two signals. A common approach to solve this problem in single-phase systems is to apply first an $\alpha\beta$ transform by keeping the original signal as the α component, and introducing a delay of 90° to the original signal to obtain the β component; then the $\alpha\beta$ signals are transformed to dq components [119].

An essential component of a synchronous frame controller is the Phase-Locked Loop (PLL), since it determines the frequency and the phase angle references at which the transform is performed, allowing the converter's voltages and currents to be synchronized with the system voltage. Additionally, thanks to the action of PLL, V_q in dq0 transform can be forced to be zero, and thus, the apparent power in dq components can be expressed as:

$$S = P_{sys} + jQ_{sys} = 0.5V_dI_d - 0.5jV_dI_q \tag{3.1}$$

All variables in this an other equations and figures in this chapter are defined in the Nomenclature. In this equation, I_d and I_q are the variables used to control P and Q. P control regulates V_{dc}, which is affected by the battery current I_b. The reference for I_d is derived from the chosen $V_{dc,ref}$, and the reference for I_q is obtained from the desired Q_{ref}; the conversion between Q_{ref} and I_{qref} is performed by the control loop referred to as Q control in Figure 3.2. The other parts of the controller in Figure 3.2 regulate the dc-link voltage and produce a final modulation signal v_{mod} obtained by a dq-$\alpha\beta$ transform, which is used to generate the coupling voltage v_c in Figure 3.1.

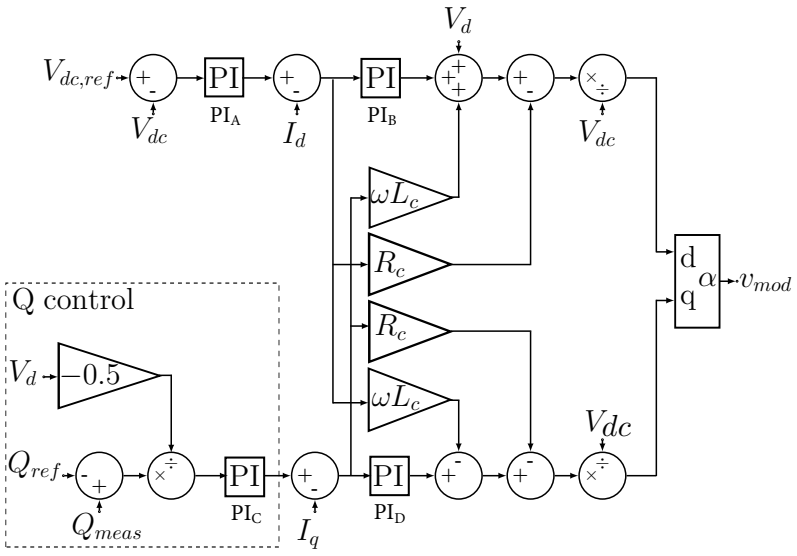

Figure 3.2: AC/DC dq controller with reactive power support.

3.2.3 DC/DC Converter Controller

The control of active power in the four-quadrant EV charger under study is performed by controlling the battery current, considering that any change in its amplitude or direction, according to charging or discharging setpoints, affect the dc-link voltage. Moreover, since the dc-link voltage is automatically regulated by the ac/dc converter controller, the changes in the dc-link voltage are compensated by an exchange of active power between the charger and the grid.

Stage 2 controller, depicted in Figure 3.3, implements three strategies that can be independently selected to establish the duty cycle of dc/dc converter's switches. The first is a Constant Power (CP) strategy, which defines the battery current reference as the output of a PI controller that receives the active power error, and then, estimates the duty cycle as the output of a PI controller fed with the battery current error. In this control, P_{meas} is the calculated real component from (3.1), and P_{ref} is the active power request at the grid interface. The other two strategies are CC and CV, which feed the battery current and voltage errors, respectively, to PI controllers to compute the duty cycle of the buck switch SW_5. CC-CV charging is typical for Li-ion EV batteries, as explained in Section 2.4.2, and found in the majority of chargers.

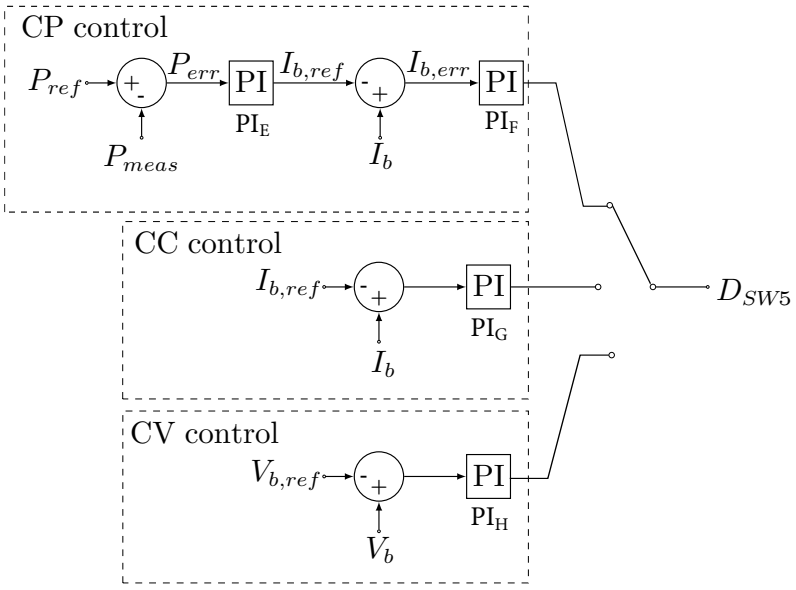

Figure 3.3: DC/DC converter control strategies.

3.3 Average Modeling

In the analysis of the impact of four-quadrant chargers on the LV distribution system, a number of these chargers need to be considered. Hence, using detailed models of the four-quadrant chargers would require a significant amount of computational time, because of the high switching frequency. Hence, an average model of the charger is developed in this section to be used in LV distribution system integration studies, as demonstrated in Section 3.5. This model can also be used to derive a small signal average model and obtain a transfer function of the smart charger controller, which are useful for design and tuning of this controller.

The following switching functions can be defined for the two legs of the full-bridge ac/dc converter of Figure 3.1, when controlled under a unipolar voltage regime:

$$SF_1 = \begin{cases} 1 \rightarrow SW_1 : ON, SW_2 : OFF \\ 0 \rightarrow SW_1 : OFF, SW_2 : ON \end{cases} \tag{3.2}$$

$$SF_2 = \begin{cases} 1 \rightarrow SW_3 : ON, SW_4 : OFF \\ 0 \rightarrow SW_3 : OFF, SW_4 : ON \end{cases} \tag{3.3}$$

One can write v_c and i_{dc} in terms of SF_1 and SF_2 as follows:

$$v_c = (SF_1 - SF_2)v_{dc} \tag{3.4}$$

$$i_{dc} = (SF_1 - SF_2)i_{sys} \tag{3.5}$$

In average modeling, SF_1 and SF_2 can be replaced by their low-frequency components, as follows:

$$SF_1 \approx 0.5 + 0.5m_1 \tag{3.6}$$

$$SF_2 \approx 0.5 + 0.5m_2 \tag{3.7}$$

where m_1 and m_2 are the modulation signals (normalized to the peak value of the triangular carrier signal) used to control the switches, represented as:

$$m_1 = Mcos(\omega t + \theta) = v_{mod} \tag{3.8}$$

$$m_2 = -Mcos(\omega t + \theta) = -v_{mod} \tag{3.9}$$

where M is the modulation index that is allowed to vary between 0 and 1 in the linear range of PWM. Therefore, from (3.4) to (3.9), and excluding the high-frequency contents, v_c and i_{dc} can be written in the following form:

$$v_c = 0.5(m_1 - m_2)v_{dc} = v_{mod}v_{dc} \tag{3.10}$$

$$i_{dc} = 0.5(m_1 - m_2)i_s = v_{mod}i_{sys} \tag{3.11}$$

Assuming complementary switch control signals for SW_5 and SW_6, two topological modes can be identified for the bidirectional buck-boost converter:

- Topological mode 1: In this case, SW_5 is ON and SW_6 is OFF, resulting in:

$$\frac{di_{L_f}}{dt} = \frac{1}{L_f}v_{dc} - \frac{1}{L_f}v_b \tag{3.12}$$

$$\frac{dv_{dc}}{dt} = \frac{1}{C_{dc}}i_{dc} - \frac{1}{C_{dc}}i_{L_f} \tag{3.13}$$

$$\frac{dv_b}{dt} = \frac{1}{C_f} i_{L_f} - \frac{1}{C_f} i_b \tag{3.14}$$

- Topological mode 2: Here, SW_5 is OFF and SW_6 is ON, yielding:

$$\frac{di_{L_f}}{dt} = -\frac{1}{L_f} v_b \tag{3.15}$$

$$\frac{dv_{dc}}{dt} = \frac{1}{C_{dc}} i_{dc} \tag{3.16}$$

$$\frac{dv_b}{dt} = \frac{1}{C_f} i_{L_f} - \frac{1}{C_f} i_b \tag{3.17}$$

Averaging the first-order differential equations (3.12)-(3.17) over a switching period, one can obtain the following expressions, where D_{SW_5} is the duty cycle for SW_5 in Figure 3.1:

$$\begin{aligned} \left.\frac{di_{L_f}}{dt}\right|_{av} =& D_{SW_5}\left(\frac{1}{L_2} v_{dc} - \frac{1}{L_f} v_b\right) + (1 - D_{SW_5})\left(-\frac{1}{L_f} v_b\right) \\ =& D_{SW_5}\frac{v_{dc}}{L_f} - \frac{v_b}{L_f} \end{aligned} \tag{3.18}$$

$$\begin{aligned} \left.\frac{dv_{dc}}{dt}\right|_{av} =& D_{SW_5}\left(\frac{1}{C_{dc}} i_{dc} - \frac{1}{C_{dc}} i_{L_f}\right) + (1 - D_{SW_5})\left(\frac{1}{C_{dc}} i_{dc}\right) \\ =& \frac{1}{C_{dc}} i_{dc} - D_{SW_5}\frac{i_{L_f}}{C_{dc}} \end{aligned} \tag{3.19}$$

$$\left.\frac{dv_b}{dt}\right|_{av} = \frac{1}{C_f} i_{L_f} - \frac{1}{C_f} i_b \tag{3.20}$$

From these average expressions, the equivalent circuit of Figure 3.4 can be derived. Note that this model does not account for converter losses to keep it simple, since considering them implies modeling non-ideal switches, diodes, capacitors and inductors, which is needed if studying the efficiency of the converter is required, which is not the case here, as the model concentrates on properly representing the dynamic response of the developed

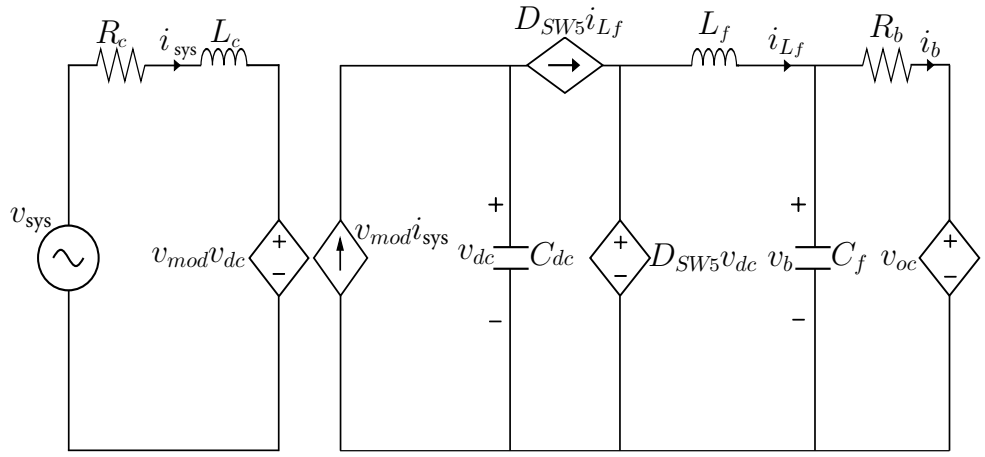

Figure 3.4: Average model of bidirectional charger.

smart charger. The losses can be readily approximated by adding resistances to the controllable voltage and current sources that represent converter switches in the model. In this thesis, the battery is modeled as a Thevenin equivalent, with v_{oc} and R_b being functions of SoC and i_b.

The proposed average model applies only to the topology presented in Figure 3.1. However, the same averaging technique can be applied to other EV charger topologies to obtain similar equivalent circuits, which can be easily integrated into simulation packages. In this case, the main purpose of the model is to speed-up time domain simulations involving several chargers in a distribution grid. The model is mainly intended to capture low-frequency dynamics, neglecting the switching frequency dynamics, which are very small due to filtering, and thus allowing to determine set points for smart charging in LV networks, which is the main application of the proposed model. The model also allows to design the smart charger controller, as it captures the main relevant dynamics for that purpose. Furthermore, it allows studying the effects on batteries of the smart charger, which will not be possible with a simpler model with a controllable load and source.

The proposed model is designed to be integrated in mathematical models of the LV distribution system network to calculate control settings of the actual smart charger. These settings are obtained here based on a heuristic approach to avoid overloading of the distribution system transformer and improve voltage profiles in the LV network, thus becoming an integral part of smart charging strategies in distribution feeders, as explained and demonstrated in detail in Section 3.5.

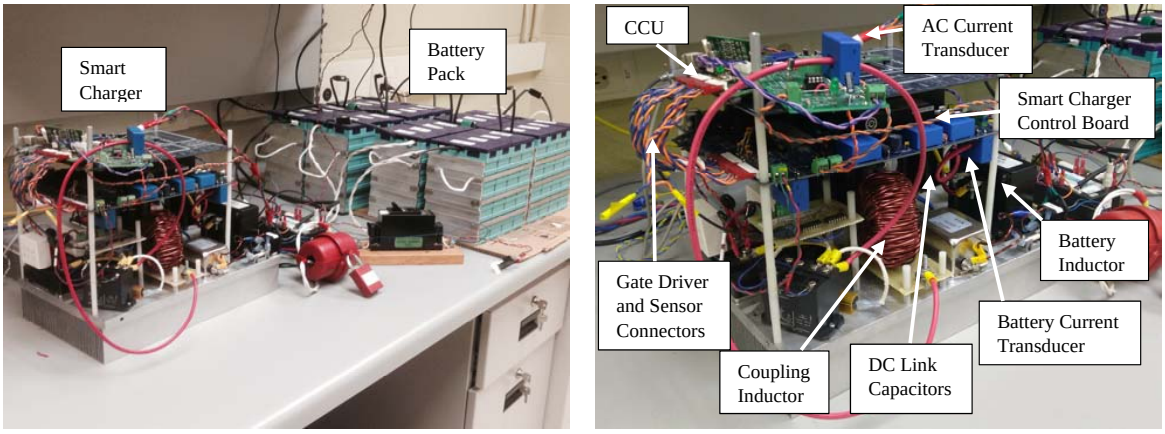

(a) (b)

Figure 3.5: Bidirectional charger prototype (a) smart charger-battery pack layout, and (b) smart charger side view [120].

3.4 Validation of Average Model

In this section, the charger's average model developed in Section 3.3 is verified against a prototype of a Level 1, 1.92 kVA/120 V four-quadrant charger built in the lab (see Figure 3.5) [120]. The prototype receives control signals through a Wi-Fi link, which allows an external agent, such as an aggregator or Distribution System Operator, to remotely control the charging or discharging of the EV battery. The main components of the prototype are:

1. The power converter, which implements the topology described in subsection 3.2.1, with the parameter values given in Table 3.1.

2. The control board, which interconnects all voltage and current transducers, gate drive modules and the Central Control Unit (CCU), that in this prototype is a TMS320F2808 DSP, and is mainly in charge of performing the control strategies described in subsections 3.2.2 and 3.2.3, using the parameters given in Tables 3.1 and 3.2. These parameters were selected following the typical design procedure found in the technical literature for full-bridge and bidirectional buck-boost converters [121], with the exception of the dc-link capacitor, which is dimensioned considering that the converter is also used as a reactive power source, as per the method described in [18].

3. The lithium-ion battery model GBS-LFMP40AH from Elite Power Solutions (4.1 kWh, 102.4 V) and the corresponding Battery Management System.

4. The communications controller, which enables the remote control of the charger using a web page that was implemented using the SN8200 EVK Wi-Fi module from Murata. Wi-Fi technology was chosen because most of the current home energy management systems (e.g., Peaksaver Plus systems in Ontario [122]) are being designed to communicate with the user and utilities through Wi-Fi interfaces and the Internet. Thus, the chosen Wi-Fi controller broadcasts a web page with a user interface to select the mode of operation of the charger (CC-CV or smart charging), so that P and Q set points can be defined in smart-charging mode. This web interface also provides operational information such as dc-link voltage, ac voltage, ac current, P, Q, battery SoC and status messages, which is useful for measuring and monitoring purposes.

Table 3.1: Smart Charger Prototype Parameters [120]

Description	**Parameter**	**Value**	**Unit**
Smart Charger VA Rating	S	1.92	kVA
Absolute Maximum Reactive Power	Q_{sys}	1.92	kVAR
Absolute Maximum Active Power	P_{sys}	1.92	kW
Grid Voltage	V_{sys}	120	V
Maximum AC Current	I_{sys}	16	A
Absolute Maximum Battery Current	I_b	20	A
Nominal Open Circuit Battery Voltage	V_{oc}	105	V
DC Link Voltage	V_{dc}	280	V
Coupling Inductor	L_C	1.65	mH
DC Link Capacitor	C_{dc}	2	mF
DC/DC Filter Inductor	L_f	1.5	mH
DC/DC Filter Capacitor	C_f	1	mF
Switching Frequency	f_{sys}	20	kHz

Table 3.2: Controller Parameters [120]

Controller	$\mathbf{PI_A}$	$\mathbf{PI_B}$	$\mathbf{PI_C}$	$\mathbf{PI_D}$	$\mathbf{PI_E}$	$\mathbf{PI_F}$	$\mathbf{PI_G}$	$\mathbf{PI_H}$
k_i	2.5	160	5	80	0.5	1	1	1
k_p	0.25	15	0.07	10	0.1	0.001	0.001	0.001

To compare the performance of the average model with that of the prototype, a charger with the same characteristics of the prototype was simulated in the PSCAD™ environment [123], using the average model. The charger parameters used in the simulation were the same as those of the prototype, as per Tables 3.1 and 3.2. The average model simulation was performed using a 50 μs time step, which was defined through trial and error as an appropriate value to capture all the variations in voltage and current signals. It is important to mention that if a switching model was used, a 50 μs time step would be insufficient to capture the dynamics of the 20 kHz PWM signal.

3.4.1 Steady-state Response

To compare the steady-state response of the average model in the four quadrants of the P-Q plane, as well as on the boundaries of the quadrants, the simulation and experimental results are presented in Figure 3.6. These plots demonstrate that the charger is capable of four-quadrant operation, with the average model representing the operation with high accuracy. Purely reactive power requests are also shown, where the current lags or leads the voltage by 90°. Observe that the steady-state current and voltage signals from the average model and the prototype are very similar for all analyzed P-Q plane operating points.

The prototype signals contain some noise, and in several cases a third harmonic can be observed in current signals, as demonstrated by the flattening of current signal around zero-crossing points. This current harmonic can appear in a full-bridge ac/dc converter when the dc-link voltage measurement signal is passed to the control loop without appropriate filtering of the second harmonic ripple [124]; potential solutions to this problem include improving the filtering of input control signals, increasing the size of the coupling inductor, and retuning the PI regulators in the ac/dc converter. There were also issues producing a stable current wave shape, which is a result of poor current tracking associated with the chosen current sensor, and the ac current conditioning circuit linking the measured current to the Analog-to-Digital Converter (ADC) on the CCU.

3.4.2 Dynamic Response

A comparison between the dynamic behavior of the prototype and the average model was also performed. For this purpose, step responses for V_{sys}, I_{sys}, P_{sys}, Q_{sys}, V_b, V_{dc}, and I_b in two transitions were analyzed. The first transition was from 1.1 kW and 0 kVAR to -1.1 kW and 0 kVAR, and the second transition was from -1.1 kW and 0 kVAR to 1.1 kW and 1.1 kVAR; the results of these scenarios are presented in Figure 3.7. Note that the dynamic responses of the average model for V_{sys}, I_{sys}, P_{sys}, Q_{sys}, V_{dc}, I_b and V_b follow very closely the corresponding prototype signals. However, observe that V_{dc} on the prototype presents larger overshoots during the transition of P and Q references, and that battery voltage values are not in close agreement. These differences can be attributed to the battery model, which only considers a voltage source behind a resistor, obtained from actual tests on a battery pack in the lab, based on a model consisting of open-circuit voltage and series resistance, and does not represent the actual dynamic behavior of the battery. To obtain a closer agreement between the results of prototype and those of the average model, a dynamic model of the battery should be used. Additionally, it can be observed that the controller has a slow response, as intended. Since there is no inherent advantage to having a fast time response, which can lead to overshoot, potentially charging the battery beyond the limit it is rated for, the dc filter values were chosen such that it would not only filter the ripple in the P-Q requests, but also slow the response down and eliminate overshoot. The response time of the active power controller is much shorter than that of the reactive power controller, since the active power controller is directly coupled to the battery current.

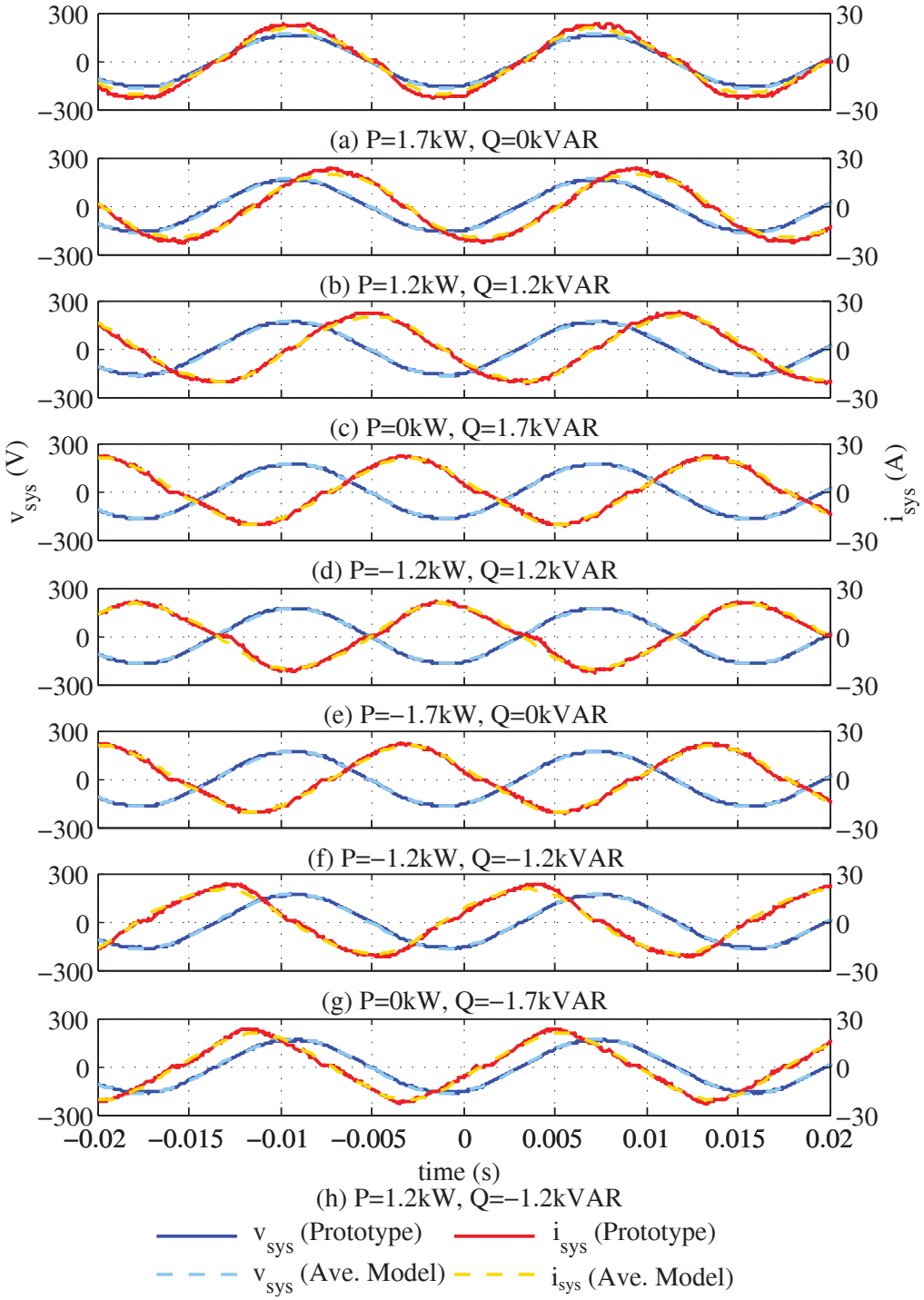

Figure 3.6: Steady-state responses of smart charger prototype and average model for different PQ requests.

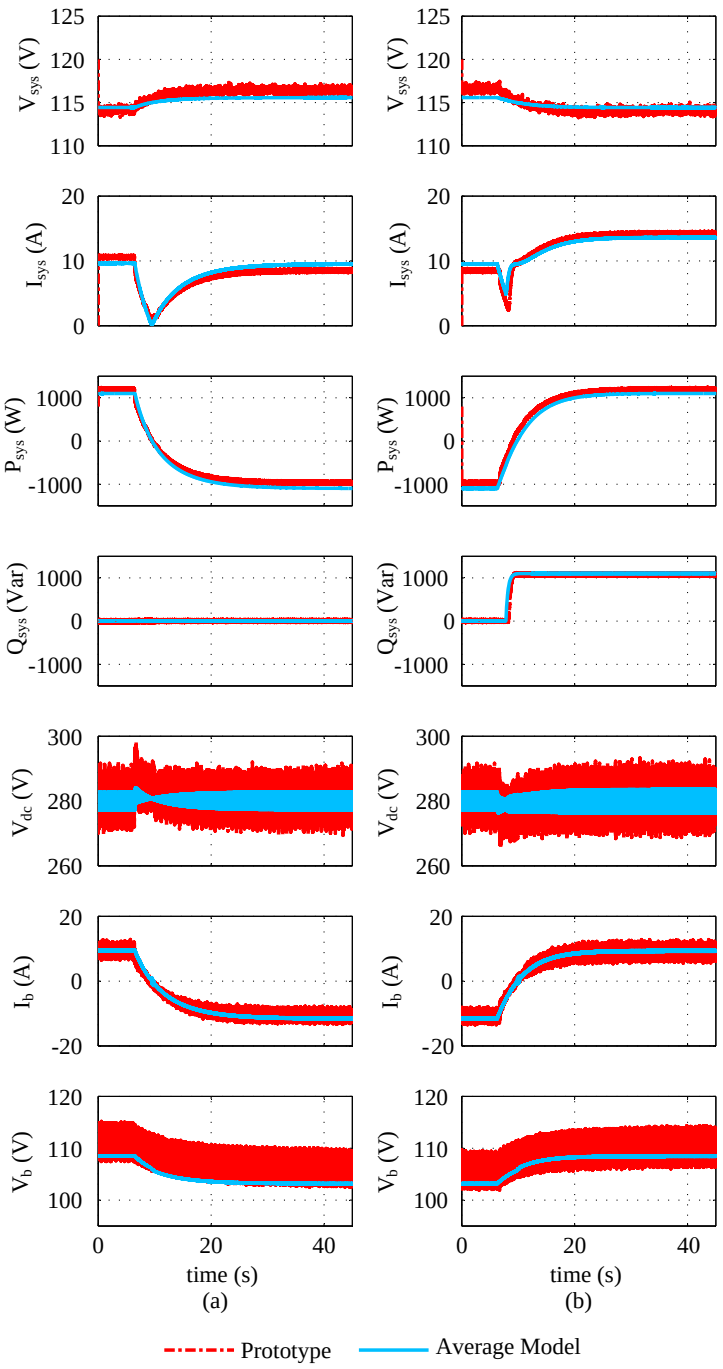

Figure 3.7: Step response (a) from P=1.1kW and Q=0 kVAR to P=-1.1 kW and Q=0 kVAR, and (b) from P=-1.1kW and Q=0 kVAR to P=1.1 kW and Q=1.1 kVAR.

3.5 Low-Voltage Distribution System EV Integration

3.5.1 Test System and Case Studies

The average model of the bidirectional charger was used to simulate a typical secondary distribution system composed of 10 residential loads, fed from a 50 kVA, 12.47 kV/240 V-120 V single-phase transformer (see Figure 3.8), and 10 EVs, each connected to a residential load. The specifications of the secondary distribution system were extracted from the residential CIGRE benchmark of a North-American secondary distribution system presented in [125]. Residential loads were assumed to be evenly distributed between the split secondary system phases, and follow the demand curves and power factors specified in the CIGRE benchmark. It was assumed that each residential load had an EV with a single-phase charger, according to the specifications of the prototype introduced in Section 3.4, i.e., 1.92 kVA/120 V, and a 16 kWh battery. The simulations were implemented using the PSCAD^{TM} software [123].

A three-winding transformer model was used for the distribution transformer, and a coupled wire model was used for service cables. Residential loads were modeled as constant-impedance loads, with the impedances determined by the given power in a time interval and the nominal voltage. The bidirectional chargers' average models were implemented using controlled voltage and current sources available in the PSCAD^{TM} library. The controllers described in Section 3.2 were implemented using the parameters given in Tables 3.1 and 3.2. For all case studies, the simulation time was 288 s, and the simulation step was 50 μs, representing an advantage in terms of simulation time step and simulation time when compared to the case where a complete model with all switching details is used, which requires much smaller simulation time steps. Each second in the simulation represents the loading conditions in a 5 minute interval to reduce simulation time, without loss of generality, given the charger time constants, which are in the order of ms, as discussed in detail in Section 3.5.2. Thus, the power references for the residential loads are adjusted each second, and active and reactive power references for bidirectional chargers are adjusted depending on the type of control, as explained next.

Three case studies were implemented to analyze the impact of EV charging and different V2G strategies on the residential system. All cases simulate CC-CV charging, assuming that all EVs start charging at 1:00 am with 20% SoC, until reaching 85% SoC. The battery voltage for all EVs is calculated using the expressions $V_{oc} = 2.9132SoC + 104.08$ for charging, and $V_{oc} = 3.5862SoC + 103.26$ for discharging, which approximate the open circuit voltage of the battery pack used in the prototype. R_b is assumed to be 0.0625 Ω

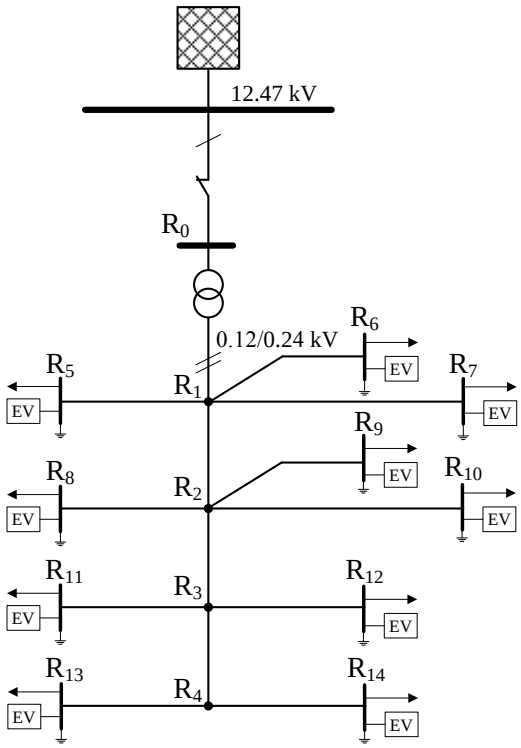

Figure 3.8: Secondary distribution system model used in the study.

for charging, and 0.05625 Ω for discharging. Charging is switched from CC to CV mode when the battery reaches an SoC of 75%.

The V2G strategies are assumed to be applied following the afternoon commuting, and EVs are divided in the following three sets to study the effect of different arriving times: Set 1 is composed of EVs at nodes R_5, R_9, R_{12}, and R_{13}, following the CIGRE benchmark notation, arriving at 6:00 pm; Set 2 is composed of EVs at nodes R_6, R_8, and R_{11}, arriving at 7:00 pm; and finally, Set 3 is composed of EVs at nodes R_7, R_{10}, and R_{14}, arriving at 8:00 pm.

The first case study presents a Q compensation control by an external agent. It is assumed that this external agent is a controller located at the distribution transformer, receiving real-time measurements of reactive power consumption of the residential network. Thus, the controller determines Q compensation requirements of the residential distribution system, and determines the Q setpoints for all EV chargers that are connected to the grid, as depicted in Figure 3.9, where N_v is the number of vehicles connected in each of the split

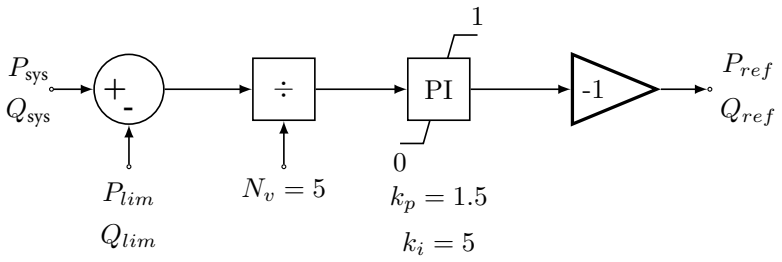

Figure 3.9: P and Q compensation control.

phases, Q_{lim} for this controller is assumed fixed at 4 kVAR, and the maximum available Q per charger is assumed to be 1 kVAR.

The second case study is based on the following voltage droop function, which is implemented locally in all bidirectional chargers, as proposed in [83] for the case of solar panel applications:

$$Q_{EV} = \begin{cases} 1 & V > 1.03 \text{ pu} \\ \frac{100}{3}(V-1) & 0.97 \text{ pu} \leq V \leq 1.03 \text{ pu} \\ -1 & V < 0.97 \text{ pu} \end{cases} \tag{3.21}$$

This function determines the reactive power set point as a function of the charger local voltage; hence, the reactive power compensation depends on the voltage at the connection point.

The third case study is referred to as P compensation and is identical to the first case, except that it is used for active power. In this case, P_{lim} for the control strategy of Figure 3.9 is assumed fixed at 36 kW, and the maximum available P per charger is assumed to be 1 kW.

A fourth case study is carried out to analyze possible dynamic interactions of bidirectional EV chargers in LV distribution networks, considering set-point changes to the EV bidirectional chargers in a short period of time. In this case, the residential loads are assumed constant and at their maximum levels, as defined in the CIGRE benchmark. EVs at nodes R_5, R_7, R_9, R_{11}, and R_{13} are assumed to absorb 1.92 kW each, and EVs at nodes R_6, R_8, R_{10}, R_{12}, and R_{14} are assumed to operate in voltage droop control mode. It is also assumed that EVs start to operate in pairs every two seconds, following the sequence R_5-R_6, R_7-R_8, R_9-R_{10}, R_{11}-R_{12}, and R_{13}-R_{14}. In this case, the simulation time is actual 30s, i.e., no time scaling is used here, and the simulation step is 50 μs, as one is interested in the transient response due to large step changes, rather than the overall daily charging profile analyzed in the three previous cases, in which the load changes between consecutive time steps are relatively small and the steady-state of voltages and currents are reached

quickly.

3.5.2 Simulation Results

Figure 3.10 presents the results for active and reactive powers at the distribution transformer. For the three cases, a new peak appears during early morning hours due to simultaneous charging of EVs; however, this peak does not surpass the normal evening peak. Q compensation and voltage droop operate by decreasing the reactive power consumption during the peak hours, slightly improving the voltage profile, as seen in Figures 3.11(a) and (b), compared to the voltage at the last node (R_{14}) without EV. The Q compensation strategy is able to inject more reactive power, since it follows the actual reactive power consumption; however, before 10 pm, the need for reactive power surpasses the capacity of EV chargers, as it can be seen in Figure 3.12(a). From Figure 3.12(b), it is evident that the chargers do not reach their reactive power limit when operating in voltage droop control. Note that Figures 3.10, 3.11, and 3.12 contain two scales, i.e., the actual simulation time and the corresponding equivalent real-time scale. The first scale corresponds to a simulation time of 288 s, while the second corresponds to 24-hours since 1 second of simulation time represents 5 minutes of real time, as previously mentioned. As seen in Figure 3.3, the charger is able to change the mode of operation among CC, CV and CP. When the charger connects, the control is switched to CP mode, and the duty cycle changes its value as per the corresponding PI controller output; hence, the transients that are seen in the graph for active power are due to the transitions caused by the change in the mode of operation and set points. To illustrate the actual duration of these transients, a 300 s simulation was carried out for a 5-minute window in which the EV chargers switch from CV to CP modes at t=150 s. The simulation took 1 hour and 2 minutes to complete running in a 1.87 GHz Intel Xeon CPU, which would result in about 13 days of simulation time to complete a full 24-hour period in this time scale; this is the reason why the simulations shown in Figures 3.10-3.12 are carried out using a faster time scale than real-time. The results of this simulation are presented in Figure 3.13; observe in Figure 3.13(a) that the transient appears as an instantaneous spike, when in reality it has a duration of almost 0.5 s, as seen in Figure 3.13(b). In practical implementations, these transients have to be minimized in order to avoid harmful effects on charger switches and EV batteries. This can be done by making the transitions in the set-points gradual.

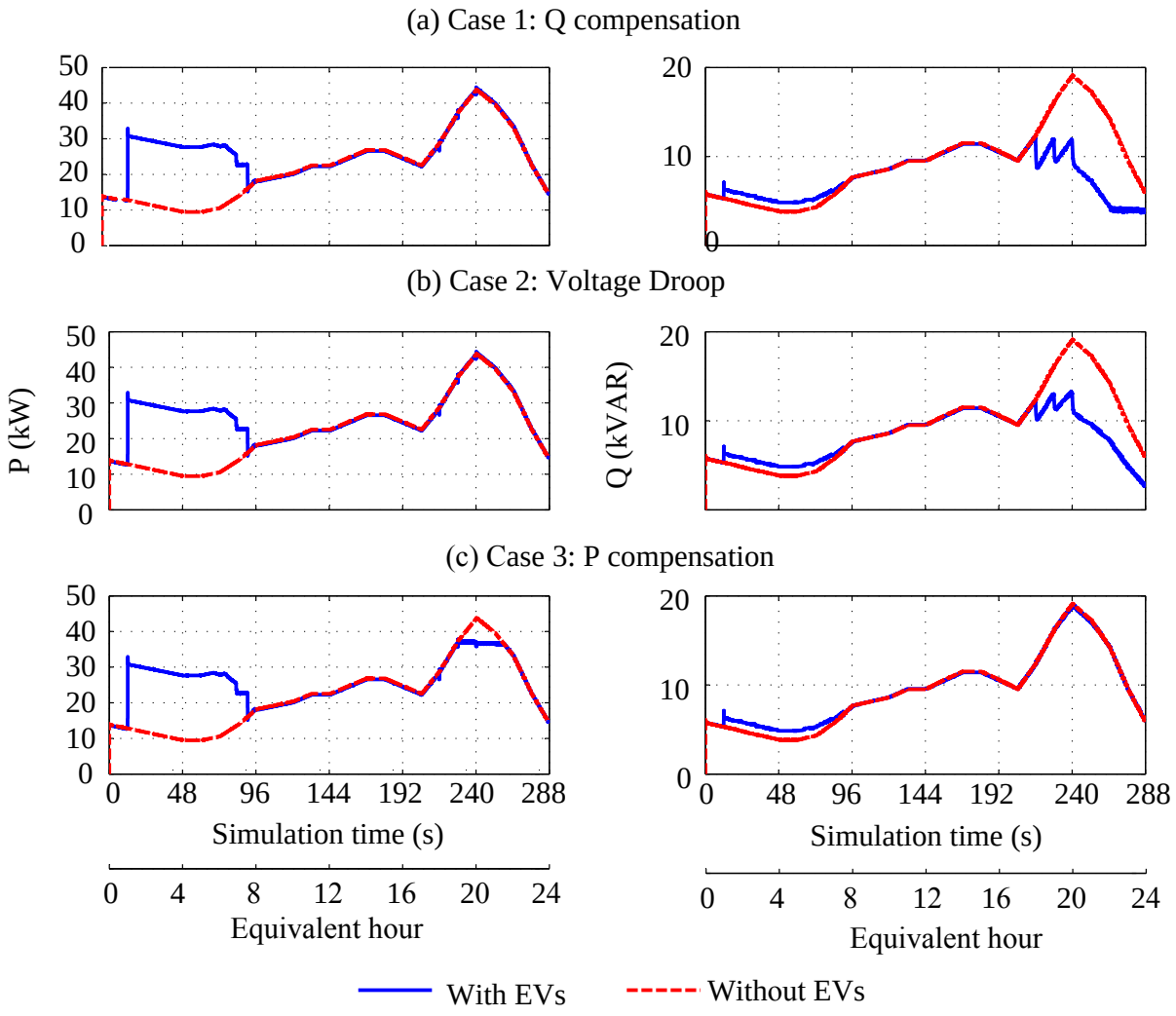

Figure 3.10: Active and reactive power at distribution transformer for three case studies.

P compensation shaves the active power curve at 36 kW during the peak period, according to the fixed limit set for the P of each charger, as seen in Figure 3.10(c). This has an effect on the voltage profile (see Figure 3.11(c)), which is also improved thanks to less current coming from the distribution transformer. As seen in Figure 3.12(c), the chargers inject P when needed after the vehicles arrive, without reaching the limit of 1 kW. Note that Figure 3.10, 3.11 and 3.12 show transients at certain points, which are due to the dynamic response of the average models following a change in reference signals.

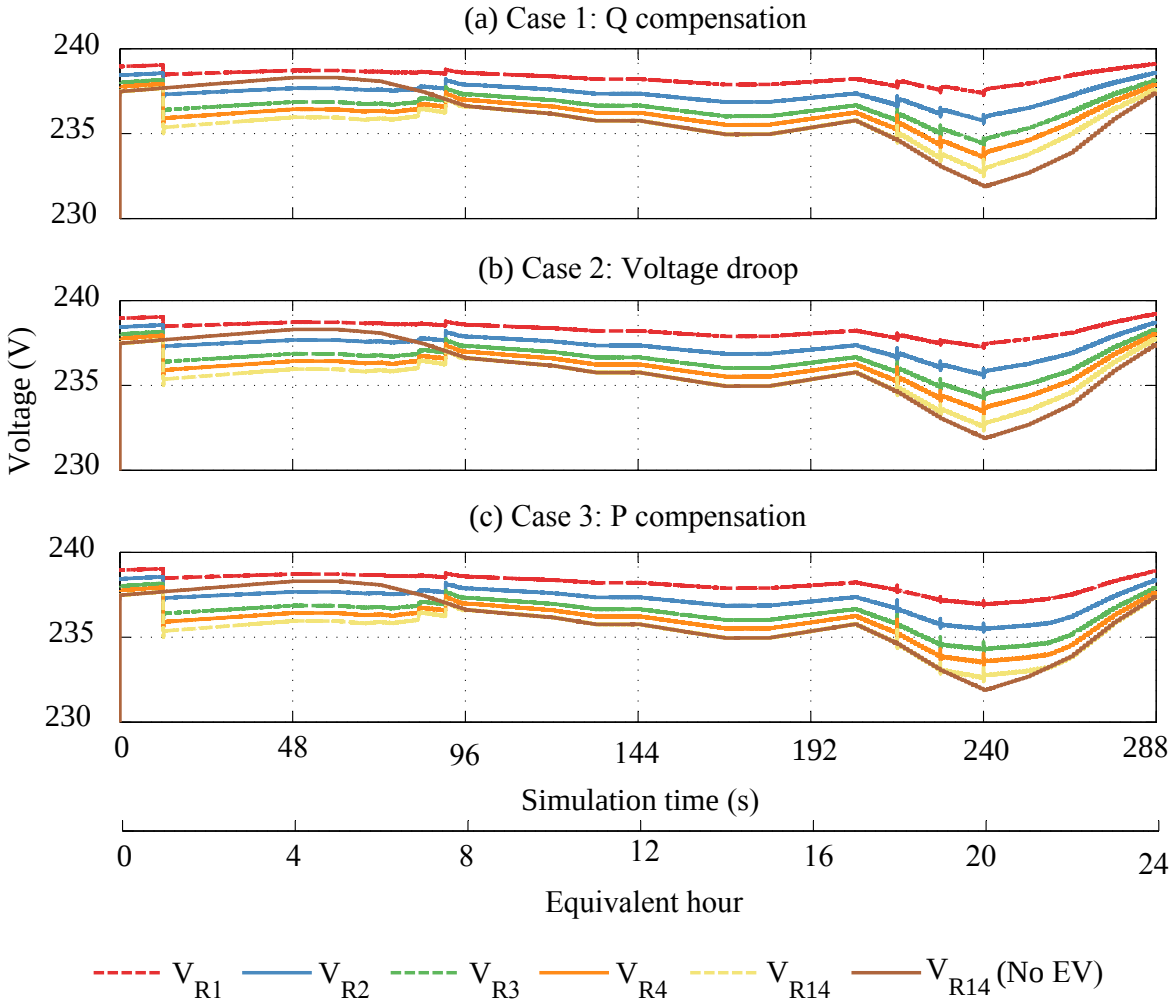

Figure 3.11: Voltage at different nodes of the secondary distribution system.

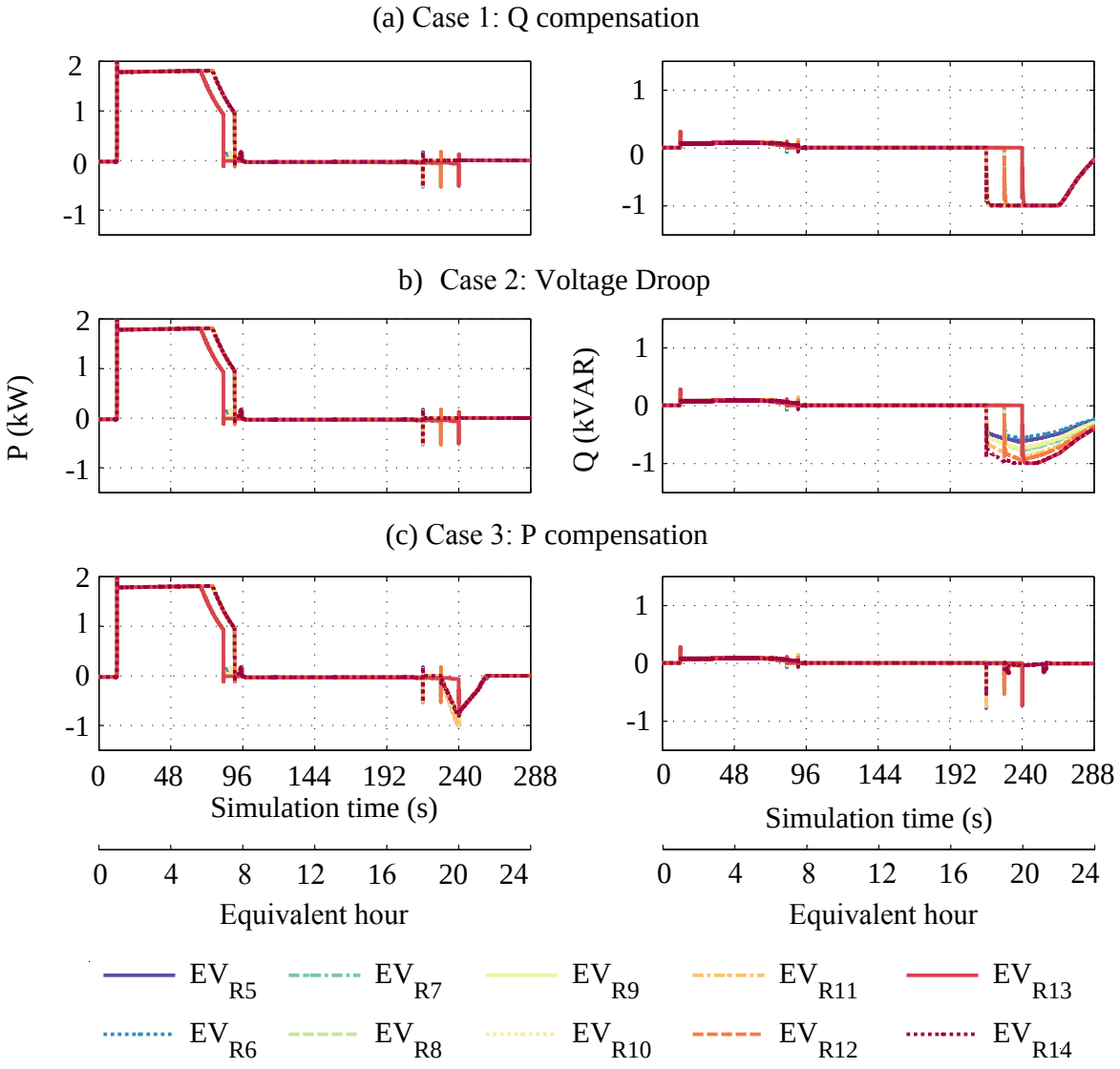

Figure 3.12: Active and reactive power at EV chargers for three case studies.

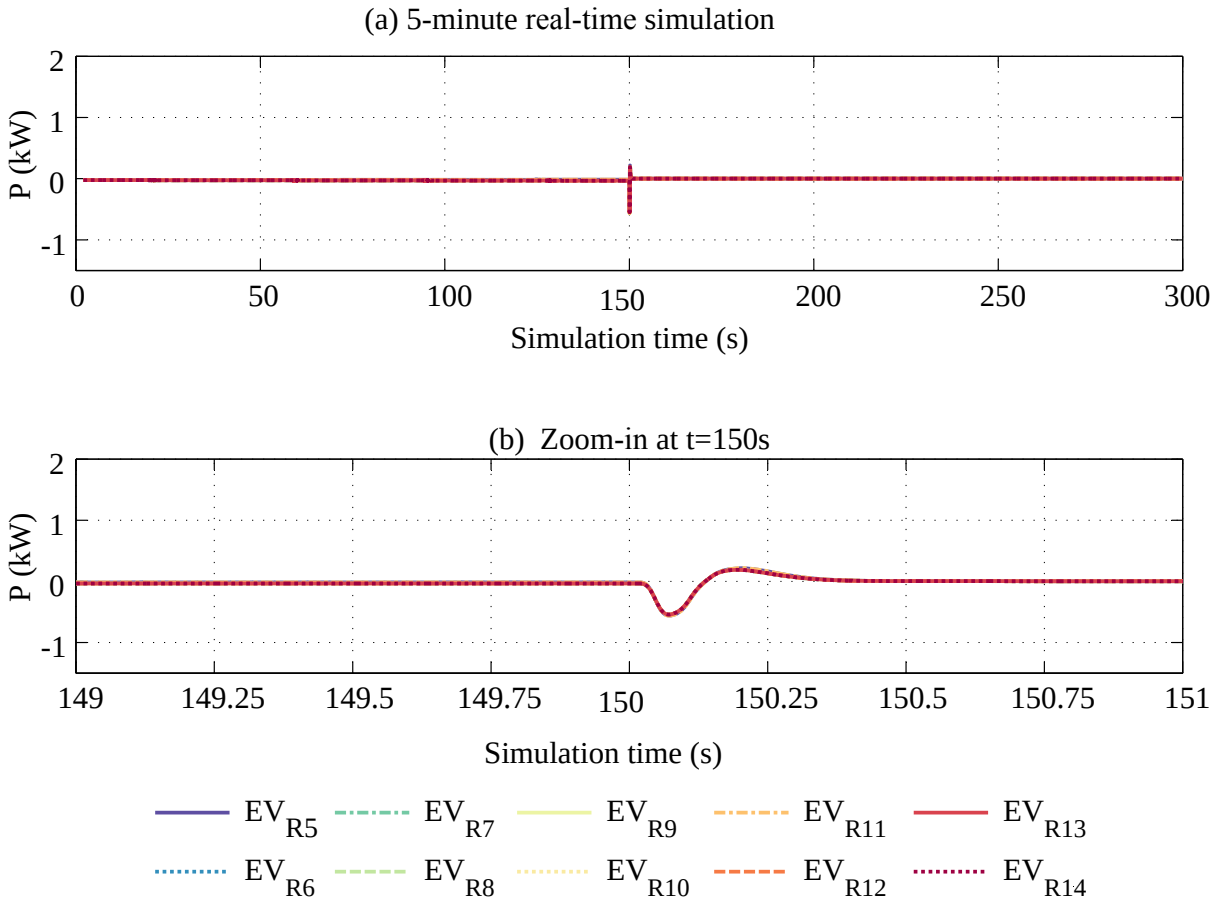

Figure 3.13: The effect of control mode transition between CV and CP on active power.

For the fourth case study, Figure 3.14 shows the details of active and reactive power dynamic transitions in EV chargers, and Figure 3.15 depicts the effects of these transitions on the distribution transformer active and reactive power loading and node voltages, with and without considering the operation of EVs in voltage droop mode. Observe that the active and reactive powers for all EVs have a slow transition, as expected from the experiments presented in Section 3.4, slowly and slightly increasing the total active power at the distribution transformer. The transients observed in Figure 3.12, which appear as a consequence of the dynamic response of the EV charger controller, also appear in Figure 3.14, and have only a small effect on the node voltages and transformer active and reactive

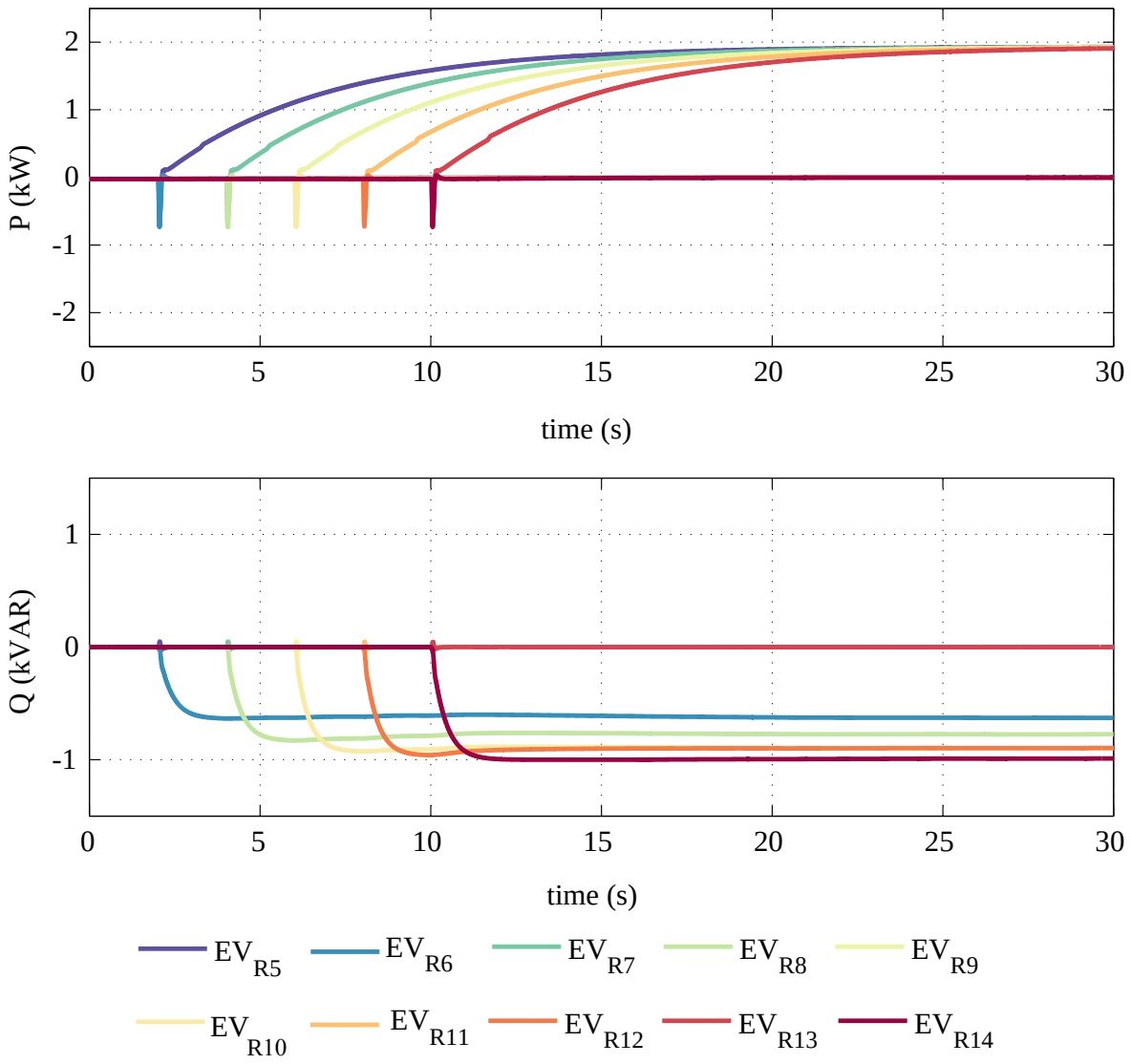

Figure 3.14: Active and reactive power for EVs in Case 4 on dynamic interactions.

power, as observed in Figure 3.15. Note that the voltages improve following the dynamics of the droop controller and the charger.

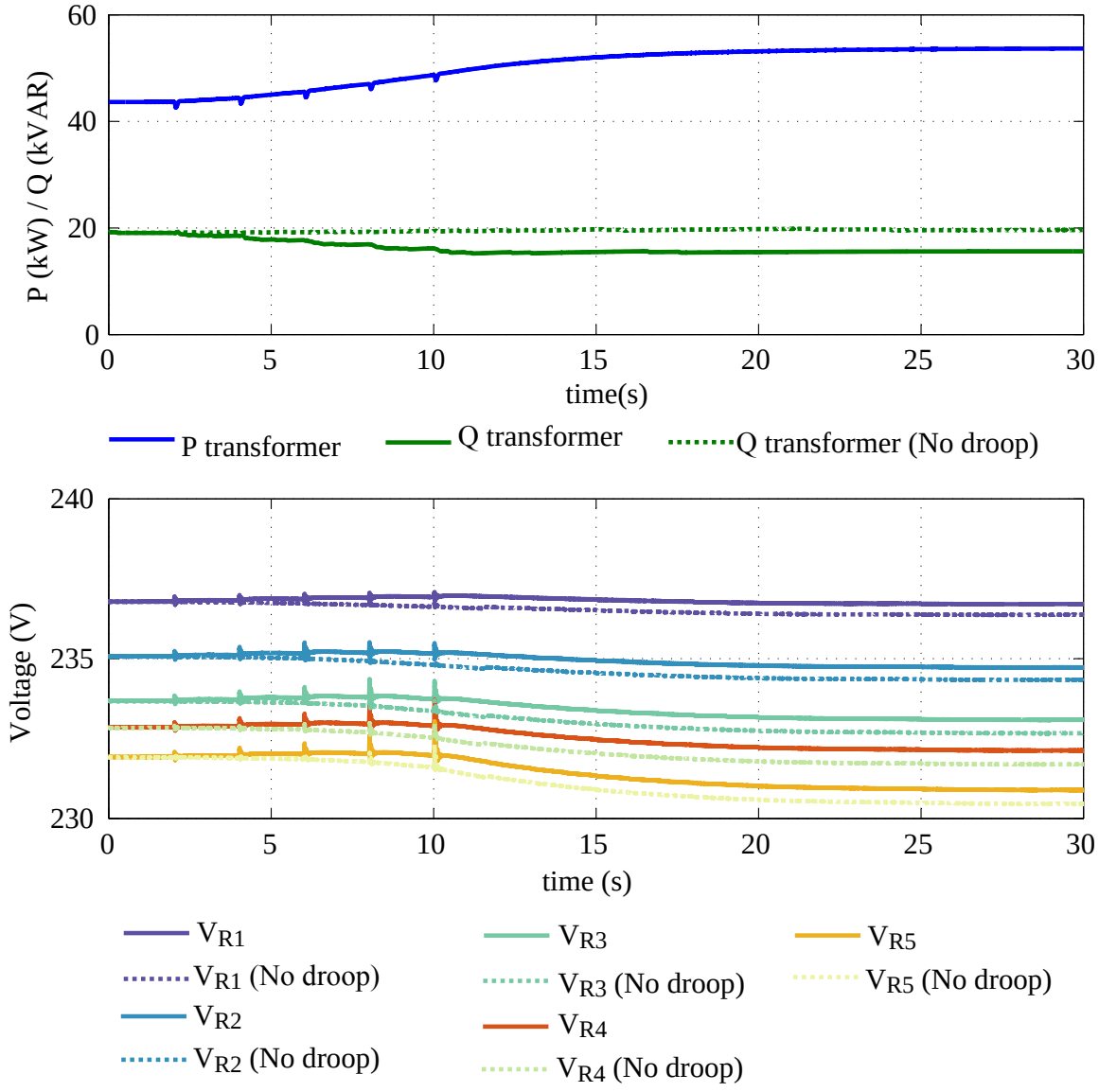

Figure 3.15: Active and reactive power at distribution transformer and node voltages in Case 4 on dynamic interactions.

3.5.3 Discussion

Options for controlling voltage profiles in LV networks are very limited; thus, the presented case studies demonstrated three control options that can be accomplished with bidirectional EV smart chargers to help with this task. The results show that P compensation strategy works better towards boosting the voltage in LV residential networks, since power factor tends to be high in residential loads. However, the main advantage of the proposed injection of reactive power from the smart charger is that it does not discharge the battery (except to compensate for the ac/dc converter losses), since this can be accomplished with the dc link capacitor. These types of chargers could also be used as an aggregated reactive power source to control the voltage profile at the medium voltage level, acting as a controllable distribution feeder capacitor, which is an approach studied in the next chapter.

The most important challenge for the integration of four-quadrant bidirectional chargers in actual distribution systems is the adequate control of P and Q to mainly charge the battery while supporting the distribution grid. This task can be complex, because P and Q are coupled and the chargers are normally located on-board the vehicles, and thus are connected to the grid for only a limited time. Since the reactive power capability of the charger only depends on the full-bridge ac/dc converter, a practical implementation approach of the proposed smart charging scheme to facilitate charging control and provide more reliable services to the grid would be to split the converter, thus integrating the Stage 1 into the EV connection box, and keeping the Stage 2 on-board the vehicle. This would require changing the ac EV charging interface to dc, which would comply well with fast charging standards.

3.6 Summary

In this chapter, the average model of a single-phase, two-stage, Level 1 four-quadrant smart charger, composed of a full bridge ac/dc converter and a bidirectional buck-boost converter, was presented. First, the topology under study was described, showing that the ac/dc converter used a dq-frame controller with an additional loop to control reactive power, and the dc/dc converter employed a PI controller with an additional loop to control active power, thus giving the charger the capability of independent P and Q control. Then, an average model of a four-quadrant EV charger was proposed and validated using measurements from an actual smart charger prototype, verifying its steady-state response in all four quadrants of the P-Q plane, as well as the response to step changing in P and Q set points. The results obtained from the average model were shown to be generally

in close agreement with those of the prototype, although some improvements could be made by using a more detailed battery model. Finally, the average model was used in the integration study of the smart charger prototype in a residential distribution system for three V2G strategies, proving to be appropriate for representing the steady-state response and cycle-to-cycle dynamics of the chargers when interacting with a distribution system.

Chapter 4

Distribution Feeder Control Strategy Considering Four-Quadrant EV Chargers

4.1 Introduction

This chapter describes a three-stage algorithm to coordinate the operation of four-quadrant EV chargers with other volt/var control devices in MV and LV distribution feeders, and presents several application cases of the proposed strategy in CIGRE's North-American MV and LV benchmark systems. Section 4.2 briefly discusses the implications of four-quadrant EV chargers in the typical distribution feeders' volt/var function, and describes the proposed three-stage architecture for distribution feeder and EV charging control. Section 4.3 introduces the mathematical model of each stage of the proposed architecture. Finally, Section 4.4 discusses the implementation and simulation results of the proposed control approach using a CIGRE's benchmark test system.

4.2 Integration of Four-Quadrant EV Chargers in Volt/var Control of Distribution Feeders

4.2.1 Volt/var Control in Distribution Feeders

The control problem in distribution feeders has been treated traditionally as a volt/var problem, as discussed in Section 2.2.4. For this purpose, LTCs at the main substation, capacitors at the substation level, capacitors at the feeder level, and SVRs are used. The objectives of typical volt/var control are to minimize voltage deviations, maintain a power factor near unity at all nodes along the feeder, minimize the power losses in the system, keep the loading of lines and transformers within limits, and minimize the total number of tap changing and switching operations.

Four-quadrant EV chargers that are able to exchange reactive power with the grid will modify the traditional way the volt/var control devices are operated. This may require communication links between the grid operator and the EV chargers, but would imply a lower number of capacitor switching and tap changing operations, and better controlability of the feeder, since more reactive power sources will be distributed along the feeder. In this context, the proposed architecture for coordinating four-quadrant EV chargers with other devices that perform volt/var control function in distribution feeders is explained next.

4.2.2 Proposed Three-Stage Architecture

Transformer taps and capacitors participate continuously in reactive power and voltage adjustment of distribution feeders under the control of LCs, with defined set-points to keep the voltage at designated nodes within a given tolerance band; however, this approach may produce a high number of operations, leading to accelerated wear of transformers and capacitors, which can be costly in terms of operation and maintenance. To reduce this adverse effect, transformer taps and capacitors in a distribution grid can be dispatched one day ahead within a volt/var control scheme, using load forecast information and constraining the number of transformer taps and capacitor operations per hour, as reported in, for example, [37] and [126]. This approach is built into the two-stage technique proposed in [46] and [47], calculating the expected day-ahead optimal transformer tap and capacitor schedule based on a load peak minimization approach, including EVs as continuous reactive power sources.

Based on the aforementioned discussion, the three-stage control architecture illustrated in Figure 4.1 is proposed here for coordination of the operation of four-quadrant EV charg-

ers, LTCs, and switched capacitors. This scheme is based on the work reported in [46] and [47], enhanced by the addition of a four-quadrant EV charger model, objective functions related to reactive power operation, and individual EV charger set-point modulation. The control architecture accounts for the uncertainty in EV operation, i.e., the energy consumed during a day, and the charger's connection and disconnection times, providing individual set points for the EV chargers connected to the LV system.

The First Stage of the proposed architecture consists of a stochastic day-ahead dispatch of taps and capacitors, considering the probabilistic modeling of EV operation in terms of battery SoC, arrival time, and departure time, as explained in some detail in Section 4.3.1. This information on EV behavior can be obtained from studies that track operational data of EVs, as is the case here. This stage considers only the MV feeder; thus, the LV loads and EVs are aggregated at the respective MV node. The inputs of this stage are the feeder's load and EV population forecasts and their probabilistic characteristics; the outputs are the best estimate for capacitor switching schedule, transformer tap schedule, and allowed peak demand for the next day. The Second Stage allocates the EV aggregated load every 5 minutes, using the tap and capacitor settings, maximum allowable load, and the actual number of EVs connected at each node. Finally, the Third Stage receives the aggregated set-points from the Second Stage and allocates P and Q set points to individual EVs connected to the system, based on the conditions calculated in the Second Stage at the MV node, and the actual household demand.

The proposed control architecture is designed to be implemented as a hierarchical distributed control. Stages 1 and 2 are conceived to be carried out by a central controller, and the third stage by distributed controllers located at the same levels as the distribution MV/LV transformers, as depicted in the conceptual scheme of Figure 4.2. Based on this, the interplay among the three stages will be hierarchical, with the distributed controllers following the signals calculated centrally, and communicating the results back to the central controller to guarantee coordination with the rest of the system.

4.3 Mathematical models

In this section, the mathematical models for different stages of the proposed control architecture are introduced and explained.

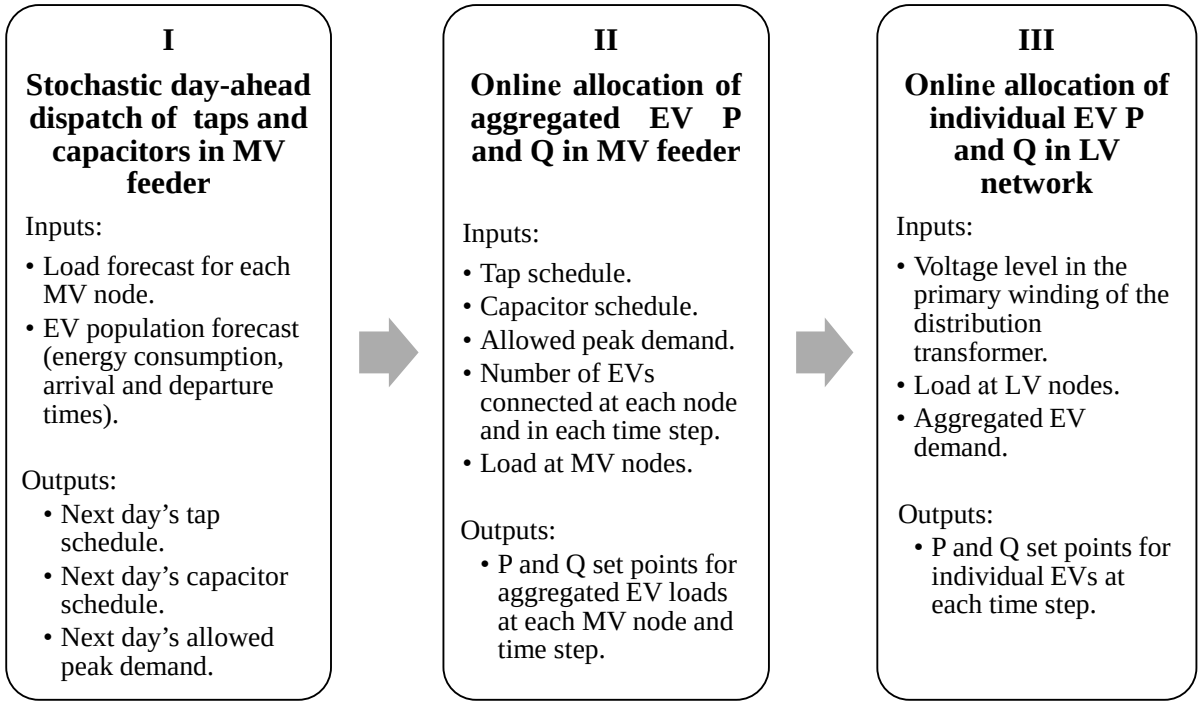

Figure 4.1: Proposed three-stage architecture for controlling four-quadrant EV chargers in distribution feeders.

4.3.1 First Stage

This stage operates one day ahead of the actual implementation, with the objective of minimizing the peak load, as follows:

$$\min P^{max} = \max_{t=1,\dots,T_{max}} \sum_{n_m=1}^{N} \left(P^{bl}_{n_m,t} + P^{agev}_{n_m,t} \right) \tag{4.1}$$

assuming that only the EV load, represented as $P^{agev}_{n_m,t}$, can be controlled. The base load profile, represented in (4.1) as $P^{bl}_{n_m,t}$, is obtained from forecast information and is not changed during the simulation; however, this is modeled as a constant impedance and hence presents deviations from the base value when the node voltages in the system are different from 1 p.u.

The constraints that accompany the objective function (4.1) are the following:

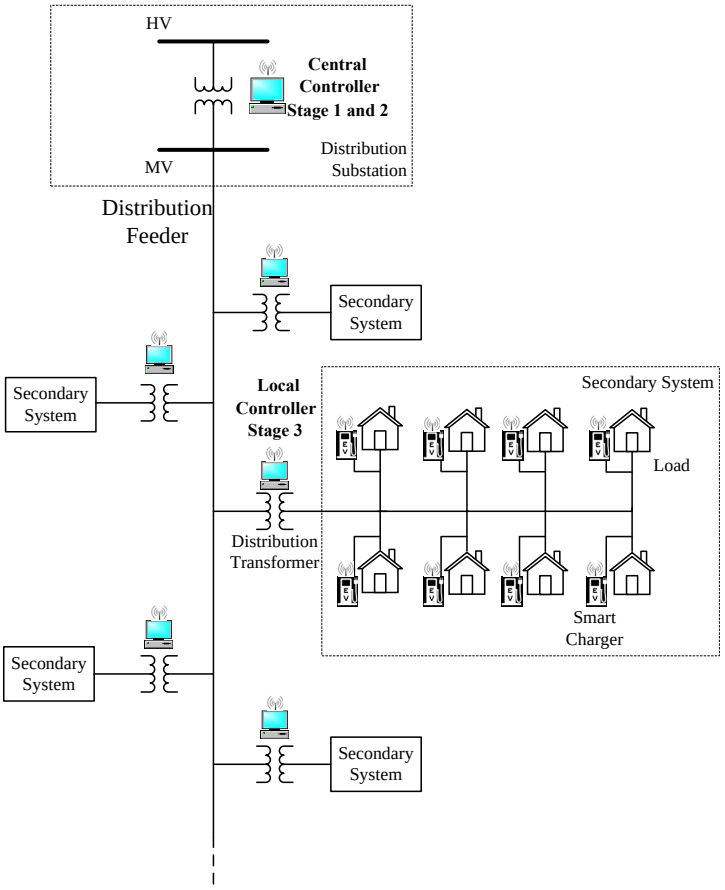

Figure 4.2: Implementation of the proposed three-stage control architecture.

$$\sum_{t=1}^{T_{max}} P_{n_m,t}^{agev} \tau_1 \leq E_{agev_{n_m}} \ \forall n_m = 1, ..., LN \tag{4.2}$$

$$\overline{E_{agev_{n_m}}} = \sum_{ev=1}^{nev_{n_m}} Bc_{ev} \ \forall n_m = 1, ..., LN \tag{4.3}$$

$$\sum_{t=1}^{T_{max}} P_{n_m,t}^{agev} \tau_1 \geq (SoC_{agev_{n_m}}^{fin} - SoC_{agev_{n_m}}^{ini}) \overline{E_{agev_{n_m}}} \ \forall n_m = 1, ..., LN \tag{4.4}$$

$$\overline{S^{agev}_{n_m,t}} = \sum_{ev=1}^{nev_{n_m},t} Cr_{ev} \ \forall n_m = 1, ..., LN, \forall t \tag{4.5}$$

$$0 \leq P^{agev}_{n_m,t} \leq \overline{S^{agev}_{n_m,t}} \ \forall n_m = 1, ..., LN, \forall t \tag{4.6}$$

$$-\overline{S^{agev}_{n_m,t}} \leq Q^{agev}_{n_m,t} \leq \overline{S^{agev}_{n_m,t}} \ \forall n_m = 1, ..., LN, \forall t \tag{4.7}$$

$$\left(Q^{agev}_{n_m,t}\right)^2 + \left(P^{agev}_{n_m,t}\right)^2 \leq \left(\overline{S^{agev}_{n_m,t}}\right)^2 \ \forall n_m = 1, ..., LN, \ \forall t \tag{4.8}$$

where the aggregated EV load constraints are represented by (4.2)-(4.8), which include the aggregated EV energy consumption (4.2) obtained from travel information, the aggregated battery capacity (4.3), and the minimum SoC that is required at the end of the day (4.4). In (4.2)-(4.4), τ_1 is the First Stage time step, $E_{agev_{n_m}}$ represents the aggregated EV energy at each MV node, $\overline{E_{agev_{n_m}}}$ is the maximum aggregated EV energy at each MV node, Bc_{ev} is the battery capacity of individual EVs, and $SoC^{fin}_{agev_{n_m}}$ and $SoC^{ini}_{agev_{n_m}}$ are the final and initial SoC values of the aggregated EV batteries. The aggregated power limits imposed by the rating of the chargers are considered in (4.5)-(4.8), where $\overline{S^{agev}_{n_m,t}}$ is the maximum aggregated EV apparent power, Cr_{ev} is the individual EV rating, and $Q^{agev}_{n_m,t}$ is the reactive power of the EV load. It is important to mention that EVs are modeled in this stage as aggregated loads that only absorb active power, as no discharge is considered in this thesis, and can inject or absorb reactive power.

For LTCs, the constraints include the maximum and minimum tap positions, and the maximum number of operations per day, as follows:

$$\underline{tap_{i_t}} \leq tap_{i_t,t} \leq \overline{tap_{i_t}} \ \forall i_t, \forall t \tag{4.9}$$

$$\left|tap_{i_t,t} - tap_{i_t,t-1}\right| \leq Mop_{tap} \ \forall i_t, \forall t \tag{4.10}$$

Substation and feeder capacitor constraints are also considered, which are very similar to those of LTCs, as follows:

$$0 \leq cap_{j_c,t} \leq \overline{cap_{j_c}} \ \forall j_c, \forall t \tag{4.11}$$

$$\left|cap_{j_c,t} - cap_{j_c,t-1}\right| \leq Mop_{cap} \ \forall j_c, \forall t \tag{4.12}$$

These constraints include the limits for switching operations (4.11) and the maximum number of operations (4.12). The tap and switching positions of LTCs and capacitors are integer variable in this problem.

The First Stage also implements maximum and minimum voltage limits at MV nodes, current limits in distribution lines, and apparent power limit at MV nodes, as follows:

$$\underline{V_{n_m}} \leq V_{n_m,t} \leq \overline{V_{n_m}} \ \forall n_m, \forall t \tag{4.13}$$

$$0 \leq I_{l_m,t} \leq \overline{I_{l_m}} \ \forall l_m, \forall t \tag{4.14}$$

$$0 \leq |S|_{n_m,t} \leq \overline{S_{n_m,t}} \ \forall n_m, \forall t \tag{4.15}$$

Finally, unbalanced three-phase power flow equations relating P, Q, and voltages are also considered, as follows:

$$P_{n_m,p,t} = \sum_{k_m=1}^{N} \sum_{q=1}^{3} V_{n_m,p,t} V_{k_m,q,t} Y_{n_m,p,k_m,q} cos(\theta_{n_m,p,k_m,q} + \delta_{n_m,p,t} - \delta_{k_m,q,t}) \ \forall n_m, \forall p, \forall t \tag{4.16}$$

$$Q_{n_m,p,t} = -\sum_{k_m=1}^{N} \sum_{q=1}^{3} V_{n_m,p,t} V_{k_m,q,t} Y_{n_m,p,k_m,q} sin(\theta_{n_m,p,k_m,q} + \delta_{n_m,p,t} - \delta_{k_m,q,t}) \ \forall n_m, \forall p, \forall t \tag{4.17}$$

where $P_{n_m,p,t}$ and $Q_{n_m,p,t}$ are the active and reactive power injections at node n_m, phase p, at time t. However, it is important to mention that, in this work, the unbalanced three-phase power flow is solved using OpenDSS, which instead of directly solving (4.16) and (4.17), employs a nodal admittance formulation to model system elements, and a fixed point method to obtain feeder voltages and currents [127], from which the necessary P and Q values can be computed.

The initial step to solve the stochastic problem of the First Stage is to randomly define an initial time, initial SoC, and final time for each EV connected to the distribution feeder nodes. This random allocation was done using PDFs derived from historical data of actual EVs; with this information, the maximum aggregated EV power and the required energy per node for the 24-hour period was determined. Then, the Mixed-Integer Nonlinear Programming (MINLP) model described by equations (4.1)-(4.17) was solved using Matlab's GA solver from the global optimization toolbox [128], and as previously mentioned, the OpenDSS package [127] to solve the power flow constraints, from which the optimal transformer tap and capacitor schedules and the maximum daily peak for each aggregated EV realization can be obtained. The nonconvex MINLP nature of the First Stage problem does not guarantee the optimality of the obtained solution; however, GA approaches have demonstrated to be likely to find solutions that are close to the global optimum due to their search strategy [104]. Moreover, the OpenDSS package is a well-known robust power flow solution tool for distribution systems.

With the previous formulations, and using the GA tool, the solution for a single realization of the EV load and forecast can be obtained in several minutes. Thus, employing a typical MCS for obtaining good expected values and confidence intervals for this optimization model for the different load and EV forecast realizations would take several hours, which is not desirable in practice. To overcome this difficulty, the non-parametric bootstrapping method is used, as proposed in [46]. This method is an alternative to MCS and consists of obtaining a reduced number of samples of the population, much smaller than the number required in an MCS, and using random sampling with replacement over these samples to obtain the statistics of a stochastic population. In this work, the aforementioned procedure to solve the First Stage optimization problem is repeated for 30 different EV load realizations, after which the non-parametric bootstrapping method is used to determine the best estimate of the maximum daily peak and the hourly tap and capacitor schedules considering EV uncertainties, as other loads are assumed here to be known, without loss of generality.

4.3.2 Second Stage

The tap and capacitor schedules, and maximum peak demand calculated in the First Stage are used as inputs in the Second Stage, which allocates the aggregated EV active and reactive power set-points, considering MV feeder constraints, every 5 minutes. This allocation is done in such a way that EVs will be able to charge in a fast and fair manner, while providing support to the grid by injecting or absorbing reactive power. In this context, the following three objective functions are proposed:

1. The first objective function is intended to allocate power in a fair manner and minimize voltage deviations:

$$\max \left(\alpha \sum_{n_m} \log \left(\frac{P_{n_m,t}^{agev}}{\overline{S_{n_m,t}^{agev}}} \right) - \beta \sum_{n_m} 100 \left(V_{n_m,t} - 1 \right)^2 \right) \forall t \tag{4.18}$$

where α and β are weight factors for the two components of the objective function. The fair allocation is done by maximizing the product of the ratios of EV active power at each node to the maximum EV charger capacity. In order to avoid scaling problems when many nodes are considered, the logarithm function is applied to the product, obtaining a summation function. The voltage deviation minimization is done by introducing the node voltage differences with respect to 1 p.u. in the maximization function. A coefficient is added for the purpose of objective function scaling.

This objective function is proposed to improve the voltage quality using the reactive power capacity of EV chargers. Since transformer taps and switched capacitors are kept constant at the position determined in the first stage, EVs provide in this case extra regulation to improve the voltage profile either by absorbing or injecting reactive power. In this case, the control of reactive power considers the combined effect on the voltages throughout the feeder by minimizing all deviations with respect to a voltage threshold.

2. In the second objective function, the aggregated EV active power is fairly allocated among the nodes, and the losses are minimized by introducing the differences between the sending and receiving end active power flows in all feeder lines in the objective function to be maximized:

$$\max \left(\alpha \sum_{n_m} \log \left(\frac{P_{n_m,t}^{agev}}{\overline{S_{n_m,t}^{agev}}} \right) - \beta \sum_{l_m} \left(P_{l_m,s,p,t} - P_{l_m,r,p,t} \right)^2 \right) \forall t \tag{4.19}$$

where $P_{l_m,s,p,t}$ and $P_{l_m,r,p,t}$ represent the active power at the sending and receiving ends of MV distribution lines.

Minimization of losses is a typical objective in volt/var regulation functions, representing a common operational goal of DSOs, which are remunerated through energy tariffs and incentives if they achieve certain loss levels [129]. In this case, EVs inject reactive power to compensate for the reactive power consumption of the base load, and thus, reduce the current in the feeders to reduce power losses. A secondary ef-

fect of this function is an increase in voltage, which may also increase the base-load energy consumption, especially in residential feeders [5].

3. The third objective function, which is referred to in this thesis as voltage droop, maximizes the sum of the proportional fairness function and the aggregated EV droop constants, represented as $K^{agev}_{n_m,t}$:

$$\max \left(\alpha \sum_{n_m} \log \left(\frac{P^{agev}_{n_m,t}}{\overline{S^{agev}_{n_m,t}}} \right) + \beta \sum_{n_m} K^{agev}_{n_m,t} \right) \ \forall t \tag{4.20}$$

$$Q^{agev}_{n_m,t} = K^{agev}_{n_m,t} \left(V_{n_m,t} - 1 \right) \ \forall n_m, \forall t \tag{4.21}$$

$$0 \leq K_{n_m,t} \leq \frac{\overline{Q^{agev}_{n_m,t}} - \underline{Q^{agev}_{n_m,t}}}{1.04 - 0.96} \tag{4.22}$$

Equations (4.21) and (4.22) force the aggregated EV chargers to inject or absorb reactive power proportionally to the differences between the node voltages and 1 p.u. The voltage limits used to calculate the droop constants upper limit are chosen to be 1.04 and 0.96 p.u., which are within the tolerance band of ±6% for MV systems, established in Canadian standards [130].

Objective function (4.20) also provides extra voltage regulation to the feeder by injecting or absorbing reactive power, but it is different from the first objective in the sense that it only follows the local voltage signals, as in the case of the voltage droop functions in power converters [131]. The droop coefficients are treated as variables that are maximized in this case to obtain a reactive power injection from the chargers to properly regulate local voltages, thus allowing the sensitivity of aggregated EV chargers to change in every time step to supply maximum available reactive power.

The formulation of this stage considers unbalanced voltages and currents in distribution lines, using ABCD parameters in a per-phase formulation, as follows:

$$\begin{bmatrix} \bar{V}_{s,p,t} \\ \bar{I}_{s,p,t} \end{bmatrix} = \begin{bmatrix} A & B \\ C & D \end{bmatrix} \begin{bmatrix} \bar{V}_{r,p,t} \\ \bar{I}_{r,p,t} \end{bmatrix} \ \forall l_m, \forall p, \forall t \tag{4.23}$$

Voltage and current expressions for loads correspond to a constant impedance model, as follows:

$$V_{L_m,p,t} = Z_{L_m,p,t} I_{L_m,p,t} \ \forall L_m, \forall p, \forall t \tag{4.24}$$

EV constraints, which include calculation of active and reactive powers for the aggregated EV loads, are represented as:

$$P^{agev}_{n_m,t} = Re\left\{\sum_p V_{n_m,t} I^{*agev}_{n_m,p,t}\right\} \ \forall n_m, \forall t \tag{4.25}$$

$$Q^{agev}_{n_m,t} = Im\left\{\sum_p V_{n_m,t} I^{*agev}_{n_m,p,t}\right\} \ \forall n_m, \forall t \tag{4.26}$$

In addition, the same first-stage constraints of active and reactive power limits imposed by the aggregated EV charger capacity (4.5)-(4.8) are included, and current balance at each node, which relates the currents in the lines, transformers, capacitors, loads and aggregated EV loads, are considered, as follows:

$$\begin{aligned}\sum_{l_m,r_{n_m}} I_{l_m,r_{n_m},p,t} = \sum_{l_m,s_{n_m}} I_{l_m,s_{n_m},p,t} + \sum_L I_{L_{n_m},p,t} + \\ \sum_C I_{C_{n_m},p,t} + \sum_{n_m} I^{agev}_{n_m,p,t} \ \forall n_m, \forall p, \forall t\end{aligned} \tag{4.27}$$

Finally, voltage limits for MV nodes (4.13), current limits for distribution lines (4.14), and power limits for each node (4.15), which reflect the capacity of the MV/LV transformer at each node are considered, plus the maximum peak demand constraint, which is obtained from running the First Stage model, which is modeled as follows:

$$\sum_{n_m} \left(P^{bl}_{n_m,t} + P^{agev}_{n_m,t}\right) \leq P_{max} \ \forall t \tag{4.28}$$

The Second Stage formulation is non-linear, with no integer constraints, since the tap and capacitor positions are kept unchanged according to the schedule found in the First Stage. Hence, this stage represents a Non-linear Programming (NLP) problem, which was readily coded in GAMS, and efficiently solved using the SNOPT solver [108].

4.3.3 Third Stage

Once the aggregated EV active and reactive powers are calculated, these signals are sent to the Third Stage, which allocates them among the EVs connected in the downstream LV system. In this stage, the allocation is done using the same fair approach as in the Second Stage. Given that the intention here is to disaggregate active and reactive power set-points, the objective function used for all cases is the following:

$$\max \sum_{ev=1}^{nev_{n_m,t}} \log\left(\frac{P_{ev,t}}{Cr_{ev}}\right) \forall t \tag{4.29}$$

The mathematical model of the Third Stage considers the following constraints:

- Voltages and currents in LV lines:

$$\begin{bmatrix} \bar{V}_{s,p,t} \\ \bar{I}_{s,p,t} \end{bmatrix} = \begin{bmatrix} A & B \\ C & D \end{bmatrix} \begin{bmatrix} \bar{V}_{r,p,t} \\ \bar{I}_{r,p,t} \end{bmatrix} \ \forall l_l, \forall p, \forall t \tag{4.30}$$

- Voltage and current relationship for impedance load models:

$$V_{L_l,p,t} = Z_{L_l,p,t} I_{L_l,p,t} \ \forall L_l, \forall p, \forall t \tag{4.31}$$

- EV active and reactive powers:

$$P_{ev,t} = Re\left\{\sum_{p} V^{ev}_{n_l,t} I^{*ev}_{n_l,p,t}\right\} \ \forall ev = 1, .., nev_{n_m}, \forall t \tag{4.32}$$

$$Q_{ev,t} = Im\left\{\sum_{p} V^{ev}_{n_l,t} I^{*ev}_{n_l,p,t}\right\} \ \forall ev = 1, .., nev_{n_m}, \forall t \tag{4.33}$$

- The limits of active and reactive power for individual chargers:

$$0 \leq P_{ev,t} \leq Cr_{ev} \ \forall ev = 1, .., nev_{n_m}, \forall t \tag{4.34}$$

$$-Cr_{ev} \leq Q_{ev,t} \leq Cr_{ev} \ \forall ev = 1, .., nev_{n_m}, \forall t \tag{4.35}$$

$$P_{ev,t}^2 + Q_{ev,t}^2 \leq Cr_{ev,t}^2 \ \forall ev = 1, .., nev_{n_m}, \forall t \tag{4.36}$$

- The following constraint guarantees that the sum of individual EVs' allocated active and reactive powers is equal to the aggregated set-points:

$$\sum_{ev=1}^{nev_{n_m}} P_{ev,t} = P_{n_m,t}^{agev} \tag{4.37}$$

$$\sum_{ev=1}^{nev_{nm}} Q_{ev,t} = Q_{n_m,t}^{agev} \tag{4.38}$$

- The formulation of this stage also considers the current balance constraints:

$$\sum_{l_l,r_{n_l}} I_{l_l,r_{n_l},p,t} = \sum_{l_l,s_{n_l}} I_{l_l,s_{n_l},p,t} + \sum_{L} I_{L_{n_l,p,t}} + \sum_{n} I_{n_l,p,t}^{ev} \ \forall n_l, \forall p, \forall t \tag{4.39}$$

  and limits of node voltages and distribution line currents:

$$\underline{V_{n_l}} \leq V_{n_l,t} \leq \overline{V_{n_l,t}} \ \forall n_l, \forall t \tag{4.40}$$

$$0 \leq I_{l_l,p,t} \leq \overline{|I|_{l_l,p,t}} \ \forall l_l, \forall p, \forall t \tag{4.41}$$

The Third Stage is also an NLP problem, which was coded in GAMS and solved using the SNOPT solver [108].

In every time step, after allocating the individual P and Q set-points for each EV, the SoC is calculated using the following equation:

$$SoC_{ev,t} = SoC_{ev,t-1} + \frac{P_{ev,t} \ \tau_2}{Bc_{ev}} \ \forall t \tag{4.42}$$

where τ_2 is the Second Stage time step. If the SoC of an EV battery pack reaches 80%, P is not allocated for that EV in the next time steps, but Q is assumed to be available until the EV is no longer connected. This upper SoC limit is recommended by several EV manufacturers to extend battery life [132].

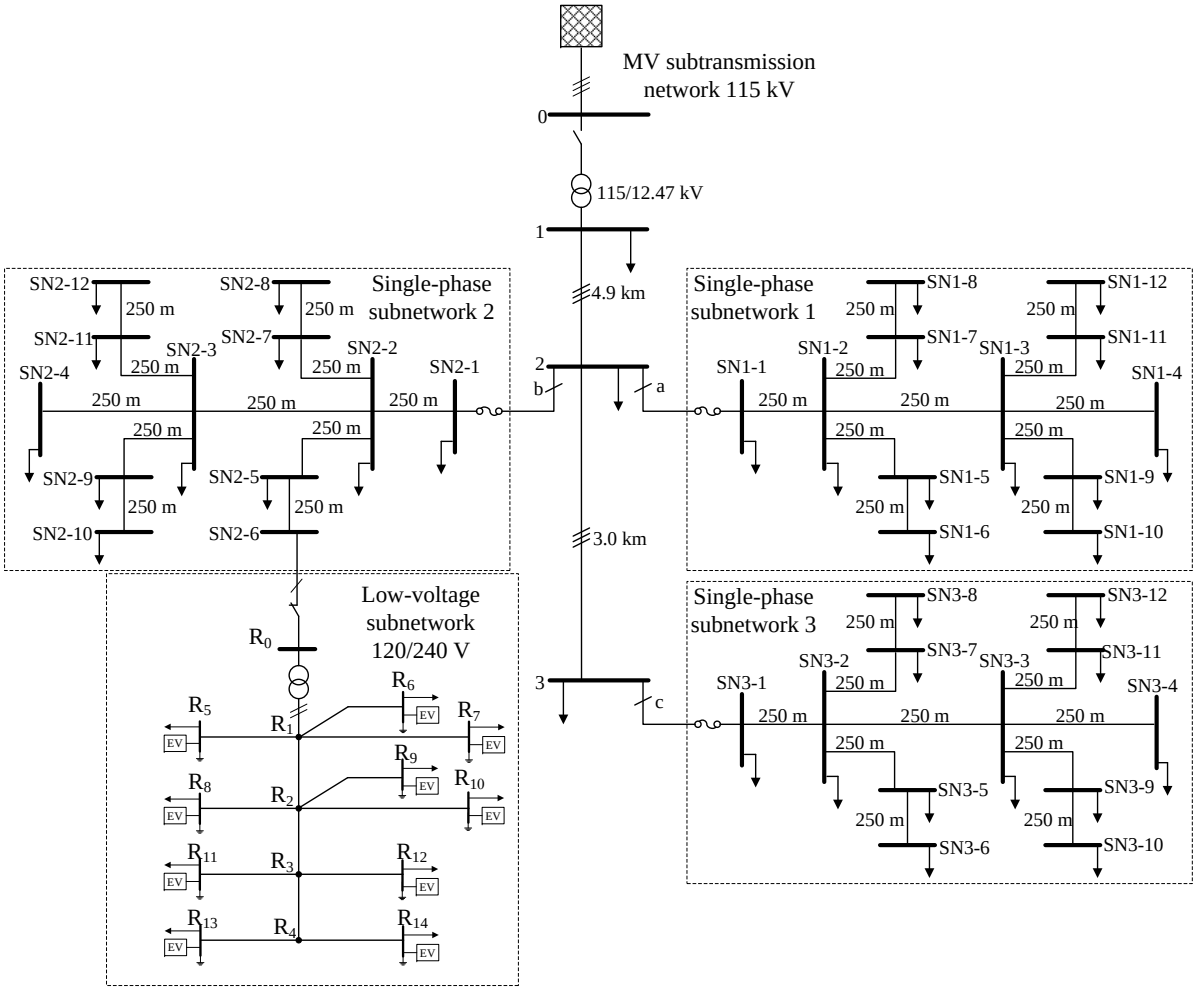

Figure 4.3: MV and LV test systems.

4.4 Simulation results and analysis

4.4.1 Input Data, Test Systems, and Assumptions

The algorithms explained in the previous sections were tested on a CIGRE's MV benchmark system [125]. The original benchmark system has a meshed feeder and a radial feeder; in this study, only the more typical radial feeder shown in Figure 4.3 was considered. This is a 12.47 kV feeder and has a length of 7.9 km. Three single-phase subfeeders, all having

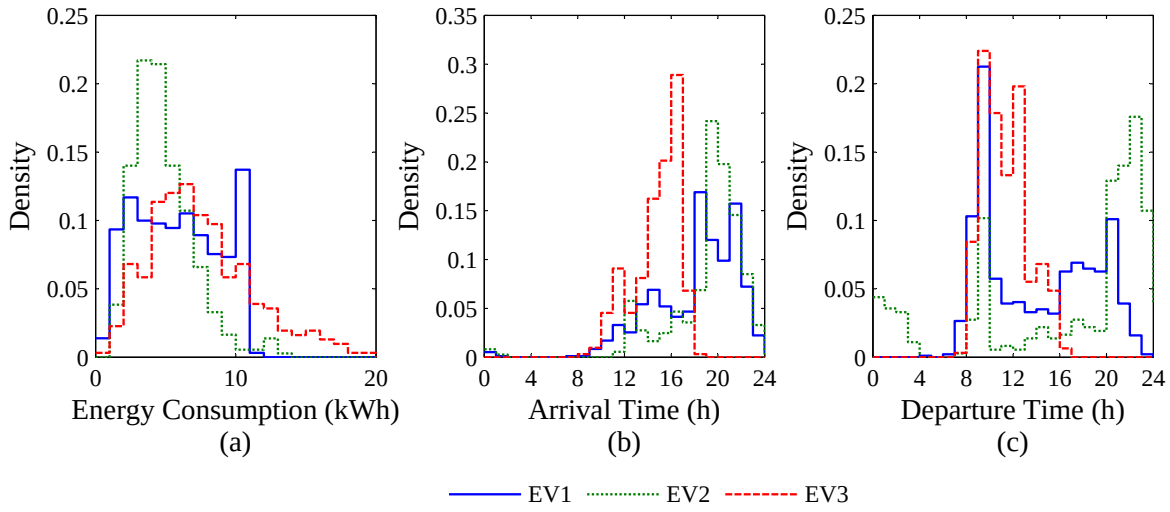

Figure 4.4: (a) Energy consumption, (b) arrival time, and (c) departure time histograms for the three EVs considered.

the same topology, are connected to the main feeder at different nodes and phases, and one subfeeder is modeled as an equivalent load at the first node.

In order to test the Third Stage of the algorithm, which operates at the LV level, the CIGRE's North American LV benchmark system from [125] was employed. This LV feeder is composed of a 50 kVA, 12.47/240-120 V transformer, and 10 residential loads, as shown at node SN2-6 in Figure 4.3. All original loads at nodes SN1-6, SN1-7, SN1-9, SN2-6, SN2-7, SN2-9, SN3-6, SN3-7, and SN3-9 in Figure 4.3 were replaced with this LV test feeder; due to space constraints, only the LV system of node SN2-6 is shown. The demand at each MV node that is not replaced by an LV system, follows the respective curves and peak values presented in [125] for the MV benchmark system; for those nodes modeled with the full LV system, the demand follows the individual household loads included in the report. Based on this, the peak base loads for the MV and individual LV systems are approximately 6000 kVA and 47 kVA, respectively, which corresponds to the original load of the benchmark system.

EVs are modeled using the actual data collected for three EVs operated in the region of Waterloo, Ontario, Canada, in a period of seventeen months[1]. These vehicles have been selected since they represent two of the bestselling EVs in Canada, and have the

[1]The data was collected through the Drive4Data program, led by the Waterloo Institute for Sustainable Energy (WISE). More information is available at https://wise.uwaterloo.ca/drive4data.

largest number of charging events for a coincident period of time in the database. The information used in this study included the consumed electricity between charging events, the arrival time, which determines the starting time for charging, and the departure time, which determines the maximum duration of the charging. Table 4.1 presents the main data for the 3 EVs considered in the study, and Figure 4.4 depicts the corresponding histograms of energy consumption, and arrival and departure times. EV chargers for this study are assumed to be rated at 3.3 kVA.

The original benchmark system considered in this study does not contain information about the number of households representing the residential loads; hence, it is assumed here that a household has a 5 kVA peak load, as per [133], and that there is an EV for each residence. Based on this assumption, Table 4.2 presents the number of EVs assumed to be connected to each node of the MV system. For the LV systems modeled, it is also assumed that each household has an EV.

An existing heuristic EV charging control method was implemented, based on the calculation of sensitivities of node voltages to active and reactive power, and the use of an LC to control the taps in the substation transformer; this heuristic technique is based on EV charging approaches described in [29] and [42]. The sensitivity factors are calculated by simulation, using dummy loads of 1 kW and 1 kVAR, which are placed at each one of the distribution system nodes to evaluate the change in voltages at all the nodes. The allocation of aggregated EV active and reactive power is done based on the following expressions:

$$P_{n_m,t}^{agev} = \min\left(\gamma \frac{\Delta V_{k,t}}{\max\left(\frac{\Delta V_{k,t}}{\Delta P_{n_m,t}}\right)}, \overline{P_{n_m,t}^{agev}}\right) \tag{4.43}$$

$$Q_{n_m,t}^{agev} = \min\left(\gamma \frac{\Delta V_{k,t}}{\max\left(\frac{\Delta V_{k,t}}{\Delta Q_{n_m,t}}\right)}, \overline{Q_{n_m,t}^{agev}}\right) \tag{4.44}$$

where γ represents a scaling factor, which in this case is equal to 0.1; $\max\left(\frac{\Delta V_{k,t}}{\Delta P_{n_m,t}}\right)$ and $\max\left(\frac{\Delta V_{k,t}}{\Delta Q_{n_m,t}}\right)$ represent the maximum sensitivity factors of all node voltages with respect to active and reactive power changes; and $\Delta V_{k,t}$ represents the desired voltage deviation at the node where the maximum sensitivity is recorded, and is calculated as follows:

$$\Delta V_{k,t} = \underline{V_{k,t}} - V_{k,t}^{bl} \tag{4.45}$$

where V_k^{bl} is the voltage at the k^{th} node calculated at the base load conditions and no EVs.

The current EV charging and feeder voltage control approach is also considered here for comparison purposes, and is referred to as Business-as-Usual (BAU). In this case, taps and capacitors are automatically controlled to keep the voltage at a certain point in the feeder fixed using an LC control, allowing EVs to absorb their maximum P and Q capacities, i.e., $\overline{P_{n_m,t}^{agev}}$ and $\overline{Q_{n_m,t}^{agev}}$, until fully charged.

Table 4.1: EV Database Summary

	EV model	Battery capacity (kWh)	Datalogging interval	# of charging events	Electricity consumed (kWh)
EV1	Chevy Volt '12	16	03/10/2014 - 08/14/2015	941	5078.05
EV2	Nissan Leaf '12	24	03/10/2014 - 08/14/2015	364	1589.78
EV3	Ford Focus EV '14	23	03/10/2014 - 08/14/2015	309	2143.39

Table 4.2: Number of EVs per MV node

MV node	# of EVs/node
SN1-5, SN1-8, SN1-11, SN1-12, SN2-5, SN2-8 SN2-11, SN2-12, SN3-5, SN3-8, SN3-11, SN3-12	2
SN1-1, SN1-2,SN1-3, SN1-4, SN1-10, SN2-1, SN2-2,SN2-3, SN2-4, SN2-10, SN3-1, SN3-2,SN3-3, SN3-4, SN3-10	3
SN1-6, SN1-7,SN1-9, SN2-6, SN2-7, SN2-9, SN3-6,SN3-7, SN3-9	10
1	636

4.4.2 Simulation Results

First, the 3 EV models described in Table 4.1 were evenly assigned to the nodes of the test system, considering the number of EVs per node described in Table 4.2, and 30 EV scenarios were created by randomly selecting one of the charging events available in the

EV database. Each of these EV scenarios were then applied to the test system, and the First Stage optimization model was solved for each scenario, considering a full day and 1-hour time steps ($\tau_1 = 1$ hr). Then, 15000 bootstrapping samples were obtained from the 30 original samples of optimal maximum demand and optimal tap position for each hour. Figure 4.5 presents the feeder maximum demand histograms for the entire day, before and after applying the nonparametric bootstrapping method. Figure 4.5(a) shows the original sample histogram, Figure 4.5(b) presents the histogram of the mean maximum demand after applying bootstrapping on the original sample, and Figure 4.5 (c) depicts the histogram of the bootstrapping points (15000×30 resamples). The shape of Figure 4.5(a) and Figure 4.5(c) are very similar, because of the high number of resamples in the bootstrapping process, with the tails of the original data set appearing in the bootstrapping histogram. The shape of Figure 4.5(b) histogram is close to a normal distribution, from which the expected value and the confidence interval of the systems mean maximum demand can be calculated. Based on the bootstrap histogram of Figure 4.5(b), the confidence interval of the mean peak demand is $CI_{(95.4\%)} = [6.3093 \text{ MW}, 6.3573 \text{ MW}]$, which is a narrow interval that guarantees that the mean approximation is close to the population mean. The mean peak demand $P_{max} = 6.3333$ MW is then applied to the second stage.

Figure 4.6(a) depicts the substation LTC tap positions for the 24-hour period after applying bootstrapping to the original sample. The solid line represents the average tap position from bootstrapping, and the error bars correspond to a confidence interval of 95.45%, or two standard deviations from the mean. The dotted blue line represents the final tap positions after rounding the average values to integer values in order to apply them to the real system. The solution for each EV realization took on average 19 minutes, using Matlab 8.3.0.532 (R2014a) running in an Intel(R) Core(TM) i7-4770 CPU at 3.40Ghz. Hence, the full solution for the First Stage took about 9.5 hours. Considering that this process is performed off-line the day before, these computational times allow for the practical application of this technique. However, these times can be significantly reduced if parallel computation approaches are used, since this stage can be readily parallelized as discussed in [46]. Figures 4.6(b) and 4.6(c) show the tap positions for the Heuristic and the BAU methods. In both cases, the LC was set to regulate the voltage at Node 3c in the main feeder to 0.99 p.u., with a band of 0.025 p.u; this voltage was chosen to obtain a total energy consumption similar to the optimization scenarios. Note that in these cases, the tap operation is more frequent compared to the First Stage results (22 and 23 operations in the Heuristic method and the BAU, respectively, and 7 in the proposed approach), so that the voltage is kept within the required range.

The Second Stage was tested by using one of the EV scenarios from the First Stage, using the tap positions calculated in the First Stage as fixed parameters for the Second

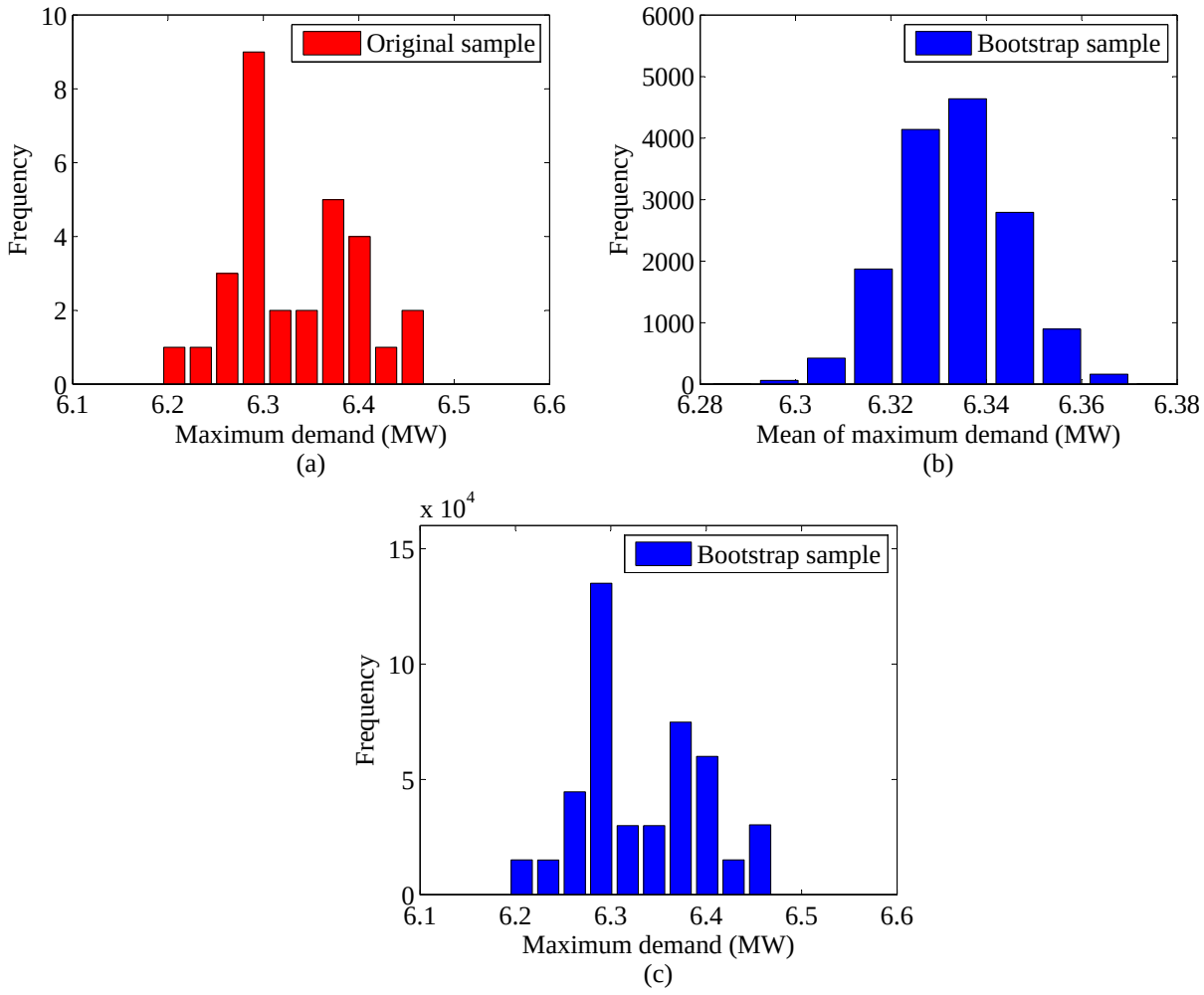

Figure 4.5: Maximum demand histogram for (a) the original sample, (b) the bootstrap mean, and (c) the bootstrap sample.

Stage model. This stage was solved for five-minute periods (τ_2=5min) using the objective functions defined in (4.18)-(4.20); hence, 288 optimization runs were performed to complete a full day. Additionally, to test the sensitivity of the Second Stage results to the weights between the EV battery charging and the provision of reactive power, the following three sets of weights were used in functions (4.18)-(4.20); α=0.9 and β=0.1; α=0.5 and β=0.5, and α=0.1 and β=0.9. The case referred hereafter as No Q control corresponds to the case in which only the control of EV active power is available, setting the EV reactive

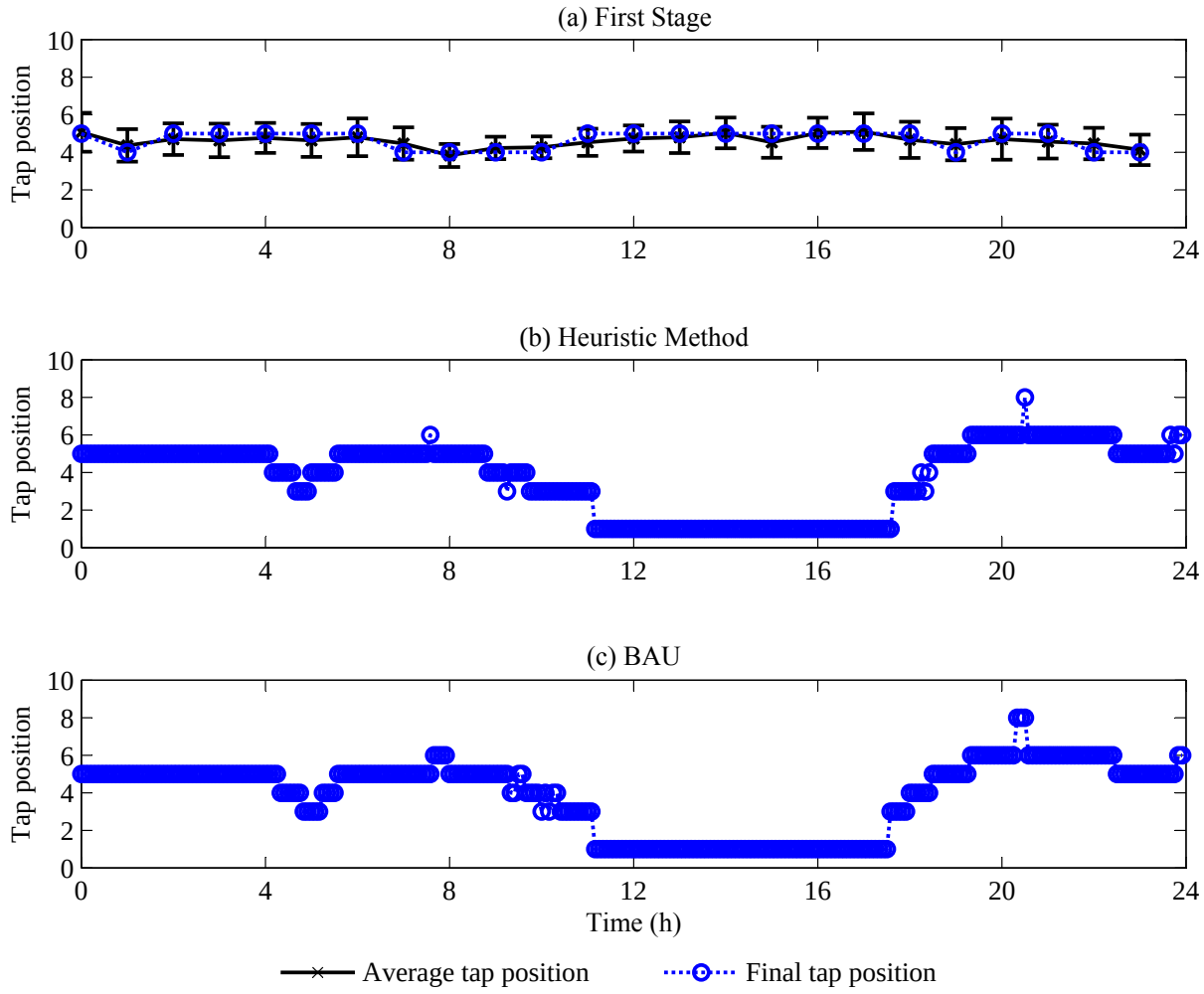

Figure 4.6: Tap simulation results.

power variables to zero, and using the weights α=1 and β=0 in the second stage objective functions.

The voltages in the MV system are depicted in Figure 4.7. Observe that for the three proposed optimization functions and no Q control, voltages are similar because they use the same tap schedule, but they tend to be higher when losses are minimized. In the Heuristic and BAU methods, the voltages are flatter compared to other cases, since taps are operated continuously to keep the voltage within a given range. In all methods, the voltages are within the defined limits (0.96-1.04).

The resulting allocations of aggregated EV active and reactive powers for nodes SN1-7, SN2-10, and SN3-12 are presented in Figure 4.8; these three nodes were selected since they are representative of different phases, demands, and number of EVs. For the three optimization functions, only the results of the pair of weights that lead to a faster EV charging are presented. These plots show that aggregated EV active power is limited during times of peak demand due to LV transformer power limits. The sharp changes in P and Q in the plots are due to EVs arriving or leaving. Furthermore, reactive power is positive most of the time for minimization of voltage deviation and voltage droop, because EV chargers try to lower the voltage, and negative for minimization of losses, since in this case the voltage is used to lower the currents and reduce losses. Each of these simulations took approximately 1.8 seconds, which demonstrates the practical feasibility of the proposed method for real-time applications. In the Heuristic method, P and Q are limited at times that do not necessarily coincide with the load peak in the corresponding LV system, thus leading to the transformer overloading. In the BAU method, this happens more often since vehicles are always allocated their maximum P and Q. This issue can be seen clearly in Figure 4.9 at node SN3-12, around hour 6, where the optimization methods reduce the EV active power, but the Heuristic and BAU methods fully allocate the available capacity, overloading the corresponding MV/LV transformers.

Table 4.3 shows the summary of the simulation results, including the total energy consumed by the EV fleet, the total energy losses, the total energy consumed in the system, and the deviation of voltages with respect to 1 p.u. as per:

$$VD = \sqrt{\frac{1}{NT}\sum_{t=1}^{T}\sum_{k=1}^{N}(V_{k,t}-1)^2} \tag{4.46}$$

The total energy losses in Table 4.3 are composed of the losses illustrated in Table 4.4, which include the losses in MV lines, losses in the LV systems modeled in detail to test the third stage, losses in the equivalent loads along the feeder and at Node 1, and losses of the substation transformer. The losses in MV lines, the LV systems modeled in detail, and the substation transformer can be obtained directly from the simulation results; for the equivalent loads connected along the feeder, the losses were estimated using the percentage of losses from the LV systems modeled in detail for the third stage, and for the equivalent load at Node 1, they were estimated with the percentage of losses of the MV feeder. These different losses and the corresponding percentages for all test cases are shown in Table 4.5.

From the results in Table 4.3, it can be seen that the minimization of voltage deviation scenarios present a lower EV energy with respect to the No Q control. The minimization of

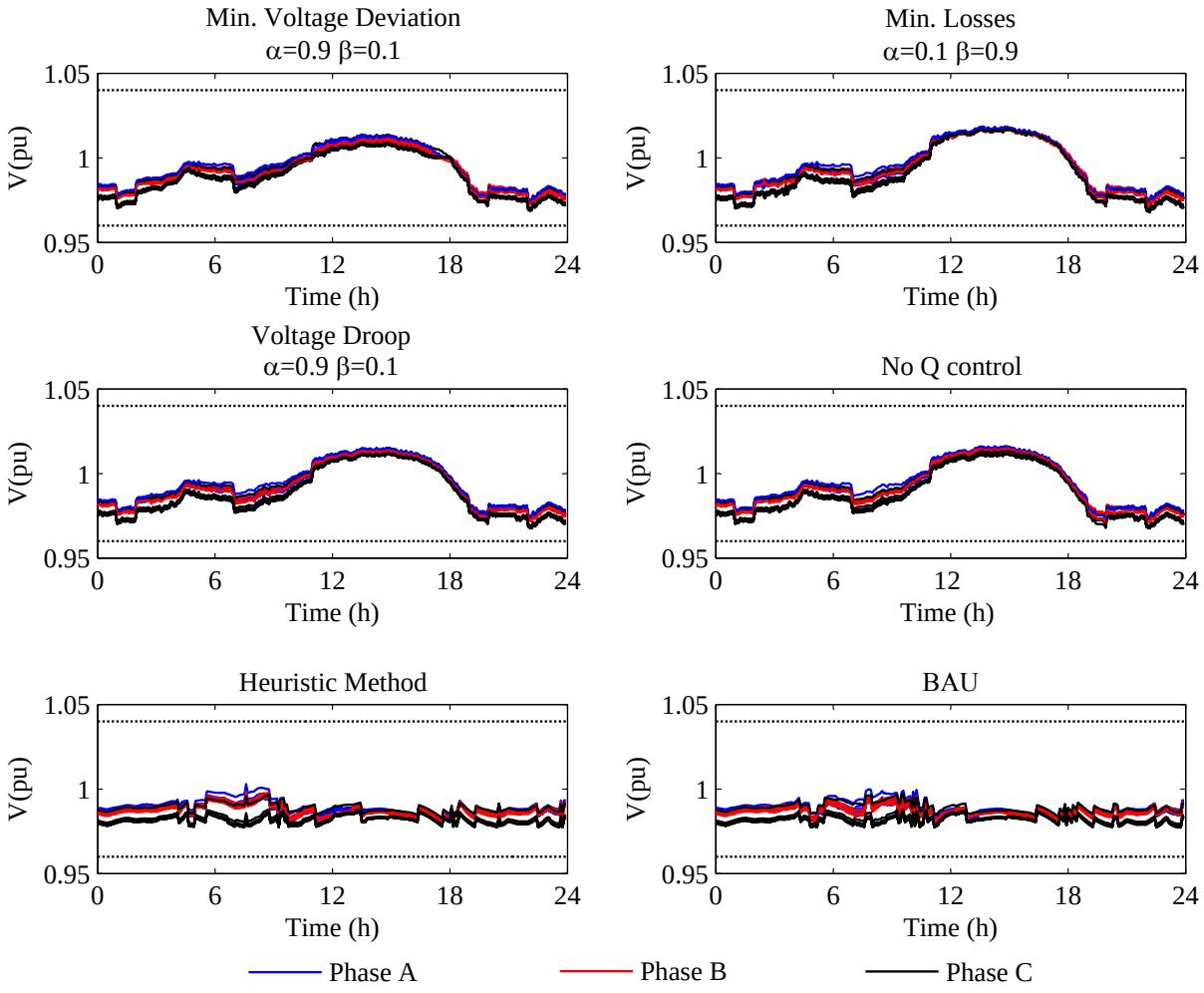

Figure 4.7: Voltages in MV system

losses scenarios also exhibit a lower EV energy, but with smaller differences. The voltage droop scenarios present the largest difference, and also the only scenario in which EV energy consumption is higher than the No Q control case. The results obtained for the Heuristic and BAU methods are very close to those of the No Q control case.

The results for energy losses in Table 4.3 show the largest reduction for the minimization of losses for α=0.1 and β=0.9, with respect to the No Q control case. Some optimization cases present an increase in total losses with respect to the No Q control case, due to the additional losses in the LV systems, produced by the injection or absorption of reactive

Table 4.3: Energy Consumption Results

	EV Energy kWh	Total Energy Losses kWh	Total Energy kWh	VD
BAU	6,065.86	3,334.06	110,651.35	1.77%
Heuristic method	5,989.62	3,070.48	110,540.44	1.76%
No Q control (α=1 β=0)	6,097.62	2,864.54	110,403.48	1.65%
Min. Voltage deviation (α=0.9 β=0.1)	5,449.71 (-10.63%)	3,008.73 (+5.70%)	109,790.72 (-0.56%)	1.46% (-0.19%)
Min. Voltage deviation (α=0.5 β=0.5)	5,237.27 (-14.11%)	2,935.84 (+3.14%)	109,583.29 (-0.74%)	1.44% (-0.21%)
Min. Voltage deviation (α=0.1 β=0.9)	5,717.01 (-6.24%)	2,823.57 (-0.81%)	110,077.03 (-0.30%)	1.40% (-0.25%)
Min. Losses (α=0.9 β=0.1)	5,908.95 (-3.09%)	2,901.95 (+1.95%)	110,256.31 (-0.13%)	1.65% (0.00%)
Min. Losses (α=0.5 β=0.5)	6,026.83 (-1.16%)	2,772.04 (-2.62%)	110,400.31 (0.00%)	1.60% (-0.05%)
Min. Losses (α=0.1 β=0.9)	5,952.69 (-2.38%)	2,736.83 (-3.85%)	110,327.14 (-0.07%)	1.59% (-0.06%)
Voltage Droop (α=0.9 β=0.1)	6,234.25 (+2.24%)	2,806.44 (-1.41%)	110,559.84 (+0.14%)	1.56% (-0.09%)
Voltage Droop (α=0.5 β=0.5)	6,091.64 (-0.10%)	2,782.02 (-2.27%)	110,419.69 (+0.01%)	1.55% (-0.10%)
Voltage Droop (α=0.1 β=0.9)	5,142.51 (-15.66%)	2,752.32 (-3.31%)	109,471.21 (-0.84%)	1.54% (-0.11%)

power that are not compensated by the energy loss savings in the MV lines, as seen in Table 4.4. The voltage droop cases, although not presenting the maximum loss reduction, consistently reduce losses for both LV systems and MV lines. It is important to highlight the fact that the losses in the MV lines are particularly low, since the currents in the main feeder and the single-phase sub feeders do not surpass 20% of the conductors' ampacity in all test cases.

The total energy consumption differences with respect to the No Q Control case are small, in a range between -0.85% and +0.12%, which is desirable, as the proposed ap-

Table 4.4: Disaggregation of Energy Losses

	Energy Losses in MV Lines kWh	Total Losses LV Systems Third Stage kWh	Total Losses for Equivalent Loads along the feeder kWh	Total Losses for Equivalent Load at Node 1 kWh	Conduction Losses at Substation Transformer kWh
BAU	198.63	105.06	323.92	2,645.55	60.9
Heuristic method	192.29	92.95	290.42	2,434.36	60.45
No Q control (α=1 $\beta = 0$)	182.53	81.17	268.95	2,255.54	58.35
Min. Volt. deviation (α=0.9 $\beta = 0.1$)	180.71 (-1.00%)	90.04 (+10.93%)	297.7 (+10.69%)	2,385.31 (+5.75%)	54.97 (-5.79%)
Min. Volt. deviation (α=0.5 β=0.5)	177.38 (-2.82%)	87.42 (+7.70%)	289.09 (+7.49%)	2,326.66 (+3.15%)	55.29 (-5.24%)
Min. Volt. deviation (α=0.1 β=0.9)	169.27 (-7.26%)	82.44 (+1.56%)	273.9 (+1.84%)	2,243.27 (-0.54%)	54.69 (-6.27%)
Min. Losses (α=0.9 β=0.1)	175.66 (-3.76%)	85.88 (+5.80%)	284.22 (+5.68%)	2,300.57 (+2.00%)	55.62 (-4.68%)
Min. Losses (α=0.5 β=0.5)	169.5 (-7.14%)	81.44 (+0.33%)	269.79 (+0.31%)	2,195.76 (-2.65%)	55.55 (-4.80%)
Min. Losses (α=0.1 β=0.9)	168.21 (-7.85%)	80.31 (-1.06%)	265.13 (-1.42%)	2,168.07 (-3.88%)	55.11 (-5.55%)
V. Droop (α=0.9 β=0.1)	177.92 (-2.53%)	80.34 (-1.02%)	266.38 (-0.9%)	2,223.54 (-1.42%)	58.26 (-0.15%)
V. Droop (α=0.5 β=0.5)	176.38 (-3.37%)	79.66 (-1.86%)	263.86 (-1.89%)	2,204.07 (-2.28%)	58.05 (-0.51%)
V. Droop (α=0.1 β=0.9)	175.91 (-3.63%)	79.49 (-2.07%)	263.11 (-2.17%)	2,176.34 (-3.51%)	57.47 (-1.51%)

proach should not affect significantly the power consumed by loads and EVs, considering the relatively low system losses, and the small variations in load voltages and EV loads, which account for 5.5% of the total demand. Finally, the minimization of voltage devia-

Table 4.5: Percentage of Losses Used with Equivalent Loads

	Total Energy LV Systems Third Stage kWh	% Losses LV Systems Third Stage	Total Energy Feeder kWh	% Losses Feeder
BAU	5,146.42	2.04	21,218.02	2.96
Heuristic method	5,077.38	1.83	21,141.93	2.72
No Q control (α=1 $\beta = 0$)	4,804.53	1.69	21,090.93	2.53
Min. Volt. deviation (α=0.9 $\beta = 0.1$)	4,823.38	1.87	21,129.16	2.69
Min. Volt. deviation (α=0.5 β=0.5)	4,814.88	1.81	21,071.05	2.63
Min. Volt. deviation (α=0.1 β=0.9)	4,776.32	1.73	20,896.00	2.52
Min. Losses (α=0.9 β=0.1)	4,822.75	1.78	21,141.05	2.58
Min. Losses (α=0.5 β=0.5)	4,823.81	1.69	21,162.58	2.46
Min. Losses (α=0.1 β=0.9)	4,838.31	1.66	21,131.77	2.43
V. Droop (α=0.9 β=0.1)	4,807.53	1.67	21,106.41	2.49
V. Droop (α=0.5 β=0.5)	4,805.89	1.66	21,075.13	2.47
V. Droop (α=0.1 β=0.9)	4,806.2	1.65	21,062.76	2.46

tion scenarios present the lowest voltage deviations, as expected, ranging from 1.40% to 1.46%, while the voltage deviations in the Heuristic and BAU methods are the highest, i.e., 1.76% and 1.77%, respectively. Note that in 6 out of 9 cases, the proposed holistic control approach reduces losses and improves the voltage profiles with respect to previously proposed EV charging control approaches and the existing method (BAU). However, this is accomplished at the expense of reducing the energy delivered to EVs, in a range of 0.1%-15%.

The benefits of Q control, which include the minimization of voltage deviation, the minimization of losses, and the voltage droop scenarios, can be seen in voltage regulation and system losses. The minimization of voltage deviation cases achieve the best voltage regulation for all scenarios, but this is accomplished by increasing system losses. The minimization of losses scenarios, albeit not improving significantly voltage regulation, result in loss reductions of up to 3.85% with respect to the No Q control case. This percentage is comparable to other methods, such as [37], in which losses are reduced by controlling transformer taps and switched capacitors in distribution feeders to minimize the energy drawn from the substation, reporting losses reductions between 0.5% and 6.7%. Finally,

the voltage droop cases improve the voltage regulation and reduce losses with respect to the No Q control case, resulting in a maximum loss reduction of 3.31%, which is close to the percentage achieved in the minimization of loss cases.

Figure 4.10 shows the individual allocation of active and reactive powers of 3 different EVs in the LV network at node SN1-7. These values are in agreement with the Second Stage results; note that the active power for each EV shows some differences with respect to the case with no Q control due to the provision of reactive power. Figure 4.11 presents voltage profiles at all buses in the LV system connected to Node SN1-7, under different control strategies; these are similar in shape to the voltages in the MV network, shown in Figure 4.7, and are within acceptable limits. Finally, Figure 4.12 depicts the SoC curves for several vehicles during the hours the EV is connected to the charger. Observe that these two figures demonstrate that the provision of reactive power to the system has just a small impact on vehicle charging, which may result in the occasional case of the battery not reaching its maximum SoC in the available charging time. The Heuristic method, however, presents a higher delay in reaching the desired SoC since this node voltage, in particular, is more sensitive to load variations, which produces a lower allocation of EV power.

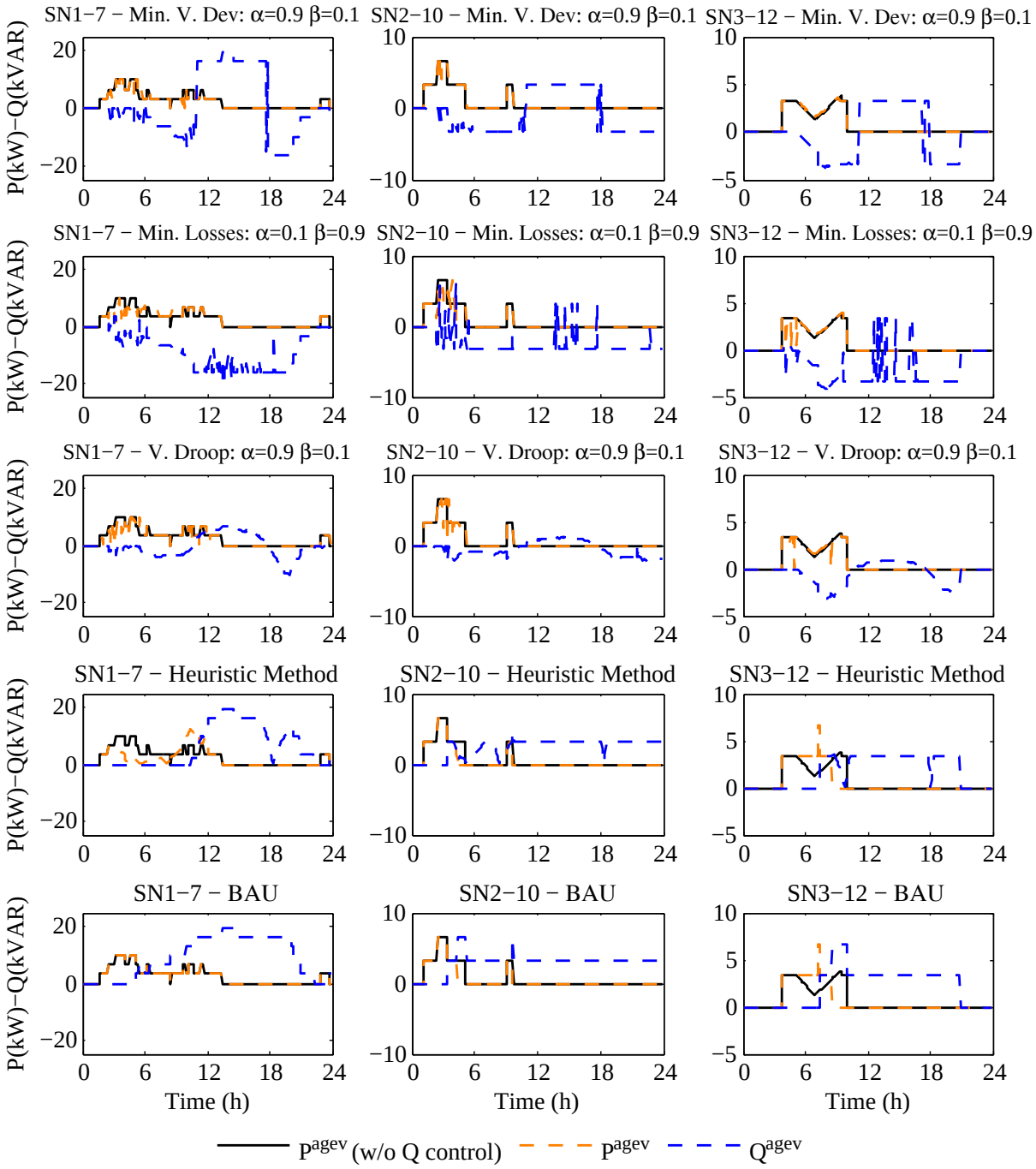

Figure 4.8: Aggregated EV P and Q allocation at nodes SN1-7, SN2-10, SN3-12

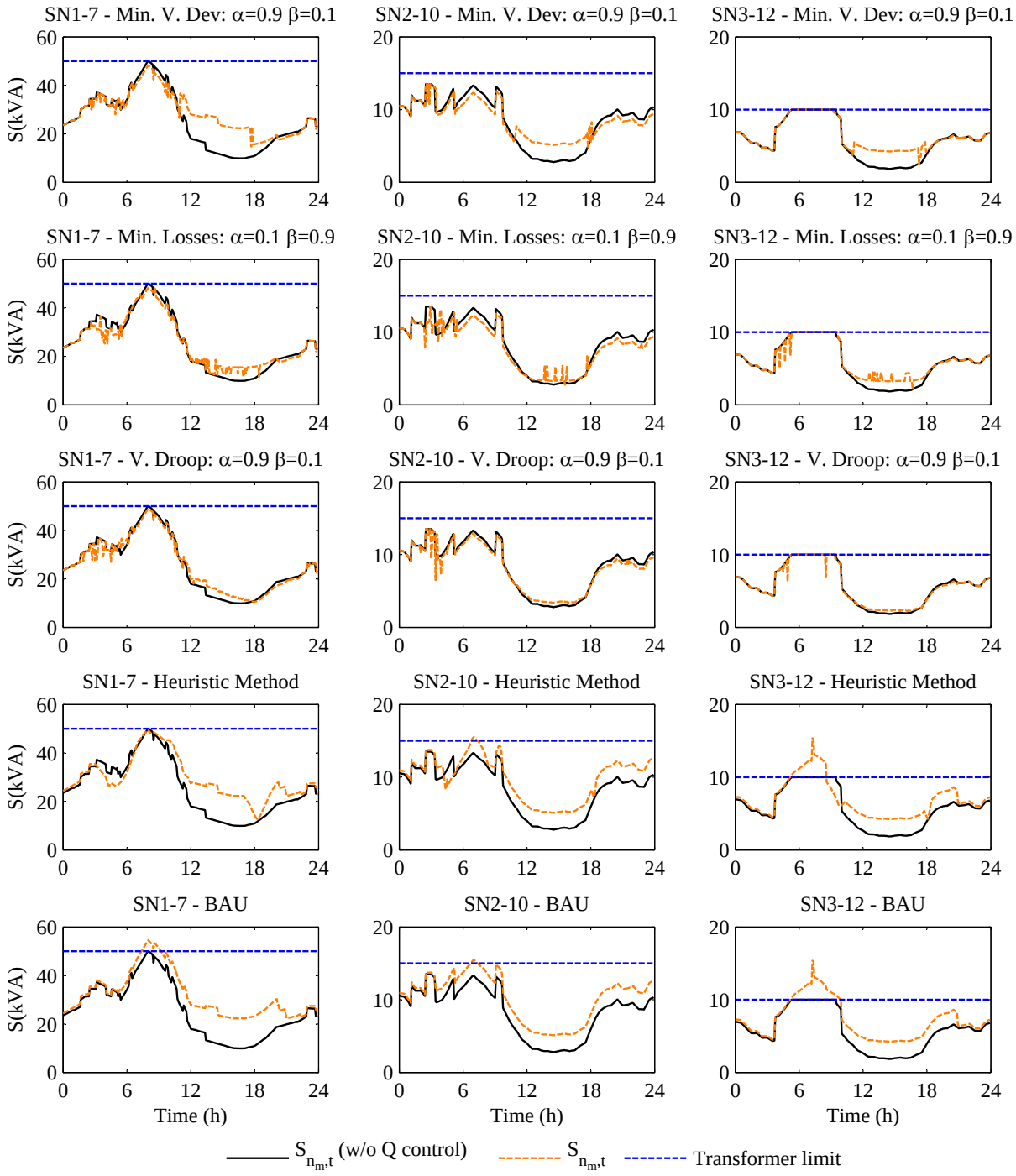

Figure 4.9: Transformer apparent power at nodes SN1-7, SN2-10, SN3-12

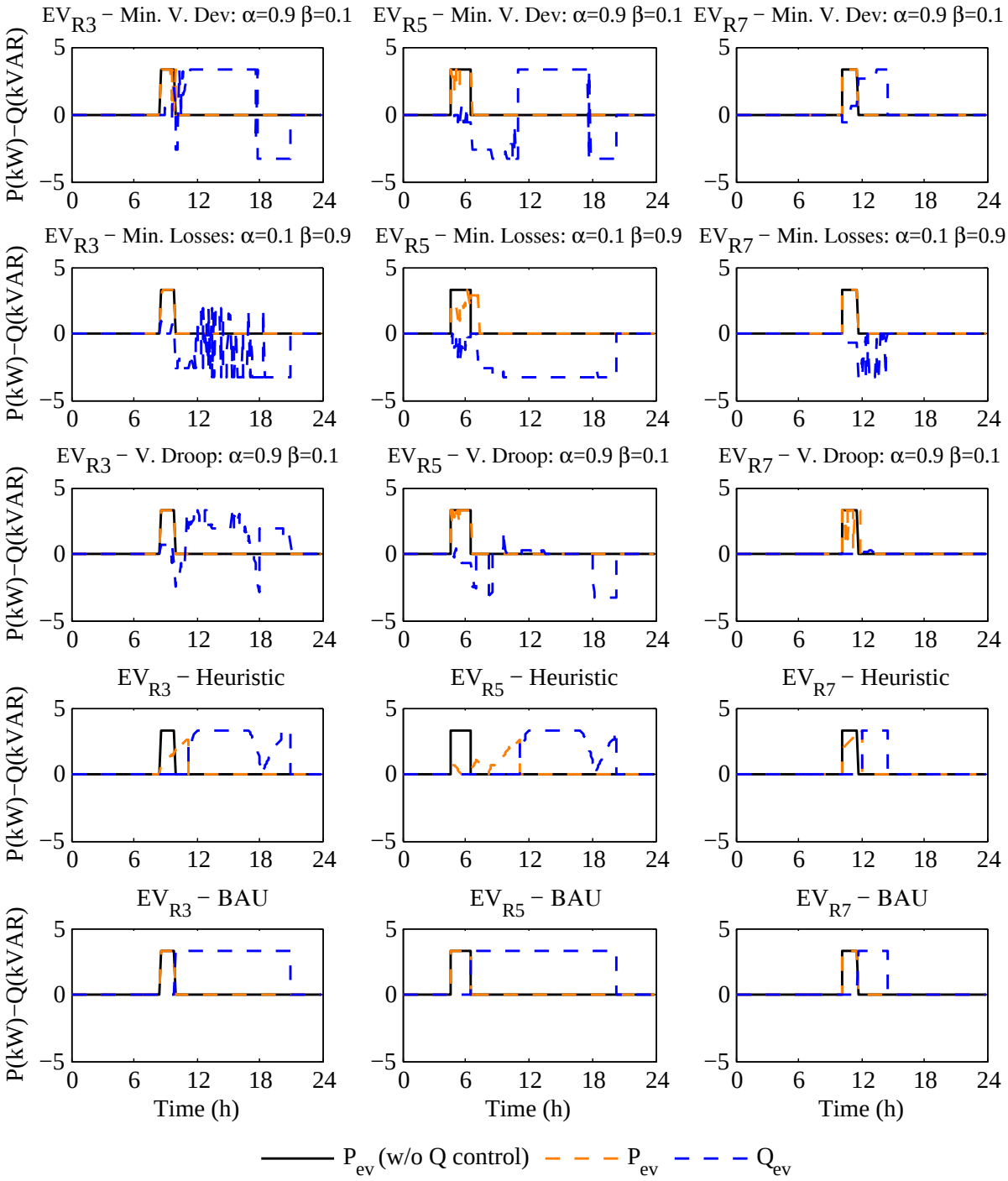

Figure 4.10: Allocation of individual P and Q for EVs at SN1-7

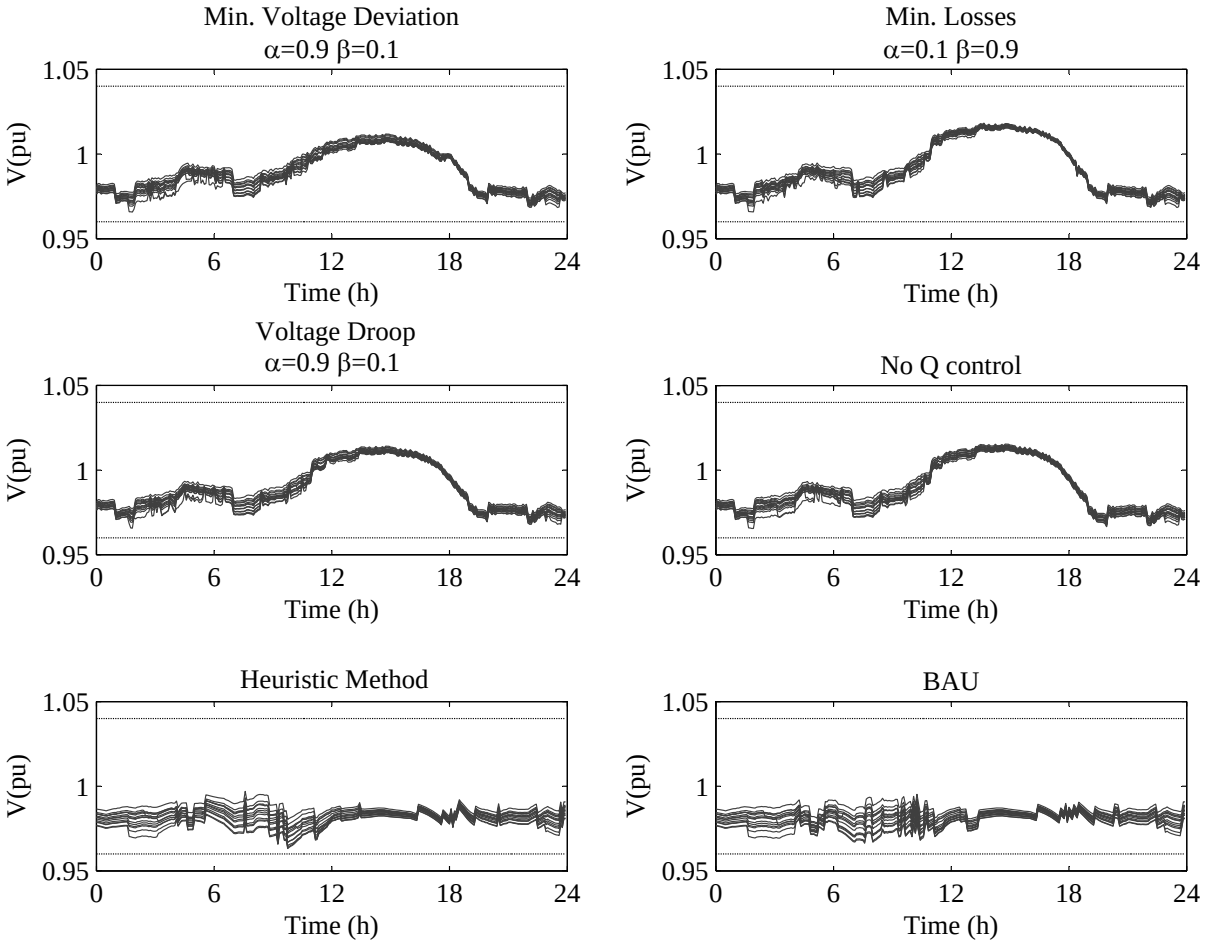

Figure 4.11: Voltages at buses connected to node SN1-7

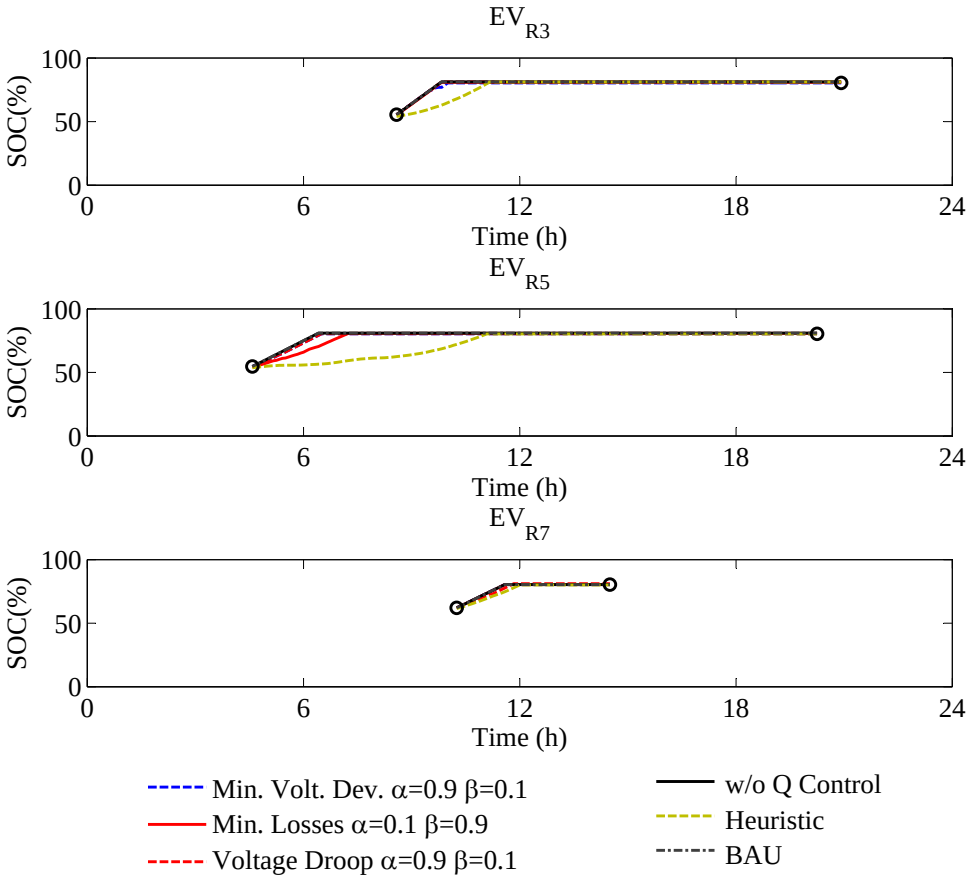

Figure 4.12: SoC of EV batteries at SN1-7

4.4.3 Discussion

So far, very few works have been published on the use of four-quadrant EV chargers to regulate voltage and reactive power in distribution feeders, considering both MV and LV levels. Hence, it is not possible to perform a full techno-economic comparison with respect to other similar works. Nevertheless, an estimation of costs of such a scheme can be obtained by considering that, based on [18], the cost of providing reactive power with a 3.3 kVA EV charger could be equal to 8.4 USD/kVAR per year (this value includes the incremental cost of upgrading a unidirectional ac/dc converter with a full bridge ac/dc converter, and the cost of additional losses), compared to 2.8 USD/kVAR per year for a typical distribution capacitor bank. However, the volt/var control implemented by EV chargers would be distributed, continuous and accurate, in contrast with the case of distribution capacitor banks. Also, the implementation of the proposed holistic approach would reduce the number of transformer taps operations and switched capacitors switchings, thus reducing wear, and hence reducing maintenance costs [126]. Finally, the proposed volt/var control would reduce losses, thus reducing energy loss costs, as with any volt/var control approach in distribution systems [63].

4.5 Summary

This chapter presented a three-stage algorithm for coordinating the operation of four-quadrant EV chargers and other volt/var control equipment in a distribution feeder. First, the proposed three-stage architecture was described, using the outputs of each stage as inputs in the following stages to define the actual set-points for EV chargers at the LV system. Then, the mathematical models describing each stage were introduced. The First Stage included the uncertainties of EV users, and employed a non-parametric bootstrapping technique to calculate the confidence intervals of the optimal expected values for transformer taps, switched capacitors, and peak demand. The Second Stage allocated active and reactive powers for the EV aggregated demand at the MV nodes, using a proportional fairness approach and three different objectives for the volt/var function. The Third Stage distributed the active and reactive power set-points calculated in the Second Stage among the individual EVs connected at the LV network.

The proposed algorithms were tested on realistic CIGRE benchmark test feeders, comparing the results for the different objective functions considered as well as with Heuristic and BAU approaches. The obtained results show that using the proposed technique and the reactive power capacity of EV chargers improves the operation of distribution feeders

by regulating the voltage and reducing losses, without having a significant effect on EV charging levels.

Chapter 5

Conclusions, Contributions and Future Work

5.1 Summary and Conclusions

This work has investigated the integration of four-quadrant EV chargers into distribution feeders, proposing first a model that can be easily used in time-domain simulations to study the dynamic interactions of these chargers in LV distribution networks, and second, a three-stage control strategy to coordinate this type of chargers with other volt/var control devices that typically operate in distribution feeders, such as LTCs and switched capacitors.

In the first main part of this thesis, an average modeling technique was employed to obtain an equivalent circuit of a Level 1, four-quadrant EV charger, which was validated using a charger prototype built in the lab. The average modeling technique was employed because it neglects the high-frequency dynamics related to switching, keeping the low-frequency dynamics necessary to study the interactions between chargers, thus speeding up time-domain simulations. The validation included a comparison of the steady-state behaviors of the average model and the prototype, using different P and Q set-points representing the operation in the four quadrants of the P-Q plane, and a dynamic study which compared P and Q transitions produced by set-point changes. A system integration study was also performed for ten four-quadrant EV chargers connected to a secondary distribution grid, simulating the voltage interactions caused during the EV charging process and the use of four-quadrant EV chargers as active and reactive power sources for three V2G strategies.

In the second main part of the thesis, a three-stage distribution feeder control strategy was proposed as an extension to previous works, adding the modeling of four-quadrant EV chargers as controllable reactive power sources, as well as the provision of reactive power services from aggregated EVs, and allocating the individual EV charger set-points located in the LV network. The first stage of the proposed approach defines, in a day-ahead time frame, the hourly schedules for transformer taps and switched capacitors, minimizing the daily peak load. The solution of the first stage accounts for the uncertainty of EV operation in terms of variables such as arriving time, departure time, and initial SoC, and combines a GA optimization solution approach with a Nonparametric Bootstrap method to obtain the expected values of the decision variables with a limited number of simulations. The second stage keeps the schedules obtained in the first stage unchanged, and allocates every five minutes active and reactive power set-points for the aggregated EV loads; this is accomplished by combining of a proportional fairness method and one of three reactive power control strategies that aim to reduce the voltage deviations and system losses. The third stage disaggregates the set-points obtained in the second stage for individual EVs located in LV networks. The algorithm was tested using the CIGRE's North American MV and LV distribution system benchmarks, and compared with a heuristic EV load allocation method and the current EV charging approach, showing good results concerning voltage regulation and loss reduction, while avoiding feeder equipment overloads, and excessive switching of voltage control equipment.

The following conclusions can be drawn from the thesis:

- The proposed four-quadrant EV charger model proved to closely represent the steady-state and dynamic behaviors of the actual prototype, and to be easily and efficiently integrated into time-domain simulations to study the interactions of multiple chargers.

- The results obtained from the implementation of the proposed three-stage EV charging feeder control strategy regarding voltage regulation and loss reduction were promising. However, it was observed that the provision of reactive power for grid services could delay EV battery charging and thus affect EV driving range.

- The provision of reactive power from a four-quadrant EV charger implies the cost of converter power losses, and the incremental cost of controllable switches and a larger dc-link capacitor, compared to a unidirectional charger. However, the results of this research demonstrated possible benefits in distribution system operation of reactive power provision from four-quadrant EV chargers, which could make up for

the extra costs by reducing losses and the volt/var control requirements of devices such as LTCs and capacitors.

5.2 Contributions

The contributions of this thesis can be summarized as follows:

- A new average model of a single-phase, four-quadrant bidirectional EV charger, which can be easily integrated into time-domain simulations to analyze the impact of this type of charger in distribution networks, has been developed and validated based on an actual bidirectional EV charger prototype.
- Three operation strategies of bidirectional EV chargers in LV distribution systems have been presented and discussed, illustrating their application through time-domain simulations based on the proposed average model.
- A new three-stage distribution feeder control approach to reduce feeder losses and peak load, provide adequate volt/var support, and fairly allocate EV charging load, based on a four-quadrant EV smart charger, has been proposed and compared with existing voltage regulation and EV charging practices, as well as with a heuristic EV charging control.
- The proposed distribution feeder control has considered both MV and LV networks, in which EV chargers represent a significant load compared to other household loads, to generate practical and feasible smart charging control signals for individual EVs connected at the LV level.

The results presented in Chapters 3 and 4 have been accepted for publication in the IEEE Transactions on Smart Grid [134, 135].

5.3 Future Work

Based on the work presented in this thesis, future research may explore the following subjects:

- Investigate distribution feeder control strategies considering simultaneous provision of active and reactive power in V2G schemes. The increasing battery capacity of new EV models will reduce the concerns for battery degradation and range anxiety, and will open more possibilities for battery discharging services.
- Study the provision of reactive power with off-board fast EV chargers, possibly connected to the MV system.
- Improve the modeling of EV charging needs with more information gathered from a larger number of actual EVs operating in different climates.

References

[1] "Adoption of the Paris Agreement," UNFCCC (United Nations Framework Convention on Climate Change), 2015. [Online]. Available: http://unfccc.int/resource/docs/2015/cop21/eng/l09r01.pdf

[2] "Ontario's Five Year Climate Change Action Plan 2016-2020," Ministry of the Environment and Climate Change, 2016. [Online]. Available: http://www.applications.ene.gov.on.ca/ccap/products/CCAP_ENGLISH.pdf

[3] "Global EV Outlook 2016," International Energy Agency, 2016. [Online]. Available: https://www.iea.org/publications/freepublications/publication/Global_EV_Outlook_2016.pdf

[4] "Paris Declaration on Electro-Mobility and Climate Change & Call to Action," 2015. [Online]. Available: http://newsroom.unfccc.int/media/521376/paris-electro-mobility-declaration.pdf

[5] T. Gonen, *Electric Power Distribution System Engineering*. CRC Press, 2008.

[6] R. C. Green, L. Wang, and M. Alam, "The impact of plug-in hybrid electric vehicles on distribution networks: A review and outlook," *Renewable and Sustainable Energy Reviews*, vol. 15, no. 1, pp. 544–553, 2011.

[7] M. G. Vayá, T. Krause, R. Waraich, and G. Andersson, "Locational marginal pricing based impact assessment of plug-in hybrid electric vehicles on transmission networks," in *CIGRE International Symposium*, Bologna, 2011, pp. 1–13.

[8] K. J. Dyke, N. Schofield, and M. Barnes, "The impact of transport electrification on electrical networks," *IEEE Trans. Ind. Electron.*, vol. 57, no. 12, pp. 3917–3926, 2010.

[9] M. Yilmaz and P. Krein, "Review of battery charger topologies, charging power levels, and infrastructure for plug-in electric and hybrid vehicles," *IEEE Trans. Power Electron.*, vol. 28, no. 5, pp. 2151–2169, 2013.

[10] ——, "Review of the impact of vehicle-to-grid technologies on distribution systems and utility interfaces," *IEEE Trans. Power Electron.*, vol. 28, no. 12, pp. 5673–5689, 2013.

[11] W. Kempton and J. Tomić, "Vehicle-to-grid power fundamentals: calculating capacity and net revenue," *Journal of Power Sources*, vol. 144, no. 1, pp. 268–279, 2005.

[12] M. Ehsani, M. Falahi, and S. Lotfifard, "Vehicle to grid services: Potential and applications," *Energies*, vol. 5, no. 10, pp. 4076–4090, 2012.

[13] "My Electric Avenue," EA Technology, 2016. [Online]. Available: http://myelectricavenue.info/

[14] "SmartV2G EU Project," Instituto Tecnológico de la Energía (ITE), 2014. [Online]. Available: http://www.smartv2g.eu/

[15] "Green eMotion Project - Electromobility in Europe," European Commision, 2016. [Online]. Available: http://www.greenemotion-project.eu/home/home.php

[16] "Smart charging system for utilities, EVSE providers and fleets," Fleetcarma, 2016. [Online]. Available: http://www.fleetcarma.com/platform/electric-vehicles/smart-charging/

[17] C. Liu, K. Chau, D. Wu, and S. Gao, "Opportunities and challenges of vehicle-to-home, vehicle-to-vehicle, and vehicle-to-grid technologies," *Proc. IEEE*, vol. 101, no. 11, pp. 2409–2427, 2013.

[18] M. C. Kisacikoglu, "Vehicle-to-grid (V2G) reactive power operation analysis of the EV/PHEV bidirectional battery charger," Ph.D. dissertation, University of Tennessee, Knoxville, 2013.

[19] K. M. Tan, V. K. Ramachandaramurthy, and J. Y. Yong, "Integration of electric vehicles in smart grid: A review on vehicle to grid technologies and optimization techniques," *Renewable and Sustainable Energy Reviews*, vol. 53, pp. 720–732, 2016.

[20] J. A. P. Lopes, F. J. Soares, and P. M. R. Almeida, "Integration of electric vehicles in the electric power system," *Proc. IEEE*, vol. 99, no. 1, pp. 168–183, 2011.

[21] J. García-Villalobos, I. Zamora, J. San Martín, F. Asensio, and V. Aperribay, "Plug-in electric vehicles in electric distribution networks: A review of smart charging approaches," *Renewable and Sustainable Energy Reviews*, vol. 38, pp. 717–731, 2014.

[22] A. Dubey and S. Santoso, "Electric vehicle charging on residential distribution systems: Impacts and mitigations," *IEEE Access*, vol. 3, pp. 1871–1893, 2015.

[23] G. Mills and I. MacGill, "Potential power system and fuel consumption impacts of plug in hybrid vehicle charging using Australian National Electricity Market load profiles and transportation survey data," *Electric Power Systems Research*, vol. 116, pp. 1–11, 2014.

[24] C. Weiller, "Plug-in hybrid electric vehicle impacts on hourly electricity demand in the United States," *Energy Policy*, vol. 39, no. 6, pp. 3766–3778, 2011.

[25] U. DOT, "The 2001 national household travel survey," *US Department of Transportation, Bureau of Transportation Statistics*, 2003.

[26] J. van der Burgt, S. P. Vera, B. Wille-Haussmann, A. N. Andersen, and L. H. Tambjerg, "Grid impact of charging electric vehicles; study cases in Denmark, Germany and The Netherlands," in *IEEE PowerTech*, Eindhoven, 2015, pp. 1–6.

[27] K. Clement-Nyns, E. Haesen, and J. Driesen, "The impact of charging plug-in hybrid electric vehicles on a residential distribution grid," *IEEE Trans. Power Syst.*, vol. 25, no. 1, pp. 371–380, 2010.

[28] E. Sortomme, M. Hindi, S. MacPherson, and S. Venkata, "Coordinated charging of plug-in hybrid electric vehicles to minimize distribution system losses," *IEEE Trans. Smart Grid*, vol. 2, no. 1, pp. 186–193, 2011.

[29] S. Deilami, A. S. Masoum, P. S. Moses, and M. A. Masoum, "Real-time coordination of plug-in electric vehicle charging in smart grids to minimize power losses and improve voltage profile," *IEEE Trans. Smart Grid*, vol. 2, no. 3, pp. 456–467, 2011.

[30] A. S. Masoum, S. Deilami, A. Abu-Siada, and M. A. Masoum, "Fuzzy approach for online coordination of plug-in electric vehicle charging in smart grid," *IEEE Trans. Sustain. Energy*, vol. 6, no. 3, pp. 1112–1121, 2015.

[31] K. Zhang, L. Xu, M. Ouyang, H. Wang, L. Lu, J. Li, and Z. Li, "Optimal decentralized valley-filling charging strategy for electric vehicles," *Energy Conversion and Management*, vol. 78, pp. 537–550, 2014.

[32] L. Gan, U. Topcu, and S. H. Low, "Optimal decentralized protocol for electric vehicle charging," *IEEE Trans. Power Syst.*, vol. 28, no. 2, pp. 940–951, 2013.

[33] O. Sundström and C. Binding, "Planning electric-drive vehicle charging under constrained grid conditions," in *International Conference on Power System Technology (POWERCON)*, Hangzhou, 2010, pp. 1–6.

[34] O. Sundström and C. Binding, "Flexible charging optimization for electric vehicles considering distribution grid constraints," *IEEE Trans. Smart Grid*, vol. 3, no. 1, pp. 26–37, 2012.

[35] I. Sharma, C. Cañizares, and K. Bhattacharya, "Smart charging of PEVs penetrating into residential distribution systems," *IEEE Trans. Smart Grid*, vol. 5, no. 3, pp. 1196–1209, 2014.

[36] O. Hafez and K. Bhattacharya, "Optimal PHEV charging in coordination with distributed generation operation in distribution systems," in *IEEE Power and Energy Society General Meeting*, San Diego, CA, 2012, pp. 1–7.

[37] S. Paudyal, C. Cañizares, and K. Bhattacharya, "Optimal operation of distribution feeders in smart grids," *IEEE Trans. Ind. Electron.*, vol. 58, no. 10, pp. 4495–4503, 2011.

[38] J. Peppanen and S. Grijalva, "Neighborhood electric vehicle charging scheduling using particle swarm optimization," in *IEEE PES General Meeting*, National Harbor, MD, 2014, pp. 1–5.

[39] A. O'Connell, D. Flynn, and A. Keane, "Rolling multi-period optimization to control electric vehicle charging in distribution networks," *IEEE Trans. Power Syst.*, vol. 29, no. 1, pp. 340–348, 2014.

[40] B. Wang, B. Hu, C. Qiu, P. Chu, and R. Gadh, "EV charging algorithm implementation with user price preference," in *IEEE Power & Energy Society Innovative Smart Grid Technologies Conference (ISGT)*, Washington, DC, 2015, pp. 1–5.

[41] P. Richardson, D. Flynn, and A. Keane, "Optimal charging of electric vehicles in low-voltage distribution systems," *IEEE Trans. Power Syst.*, vol. 27, no. 1, pp. 268–279, 2012.

[42] ——, "Local versus centralized charging strategies for electric vehicles in low voltage distribution systems," *IEEE Trans. Smart Grid*, vol. 3, no. 2, pp. 1020–1028, 2012.

[43] M. F. Shaaban, M. Ismail, E. F. El-Saadany, and W. Zhuang, "Real-time pev charging/discharging coordination in smart distribution systems," *IEEE Trans. Smart Grid*, vol. 5, no. 4, pp. 1797–1807, 2014.

[44] O. Ardakanian, S. Keshav, and C. Rosenberg, "Real-time distributed control for smart electric vehicle chargers: From a static to a dynamic study," *IEEE Trans. Smart Grid*, vol. 5, no. 5, pp. 2295–2305, 2014.

[45] M. D. Galus, S. Art, and G. Andersson, "A hierarchical, distributed PEV charging control in low voltage distribution grids to ensure network security," in *IEEE PES General Meeting*, San Diego, CA, 2012, pp. 1–8.

[46] N. Mehboob, C. Cañizares, and C. Rosenberg, "Day-ahead dispatch of distribution feeders considering temporal uncertainties of PEVs," in *IEEE PowerTech*, Eindhoven, 2015, pp. 1–6.

[47] N. Mehboob, "Smart charging of plug-in electric vehicles in distribution systems considering uncertainties," Ph.D. dissertation, University of Waterloo, 2016.

[48] A. Di Giorgio, F. Liberati, and S. Canale, "Electric vehicles charging control in a smart grid: A model predictive control approach," *Control Engineering Practice*, vol. 22, pp. 147–162, 2014.

[49] B.-R. Lin, D.-J. Chen, and H.-R. Tsay, "Bi-directional ac/dc converter based on neutral point clamped," in *Proc. IEEE International Symposium on Industrial Electronics (ISIE)*, vol. 1, 2001, pp. 619–624.

[50] B. Lin, T. Hung, and C. Huang, "Bi-directional single-phase half-bridge rectifier for power quality compensation," *IEE Proceedings-Electric Power Applications*, vol. 150, no. 4, pp. 397–406, 2003.

[51] X. Zhou, G. Wang, S. Lukic, S. Bhattacharya, and A. Huang, "Multi-function bi-directional battery charger for plug-in hybrid electric vehicle application," in *Proc. IEEE Energy Conversion Congress and Exposition*, 2009, pp. 3930–3936.

[52] M. Kisacikoglu, B. Ozpineci, and L. Tolbert, "EV/PHEV bidirectional charger assessment for V2G reactive power operation," *IEEE Trans. Power Electron.*, vol. 28, no. 12, pp. 5717–5727, 2013.

[53] T. Tanaka, T. Sekiya, H. Tanaka, M. Okamoto, and E. Hiraki, "Smart charger for electric vehicles with power-quality compensator on single-phase three-wire distribution feeders," *IEEE Trans. Ind. Appl.*, vol. 49, no. 6, pp. 2628–2635, 2013.

[54] V. Monteiro, J. G. Pinto, B. Exposto, H. Goncalves, J. C. Ferreira, C. Couto, and J. L. Afonso, "Assessment of a battery charger for Electric Vehicles with reactive power control," in *Industrial Electronics Conference (IECON)*, Montreal, QC, 2012, pp. 5142–5147.

[55] M. Kesler, M. C. Kisacikoglu, and L. M. Tolbert, "Vehicle-to-grid reactive power operation using plug-in electric vehicle bidirectional offboard charger," *IEEE Trans. Ind. Electron.*, vol. 61, no. 12, pp. 6778–6784, 2014.

[56] M. Kisacikoglu, M. Kesler, and L. Tolbert, "Single-phase on-board bidirectional PEV charger for V2G reactive power operation," *IEEE Trans. Smart Grid*, vol. 6, no. 2, pp. 767–775, March 2015.

[57] A. Dubey, S. Santoso, and M. P. Cloud, "Average-value model of electric vehicle chargers," *IEEE Trans. Smart Grid*, vol. 4, no. 3, pp. 1549–1557, 2013.

[58] D. Maksimović, A. M. Stanković, V. J. Thottuvelil, and G. C. Verghese, "Modeling and simulation of power electronic converters," *Proc. IEEE*, vol. 89, no. 6, pp. 898–912, 2001.

[59] R. Zhang, M. Cardinal, P. Szczesny, and M. Dame, "A grid simulator with control of single-phase power converters in dq rotating frame," in *Proc. IEEE 33rd Power Electronics Specialists Conference (PESC)*, vol. 3, 2002, pp. 1431–1436.

[60] Y. Zhang, Z. Jiang, and X. Yu, "Small-signal modeling and analysis of parallel-connected voltage source inverters," in *Proc. IEEE 6th International Power Electronics and Motion Control Conference*, 2009, pp. 377–383.

[61] A. Yazdani and R. Iravani, *Voltage-sourced converters in power systems: modeling, control, and applications*. John Wiley & Sons, 2010.

[62] M. R. Abedi, B.-M. Song, and R.-Y. Kim, "Dynamic performance improvement of bidirectional battery chargers using predictive current control," in *IEEE PES General Meeting*, San Diego, CA, 2012, pp. 1–8.

[63] T. Niknam, A. Ranjbar, and A. Shirani, "Impact of distributed generation on Volt/Var control in distribution networks," in *IEEE PowerTech*, vol. 3, Bologna, 2003, pp. 1–8.

[64] B. A. Robbins, C. N. Hadjicostis, and A. D. Domínguez-García, "A two-stage distributed architecture for voltage control in power distribution systems," *IEEE Trans. Power Syst.*, vol. 28, no. 2, pp. 1470–1482, 2013.

[65] P. Jahangiri and D. C. Aliprantis, "Distributed Volt/VAr control by PV inverters," *IEEE Trans. Power Syst.*, vol. 28, no. 3, pp. 3429–3439, 2013.

[66] A. Kechroud, P. F. Ribeiro, and W. L. Kling, "Distributed generation support for voltage regulation: an adaptive approach," *Electric Power Systems Research*, vol. 107, pp. 213–220, 2014.

[67] Y. Mitsukuri, R. Hara, H. Kita, E. Kamiya, N. Hiraiwa, and E. Kogure, "Voltage regulation in distribution system utilizing electric vehicles and communication," in *IEEE PES T&D Conference and Exposition*, Orlando, FL, 2012, pp. 1–6.

[68] H. Nafisi, S. M. M. Agah, H. A. Abyaneh, and M. Abedi, "Two-stage optimization method for energy loss minimization in microgrid based on smart power management scheme of PHEVs," *IEEE Trans. Smart Grid*, vol. 7, no. 3, pp. 1268–1276, 2016.

[69] B. Jiang and Y. Fei, "Decentralized scheduling of PEV on-street parking and charging for smart grid reactive power compensation," in *IEEE PES Innovative Smart Grid Technologies Conference (ISGT)*, Washington, DC, 2013, pp. 1–6.

[70] M. N. Mojdehi, M. Fardad, and P. Ghosh, "Technical and economical evaluation of reactive power service from aggregated EVs," *Electric Power Systems Research*, vol. 133, pp. 132–141, 2016.

[71] M. Manbachi, H. Farhangi, A. Palizban, and S. Arzanpour, "A novel volt-var optimization engine for smart distribution networks utilizing vehicle to grid dispatch," *International Journal of Electrical Power & Energy Systems*, vol. 74, pp. 238–251, 2016.

[72] M. A. Azzouz, M. F. Shaaban, and E. F. El-Saadany, "Real-time optimal voltage regulation for distribution networks incorporating high penetration of PEVs," *IEEE Trans. Power Syst.*, vol. 30, no. 6, pp. 3234–3245, 2015.

[73] W. H. Kersting, *Distribution System Modeling and Analysis*. CRC Press, 2001.

[74] T. A. Short, *Electric power distribution handbook*. CRC Press, 2003.

[75] Hydro One Networks Inc., "Distribution Customers Conditions of Service," p. 134, 2013. [Online]. Available: http://www.hydroone.com/MyHome/MyAccount/ConditionsofService/Documents/Hydro_One_Conditions_of_Service_2013_ENGLISH.pdf

[76] IEEE Task Force on Load Representation for Dynamic Performance, "Load representation for dynamic performance analysis," *IEEE Trans. Power Syst.*, vol. 8, no. 2, pp. 472–482, 1993.

[77] J. V. Milanović, "On unreliability of exponential load models," *Electric power systems research*, vol. 49, no. 1, pp. 1–9, 1999.

[78] D. Kosterev and A. Meklin, "Load modeling in WECC," in *IEEE PES Power Systems Conference and Exposition*, Atlanta, GA, 2006, pp. 576–581.

[79] A. Bokhari, A. Alkan, R. Dogan, M. Diaz-Aguiló, F. de León, D. Czarkowski, Z. Zabar, L. Birenbaum, A. Noel, and R. E. Uosef, "Experimental determination of the zip coefficients for modern residential, commercial, and industrial loads," *IEEE Trans. Power Del.*, to be published.

[80] M. E. Baran and M.-Y. Hsu, "Volt/var control at distribution substations," *IEEE Trans. Power Syst.*, vol. 14, no. 1, pp. 312–318, 1999.

[81] "IEEE standard for interconnecting distributed resources with electric power systems," *IEEE Std 1547-2003*, pp. 1–28, July 2003.

[82] "IEEE standard for interconnecting distributed resources with electric power systems - amendment 1," *IEEE Std 1547a-2014 (Amendment to IEEE Std 1547-2003)*, pp. 1–16, May 2014.

[83] K. Turitsyn, P. Sulc, S. Backhaus, and M. Chertkov, "Options for control of reactive power by distributed photovoltaic generators," *Proc. IEEE*, vol. 99, no. 6, pp. 1063–1073, 2011.

[84] I. Roytelman and V. Ganesan, "Coordinated local and centralized control in distribution management systems," *IEEE Trans. Power Del.*, vol. 15, no. 2, pp. 718–724, 2000.

[85] N. Mohan, W. P. Robbins, T. M. Undeland, R. Nilssen, and O. Mo, "Simulation of power electronic and motion control systems-an overview," *Proc. IEEE*, vol. 82, no. 8, pp. 1287–1302, 1994.

[86] S. Banerjee and G. C. Verghese, *Dynamic Models of Power Converters*. Wiley-IEEE Press, 2001, pp. 25–52. [Online]. Available: http://ieeexplore.ieee.org/xpl/articleDetails.jsp?arnumber=5263175

[87] S. Bacha, I. Munteanu, A. I. Bratcu *et al.*, "Power electronic converters modeling and control," *Advanced Textbooks in Control and Signal Processing*, vol. 454, 2014.

[88] L. Dickerman and J. Harrison, "A new car, a new grid," *IEEE Power and Energy Magazine*, vol. 8, no. 2, pp. 55–61, March 2010.

[89] M. C. Falvo, D. Sbordone, I. S. Bayram, and M. Devetsikiotis, "EV charging stations and modes: International standards," in *International Symposium on Power Electronics, Electrical Drives, Automation and Motion (SPEEDAM)*, Ischia, June 2014, pp. 1134–1139.

[90] "Technical specifications of quick charger for the electric vehicle," CHAdeMO Association, 2010.

[91] "SAE charging configurations and ratings terminology," SAE International. [Online]. Available: http://www.sae.org/smartgrid/chargingspeeds.pdf

[92] S. Vazquez, S. M. Lukic, E. Galvan, L. G. Franquelo, and J. M. Carrasco, "Energy storage systems for transport and grid applications," *IEEE Trans. Ind. Electron.*, vol. 57, no. 12, pp. 3881–3895, 2010.

[93] K. Young, C. Wang, L. Y. Wang, and K. Strunz, "Electric vehicle battery technologies," in *Electric Vehicle Integration into Modern Power Networks*. Springer, 2013, pp. 15–56.

[94] "Electric cars available in Canada," Plug'n Drive, 2016. [Online]. Available: https://www.plugndrive.ca/electric-cars-available-in-canada

[95] K. Bao, S. Li, and H. Zheng, "Battery charge and discharge control for energy management in EV and utility integration," in *IEEE PES General Meeting*, San Diego, CA, 2012, pp. 1–8.

[96] H. Wang, A. Hasanzadeh, and A. Khaligh, "Transportation electrification: Conductive charging of electrified vehicles." *IEEE Electrification Magazine*, vol. 1, no. 2, pp. 46–58, 2013.

[97] M. Chen and G. A. Rincon-Mora, "Accurate electrical battery model capable of predicting runtime and IV performance," *IEEE Trans. Energy Conversion*, vol. 21, no. 2, pp. 504–511, 2006.

[98] F. Soares, P. R. Almeida, and J. A. P. Lopes, "Advanced models and simulation tools to address electric vehicle power system integration (steady-state and dynamic behavior)," in *Electric Vehicle Integration into Modern Power Networks*. Springer, 2013, pp. 155–202.

[99] M. D. Galus, "Agent-based modeling and simulation of large scale electric mobility in power systems," Ph.D. dissertation, Eidgenössische Technische Hochschule ETH Zürich, Nr. 20288, 2012.

[100] Ontario Ministry of Energy, "Smart meters and time-of-use prices." [Online]. Available: http://www.energy.gov.on.ca/en/smart-meters-and-tou-prices/#.UzmIG8VA2fZ

[101] D. Richardson, "Electric vehicles and the electric grid: A review of modeling approaches, impacts, and renewable energy integration," *Renewable and Sustainable Energy Reviews*, vol. 19, pp. 247–254, 2013.

[102] K. Clement-Nyns, E. Haesen, and J. Driesen, "The impact of vehicle-to-grid on the distribution grid," *Electric Power Systems Research*, vol. 81, no. 1, pp. 185–192, 2011.

[103] C. Pang, P. Dutta, and M. Kezunovic, "BEVs/PHEVs as dispersed energy storage for V2B uses in the smart grid," *IEEE Trans. Smart Grid*, vol. 3, no. 1, pp. 473–482, 2012.

[104] S. S. Rao, *Engineering optimization: theory and practice*. John Wiley & Sons, 2009.

[105] E. Castillo, R. Mínguez, A. Conejo, and R. Garcia-Bertrand, *Decomposition techniques in mathematical programming*. Springer Berlin, 2006.

[106] R. L. Haupt and S. E. Haupt, *Practical genetic algorithms*. John Wiley & Sons, 2004.

[107] J. Nocedal and S. Wright, *Numerical optimization*. Springer Science & Business Media, 2006.

[108] P. E. Gill, W. Murray, M. A. Saunders, A. Drud, and E. Kalvelagen, "GAMS/SNOPT: an SQP algorithm for large-scale constrained optimization," *GAMS-The Solver Manuals*, 2000.

[109] A. C. Davison and D. V. Hinkley, *Bootstrap methods and their application*. Cambridge university press, 1997, vol. 1.

[110] Z. Yang, M. Zwolinski, and C. Chalk, "Bootstrap, an alternative to monte carlo simulation," *Electronics Letters*, vol. 34, no. 12, 1998.

[111] A. M. Zoubir and D. R. Iskandler, "Bootstrap methods and applications," *IEEE Signal Processing Magazine*, vol. 24, no. 4, pp. 10–19, 2007.

[112] R. J. Tibshirani and B. Efron, "An introduction to the bootstrap," *Monographs on Statistics and Applied Probability*, vol. 57, pp. 1–436, 1993.

[113] N. Wong and M. Kazerani, "A review of bidirectional on-board charger topologies for plugin vehicles," in *Proc. IEEE 25th Canadian Conference on Electrical & Computer Engineering (CCECE)*, 2012, pp. 1–6.

[114] M. C. Kisacikoglu, B. Ozpineci, and L. M. Tolbert, "Examination of a PHEV bidirectional charger system for V2G reactive power compensation," in *Proc. IEEE 25th Applied Power Electronics Conference and Exposition (APEC)*, 2010, pp. 458–465.

[115] M. Yilmaz and P. Krein, "Review of the impact of vehicle-to-grid technologies on distribution systems and utility interfaces," *IEEE Trans. Power Electron.*, vol. 28, no. 12, pp. 5673–5689, 2013.

[116] L. Shi, A. Meintz, and M. Ferdowsi, "Single-phase bidirectional ac-dc converters for plug-in hybrid electric vehicle applications," in *Proc. IEEE Vehicle Power and Propulsion Conference (VPPC)*, 2008, pp. 1–5.

[117] M. P. Kazmierkowski and L. Malesani, "Current control techniques for three-phase voltage-source PWM converters: a survey," *IEEE Trans. Ind. Electron.*, vol. 45, no. 5, pp. 691–703, 1998.

[118] N. Wong, K. Zhuge, and M. Kazerani, "A comparative evaluation of control techniques for grid-side ac-dc converter in a two-stage level-two bidirectional battery charger," in *Proc. IEEE Transportation Electrification Conference and Expo (ITEC)*, 2013, pp. 1–5.

[119] M. Gonzalez, V. Cardenas, and F. Pazos, "DQ transformation development for single-phase systems to compensate harmonic distortion and reactive power," in *Proc. 9th IEEE International Power Electronics Congress*, 2004, pp. 177–182.

[120] J. Morris, "Design and Testing of a Bidirectional Smart Charger Prototype," Master's thesis, University of Waterloo, 2015.

[121] N. Mohan and T. M. Undeland, *Power electronics: converters, applications, and design*. John Wiley & Sons, 2007.

[122] "Peaksaver plus ®," Hydro One Inc., 2015. [Online]. Available: http://www.hydroone.com/MyHome/SaveEnergy/Pages/Peaksaver.aspx

[123] "Users guide on the use of PSCAD v4.3.1," Manitoba-HVDC Research Center, p. 492, 2010. [Online]. Available: https://hvdc.ca/uploads/ck/files/reference_material/PSCAD_User_Guide_v4_3_1.pdf

[124] J. R. Rodríguez, J. W. Dixon, J. R. Espinoza, J. Pontt, and P. Lezana, "PWM regenerative rectifiers: state of the art," *IEEE Trans. Ind. Electron.*, vol. 52, no. 1, pp. 5–22, 2005.

[125] K. Strunz *et al.*, "Benchmark systems for network integration of renewable and distributed energy resources," Tech. Rep. CIGRE Task Force C.04.02, 2013.

[126] M. Liu, C. A. Cañizares, and W. Huang, "Reactive power and voltage control in distribution systems with limited switching operations," *IEEE Trans. Power Syst.*, vol. 24, no. 2, pp. 889–899, 2009.

[127] "Simulation Tool - OpenDSS," Electric Power Research Institute, Inc. , 2011. [Online]. Available: http://smartgrid.epri.com/SimulationTool.aspx

[128] "Global optimization toolbox documentation," The MathWorks, Inc., 2016. [Online]. Available: http://www.mathworks.com/help/gads/index.html

[129] I. J. Pérez-Arriaga *et al.*, *Regulation of the power sector*. Springer, 2013.

[130] CSA, "CAN3-C23583: Preferred voltage levels for ac systems 0 to 50000 V electric power transmission and distribution," 2015.

[131] A. Mohd, E. Ortjohann, D. Morton, and O. Omari, "Review of control techniques for inverters parallel operation," *Electric Power Systems Research*, vol. 80, no. 12, pp. 1477–1487, 2010.

[132] J. Smart and S. Schey, "Battery electric vehicle driving and charging behavior observed early in the EV project," *SAE International Journal of Alternative Powertrains*, vol. 1, no. 2012-01-0199, pp. 27–33, 2012.

[133] M. T. Wishart, F. Shahnia, A. Ghosh, and G. Ledwich, "Multi objective decision making method for demand side management of LV residential distribution networks with plug-in electric vehicles," in *IEEE Power and Energy Society General Meeting*, San Diego, CA, 2011, pp. 1–8.

[134] M. Restrepo, J. Morris, M. Kazerani, and C. Cañizares, "Modeling and testing of a bidirectional smart charger for distribution system EV integration," *IEEE Trans. Smart Grid*, accepted March 2016.

[135] M. Restrepo, C. Cañizares, and M. Kazerani, "Three-stage distribution feeder control considering four-quadrant EV chargers," *IEEE Trans. Smart Grid*, accepted December 2016.